UNIVERSITY OF CALIFORNIA SANTA CRUZ

The Influence of Anthropogenic Nitrogen and Sulfur on Mercury Methylation: from Wetland Sediment to Upland Soil

A dissertation submitted in partial satisfaction of the requirements for the degree of

DOCTOR OF PHILOSOPHY

in

OCEAN SCIENCES

by

Jeannette I. Calvin

June 2024

The Dissertation of Jeannette Calvin is approved:

_____
Professor Carl Lamborg, chair

_____
Peter Weiss-Penzias, Ph.D.

_____
Professor Phoebe Lam

_____
Professor Chad Saltikov

_____
Asst. Professor Priya Ganguli

_____
Peter Biehl
Vice Provost and Dean of Graduate Studies

TABLE OF CONTENTS

LIST OF TABLES

LIST OF FIGURES

ABSTRACT

The Influence of Anthropogenic Nitrogen and Sulfur on Mercury Methylation: From Wetland Sediment to Upland Soil

Jeannette Isabella Calvin

Monomethylmercury (MeHg, CH_3Hg^+) is a neurotoxin that bioaccumulates in the food web. Previous investigations have found eutrophication to be associated with both increases and decreases in MeHg accumulation. We embarked on a time series study at Younger Lagoon Reserve, adjacent to agricultural fields, to investigate the influence of anthropogenic nitrate on MeHg production in a local lagoon. Our work hints at why it is possible for dichotomous results to exist, and also again demonstrates that sulfur is an important control on MeHg production. MeHg production in soils has received less attention than wetland and marine environments, yet agricultural soils such as vineyards are of interest as they receive elemental sulfur applications. Our research reveals the results of a first inquiry into the fate of sulfur in vineyards and its implications for potential methylation.

ACKNOWLEDGEMENTS

A number of people and institutions helped me achieve the completion of the presented research and I am deeply grateful to everyone for their contributions. Knowing that this list is far from complete, and that some folks have participated in multiple categories, I would like to thank some individuals for specific efforts:

- Dr. Carl Lamborg for taking me as a student, taking me as I am, getting me hooked on Hg research, and believing in my ability to succeed (and code!) even when I doubted myself.

- Dr. Peter Weiss-Penzias for taking me as a student at just the right time so that a Master's 2.5+ could become a PhD after all, for taking me seriously, and for modeling optimism when the going got tough.

- Drs. Phoebe Lam and Chad Saltikov for your many helpful comments for improving the writing, captions, and interpretations of my dissertation, and for helping me overcome research challenges along the way.

- Drs. Priya Ganguli and Myra Finkelstein for listening to me, really understanding me, and providing reassurance when it felt for certain graduate school might break me.

- Rabbi Shifra Penzias for helping facilitate the connection to becoming a PhD student and for providing free and much needed self-advocacy and assertiveness training.

- Private landowners in Napa Valley, CA, who allowed access to their land for this research project.

- Younger Lagoon Reserve staff & stewards and the UC Natural Reserve System for granting permission to conduct research at the lagoon.

- Weiss-Penzias Lab comrades Michelle Rothman and Travis Esquivel for being real, for truly getting it, and for being my grad school buddies at AGU and always.

- Lam-borg Lab Suite colleagues Xinyun Cui, Marissa Despins, Kristine Prelich, Vinicius Amaral, Allison Laubach, Jong-Mi Lee, Yang Xiang, and Katherine Mateos for sharing the space so kindly, providing helpful hints, and being my built-in friends when COVID and long hours in the lab kept me cut off from social contacts.

- Mom & Dad, Phil & Celeste, Debbie & Doug, and Bob & Cindy for generous emotional and financial support this whole time.

- Norks, the gem of my heart, you bring me joy whenever we can be together.

- Zee Byrd Moffatt for enduring 5 years apart, still loving me after seeing me at my worst, and remaining supportive of me finishing, even with an extra 2 years.

- Beecher Battle for taking the full force of the tears and rage that I worked so hard to hide from everyone else, and for sticking with me anyway.

- Drs. Carl Mitchell, Holger Hintelmann, Bryan Dreyer, Rachel Strickland & Rebecca Neumann for providing advice about mercury isotope measurements and calculations.

- Drs. Claudie Beaulieu & Matthew Clapham for providing totally essential help with statistics questions and indispensable training in R.

- Drs. Alyson Santoro & Silvia Newell for help with microbial interpretations.

- Drs. Kendra Turk-Kubo, Esther Mak, Katlin Bowman, and Nicole Schrad for advice on microbial experiments, DNA extraction, sequencing & data processing.

- MCD Bio colleagues Dr. Jimmy Shanks, Sara Claus, Suki Arnold & Alexis Rodriguez for being the folks who brought a smile to my face when I was in microbiology mode.

- Andi Greene, Jenny Pensky, & Emilio Grande for Lachat nutrient analyzer training.

- Undergraduate lab assistants Katie Collins, McKenna Smith, Vanessa Pham, Olivia Driscoll, Lizzie Pechulis, Kit Vu, Matthew Geller, & Molly Hoffman for taking on lab duties that freed my time for other work.

- Carolina Lazari and Mar Arroyo for standing beside me through the trials of grad school, letting me vent, giving me hugs, and never letting me doubt that I could finish a PhD despite the obstacles.

- Blender Buddies Monty, Riley, Mira & Genni for queer community.

- Yan Zhang, Ily Iglesias, Eve Pugsley, Aubrey Trapp, JB Novak, Jasen Jacobsen, Anna Schartman, and Marco Conci for being amazing Ocean Sciences colleagues and supporting my survival in grad school, each in your own way.

- Charles Martin for rescuing me in year one for helping me move. You went above and beyond and I am forever grateful.

- Ethan Marquez and Rick Wood for cheering me up and being my buddies wherever our paths crossed (and for delivering waste containers and packages!).

- UCSC Dining staff for making it possible to stay on campus for as many hours as it took to get the work done.

Funding Sources

Research presented in this dissertation received funding from the following sources:

Myers Oceanographic & Marine Biology Trust

UC Regents Fellowship & Materials Award

Marilyn C. Davis Re-entry Scholarship

SC Women's Club Rita Pistor Award

Bryant Frech & Marvin Lamborg Fund

UCSC STARS Scholarship

Kathryn D. Sullivan Research Impact Award

USDA Grant #13376262

NSF OPP #2232981

DEDICATION

The work is dedicated to my family, both biological and chosen

CHAPTER 1. Introduction

Mercury (Hg) can occur in the elemental form, Hg^0, which is gaseous, as an ion, inorganic Hg(II), and also exists in organometallic forms. Combustion of fossil fuels is a source of anthropogenic Hg to the atmosphere, as Hg stored in coal deposits is released. Atmospheric wet and dry deposition of Hg(II) and Hg^0 are one source of total mercury (HgT) to a given locale. Thus, processes such as litterfall from trees provide a source of Hg to terrestrial soil and mobilization of terrigenous material delivers Hg to the sediments of lakes and coastlines. In addition, a region may have elevated Hg as a consequence of historic or recent processes such as effluent from chlor-alkali plants, ores from Hg mining, or release of Hg^0 from artisanal Au mining.

When Hg(II) becomes methylated, it is converted to organometallic forms, monomethylmercury ($MMHg^+$) and dimethylmercury (DMHg), which collectively are often referred to as MeHg. While all forms of Hg are toxic, MeHg poses a greater risk to humans than the others because it most readily bioaccumulates in organisms and is biomagnified with trophic transfer, which allows for concentrated Hg exposure when MeHg-enriched food is consumed (Clarkson et al. 2003; Zhang et al. 2010; Karimi et al. 2012). Hg(II) can become methylated abiotically or biotically. While it has been given less research attention, the MeHg degradation process, demethylation, also occurs by both abiotic and biotic mechanisms. Some abiotic demethylation processes are photocatalyzed (Lehnerr et al. 2009) and some occur under dark conditions (Kronberg et al. 2018; West et al. 2020). However, geochemical influences on biotic processes are the focus of the work presented here.

Over the past three to four decades, biotic Hg methylation, a process thought to be mediated exclusively by anaerobic microbes (Gilmour et al. 2013), has received research attention focused on unraveling drivers of net MeHg production and elucidating which organisms are involved. Locations of high MeHg production are typically anoxic or hypoxic

environments, though there is mounting evidence that anoxic microsites within particulates in the water column (Ortiz et al. 2015; Gascón Díez et al. 2016), periphyton (Hamelin et al. 2011), and soils (Huang and Mitchell, 2023) support methylation by anaerobic bacteria in broadly oxic environments.

To date, a myriad of microbes, including sulfate-reducing and iron-reducing bacteria, methanogens, and archaea have been confirmed to methylate mercury. Parks et al. (2013) revealed that the ability to methylate was associated with possession of the gene pair *hgcAB* and subsequent studies have focused on associating this gene and its abundance with biogeochemical conditions and concentrations of analytes or microbial types in various environments (Podar et al. 2015; Ma et al. 2017; Wang Y-L et al. 2024). The current knowledge of organisms reported with *hgcA*, or similar sequences, along with the sequences and identities with those who have been confirmed to methylate Hg has been expertly summarized in a database called Hg-MATE (Gionfriddo et al. 2021). Like methylation, biotic demethylation is also thought to be catalyzed by microbial enzymes, and three pathways have been proposed: reductive demethylation (Spangler et al. 1973; Parks et al 2009) (also called *mer*-dependent demethylation (Barkay and Gu, 2022), oxidative demethylation (Oremland et al. 1991), and most recently, methanotrophic demethylation (Lu et al. 2017).

Microbial identity and possession of HgcA or a similar protein is only a limited part of the story of unraveling environmental Hg methylation and demethylation dynamics. Geochemical parameters are also at play, and accordingly, LOI (a proxy for organic carbon content), salinity, pH, nitrogen species, sulfur species, and other variables have been examined and implicated as influential in different environments. While an environment would require Hg(II) to be present to get methylated, once that condition is met there is a lack of consensus as to which other geochemical variables control the process of MeHg production, as results are frequently site specific.

The research presented here is on Hg cycling dynamics in both wetland and upland environments, though the Hg story became inseparable from studying mercury's near-

constant companion, sulfur. Hg is a chalcophile and enters into complexation with sulfide to form cinnabar, HgS_{solid}, and other dissolved HgS species, and is known to have a high affinity for organic matter likely as a consequence of reacting with S-containing cysteine residues. Indeed, sulfur species come into play throughout this work, in Chapter 2 by contributing to a hindering matrix effect requiring method development to overcome, in Chapter 3 as a fuel (sulfate) and a byproduct (sulfide) of bacterial metabolism, and in Chapter 4, in the form of elemental sulfur, S^0, as an agricultural amendment. Sulfur (oxidized and reduced forms) have been implicated in Hg methylation but can have bi-directional effects on the process. Sulfate can stimulate MeHg production by sulfate-reducing bacteria, up to a threshold concentration, but too much sulfide accumulation as a result of sulfate-reduction limits Hg bioavailability to microbes. The process is summarized in Figure 1, which is based on the work of Benoit and colleagues (Benoit et al. 1999a; Benoit et al. 1999b; Benoit et al. 2001a; Benoit et al. 2001b).

Organic carbon fuels the metabolisms of heterotrophic organisms, and so their metabolic activity depends on its availability. Studies have extensively examined how microbial metabolisms respond to the quantity, structure, and bioavailability of organic matter. Organic carbon has also been suggested to play a role in the bioavailability of Hg(II) to microbes (Chiasson-Gould et al. 2014), and a large amount of OM has been associated with reducing accumulation of MeHg in the marine food web (Driscoll. et al. 2012). While Chapter 3 discussion goes into a more comprehensive discussion, nitrate and OM are both involved in biotic Hg cycling. The free energy of available electron acceptors can induce competition for OM by microbes (e.g., Bentzen, 1995), which affects who survives, and can impact Hg cycling. Previous results have found stimulation of demethylation and suppression of methylation under nitrate addition. (Hines et al., 2012; Todorova et al. 2009). Future work will tell us what role, if any, nitrate-reducers (by denitrification or DNRA), ammonia-oxidizers, and nitrite-oxidizers play in MeHg cycling.

As the influences of these variables, and others, cannot be easily isolated in the environment, researchers have turned to microcosm studies to help to unravel the effects of geochemical parameters. These are (usually) anoxic experiments conducted in vessels containing environmental media (sediment, soil, periphyton, or seawater) in which the native microbial community has been preserved to the extent possible. The media is amended with enriched Hg-isotope spikes, in the forms of $^{XXX}Hg(II)$ for tracking MeHg formation and $^{XXX}CH_3Hg$ for tracking demethylation (Hintelmann and Evans, 1997). The pseudo-first-order rate constants, k_{meth} and k_{demeth} (day^{-1}), can be determined by the calculations described in Ourdane et al. (2009). While these studies provide a technique for isolating variables of interest in a complex biogeochemical framework, they can have limited relationships to observations in the environment and are typically described as methylation or demethylation "potentials" (Mitchell and Gilmour, 2008). However, this type of study provides snapshots of responses to perturbations, for example, in chemical transformations of Hg, N, S, or C by microbes, and/or of the microbial community composition at points in time after chemical amendments. Table 1 presents some of the findings specifically of the influences of N and S amendments, though a much more elaborate variety of experiments has been performed with other nutrients, microbial inhibitors, radiotracers, and genomic techniques.

The work presented in Chapter 3 began as a time series experiment at Younger Lagoon Reserve, with an aim of tracking relationships between HgT concentrations, MeHg concentrations, and nitrate concentrations in surface and porewaters, along with other parameters, over the course of a whole year. The initial design called for one sampling event per season, however a June time point was pushed to August due to the COVID-19 pandemic. Arrival of wildfires and ashfall in August precluded fieldwork and sampling was pushed to October 2020, which then represented the Autumn time point. Autumn was the season the sediment for the microcosm experiments was collected, though the original plan was to sample in Summer when microbial load was anticipated to be highest. The Autumn sampling was repeated in October 2022 for consistency in observations, though it is

important to note that high sulfide conditions in October most likely had an effect on methylation and demethylation potentials determined in the microcosms, and that samples from a different season could have yielded a different result. Furthermore, after 2020, the agricultural fields surrounding the lagoon were fallow, and did not receive N amendments as they had in previous years. Therefore, the system examined in 2022 experienced a different range of nitrate concentrations. At Beach Zone, December 2022-June 2023 had nitrate concentrations ranging between 0-40 uM nitrate (K. Prelich,personal communication, June 2, 2024) whereas the range of nitrate concentrations from 2019-2020 was 0-163 uM between December 2019-April 2020. It is possible that the response to amendments in 2022 microcosms is not directly comparable to those from 2020, as the microbial community composition may have been different, and was not characterized in Autumn 2022.

It is worth noting that k_{meth} in the brackish estuarine sediment of Younger Lagoon, at sandy Beach Zone, are on the order of ~1%/day, and in the further inland location of YL, East Fork, anticipated to be more influenced by the agricultural fields surrounding the reserve, are ~0.1%/day. Rates within agricultural soils and upland soils are on the order of 0.01%/per day and overlap with those at East Fork. It appears that East Fork sediment is composed partially of the sandy, ocean-influenced wetland endmember and also from an organic-rich and clay-rich agricultural and terrestrial soil endmember. Even though East Fork is saturated and the upland forest soil site is not, the two sites had similar k_{meth}, HgT concentrations, and organic matter percentages (w/w), with vineyards and grassland having lower k_{meth} and lower organic matter percentages and HgT concentrations. Beach Zone, with <1% (w/w) organic matter and a smaller HgT concentration, had higher k_{meth} values, but lower MeHg concentrations. If crude estimates of rates of MeHg production are calculated based on the average k_{meth} (per day) multiplied by the average HgT concentration at each site, upland forest sites and East Fork sediment have similar rates of ~0.19 ng g^{-1} day^{-1} and ~0.18 ng g^{-1} day^{-1}, respectively. Estimated rates of MeHg production in wet vineyards would be lower, at ~ 0.065 ng g^{-1} day^{-1} and at Beach Zone, higher, with a rate of ~ 0.36 ng g^{-1} day^{-1}. Beach

Zone is notable as it has the lowest organic matter content of the sites compared, and the lowest HgT concentrations, but the highest k_{meth} values and the highest estimated rates of production. An absence of high MeHg concentration at Beach Zone may be as a result of limited amounts of organic matter to bind the MeHg, which allows it to enter porewater and mobilize, rather than accumulating in the sediment.

Within the lagoon sediments and in the upland soils, reduced forms of sulfur and ambient sulfate concentration respectively were associated with a suppression of k_{meth}. The findings may have been due to limited bioavailability of Hg(II) as a result of sulfide accumulation, though more work would need to be done to confirm this hypothesis. Nitrate was associated with a suppression of k_{demeth} at Beach Zone, while k_{meth} was unaffected. As microbes expected to be outcompeted by nitrate reducers would be expected to impact both methylation and demethylation potentials, why k_{meth} and k_{demeth} did not move in concert at YL Beach Zone is unknown. Metabolic flexibility of heterotrophic SRB capable of switching to nitrate-reduction was proposed as a speculative mechanism by which k_{meth} could go unchanged while demethylation was suppressed under nitrate treatment. Such an argument depends on the assumptions that SRB could still methylate Hg while performing nitrate reduction and that heterotrophic denitrifiers would have contributed significantly to demethylation were they not outcompeted for organic carbon by SRB utilizing nitrate. Despite a lack of evidence for direct stimulation to Hg methylation by nitrate, the results of microcosm assays indicate that nitrate from anthropogenic sources could lead to net Hg methylation within a system through a mechanism of lessened demethylation.

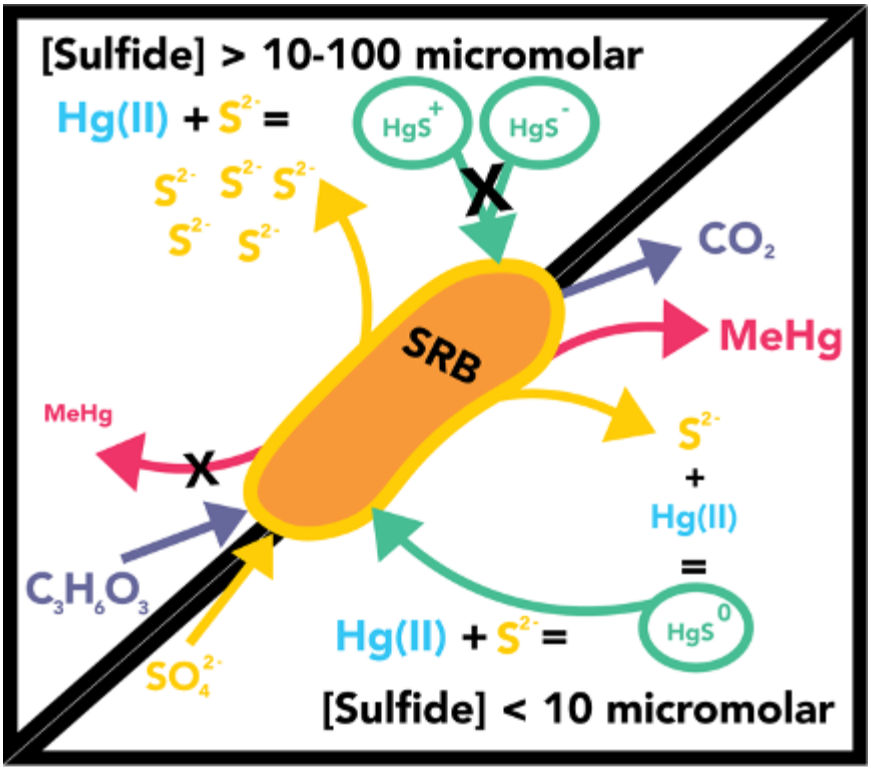

Figure 1. A cartoon depicting the biogeochemical controls on the production of MeHg. The upper left wedge of the figure shows a generic, heterotrophic, sulfate-reducing bacterium (SRB) operating under conditions of elevated sulfide (>10 uM). These conditions favor the formation of charged HgS complexes, which do not diffuse readily across bacteria cell membranes. Black X's indicate processes which are suppressed under this range of sulfide conditions. The lower right wedge of the figure shows SRB behavior under conditions of lower sulfide, where uncharged HgS complex formation is favored, Hg is bioavailable to SRB cells, and Hg methylation occurs.

Table 1. A comparison of methylation and demethylation potentials across studies with nitrogen and sulfur amendments. Methylation and demethylation pseudo-first-order rate constants were multiplied by 100 to report all in units of percent per day. BD indicates below the limit of detection. ND indicates no data available and NA indicates not applicable.

Source	Description of Potential Rate Constant Experiment	Environment	kmeth (percent per day)	kdemeth (percent per day)	Sulfate Concentration	Sulfide or Reduced Sulfur	Nitrate Concentration	Amendments' Effect on Methylation	Amendments' Effect on Demethylation
Roth et al., 2021	Ambient (Control)	Peat Soil, Alaska, USA	9.3	ND	<1 uM	0.6 uM	ND	NA	NA
Roth et al., 2021	Sulfate Amendment Experiment	Peat Soil, Alaska, USA	17	ND	0.11 mM	ND	NA	increased (sulfate)	ND
Todorova et al., 2009	Ambient (Control)	Lake Sediment, New York, USA	4	0.4	ND	ND	ND	NA	NA
Todorova et al., 2009	Nitrate Amendment Experiment	Freshwater Lake Sediment, New York, USA	< 0.025	0.37	ND	ND	1.0 mM	decrease (nitrate)	no change (nitrate)

Table 1. Continued: A comparison of methylation and demethylation potentials across studies with nitrogen and sulfur amendments.

Source	Description of Potential Rate Constant Experiment	Environment	kmeth (percent per day)	kdemeth (percent per day)	Sulfate Concentration	Sulfide or Reduced Sulfur	Nitrate Concentration	Amendments' Effect on Methylation	Amendments' Effect on Demethylation
Chen et al., 2023	Ambient (Control)	Rice Paddy Soil, Guizhou Province, China	0.03-2.5	60-160	0-52 uM	0.62-2.2 uM	NA	NA	NA
Chen et al., 2023	Nitrate Amendment Experiment	Rice Paddy Soil, Guizhou Province, China	0.005-1.25	25-125	0-1.7 mM	0.62-1.6 uM	200 mg N /kg	decrease (nitrate)	decrease (nitrate)
Hines et al., 2012	Ambient (Control)	Sediment, Marano and Grado Lagoons, Italy	~0.63 for control	~3 for control	ND	ND	ND	NA	NA
Hines et al., 2012	Nitrate Amendment Experiment	Sediment, Marano and Grado Lagoons, Italy	0.04	16.5-19.5	ND	ND	2.0 mM	decrease (nitrate)	increase (nitrate)

Table 1. Continued: A comparison of methylation and demethylation potentials across studies with nitrogen and sulfur amendments.

Source	Description of Potential Rate Constant Experiment	Environment	kmeth (percent per day)	kdemeth (percent per day)	Sulfate Concentration	Sulfide or Reduced Sulfur	Nitrate Concentration	Amendment' Effect on Methylation	Amendments' Effect on Demethylation
Gilmour et al.,1998	Ambient (Control)	Surficial Sediments. Florida Everglades, USA	2.5-3	3-23 (Marvin-DiPasquale et. al., 2003)	0-400 uM	0-300 uM	uM range	NA	NA
Gilmour et al.,1998	Nitrate Amendment Experiment	Surficial Sediments. Florida Everglades, USA	~0.5	ND	0-400 uM	200 uM ambient	100 uM	decrease (nitrate)	ND
Gilmour et al.,1998	Sulfate Amendment Experiment	Surficial Sediments. Florida Everglades, USA	3-4.8	ND	2.5 mM	200 uM ambient	uM range	slight increase (sulfate)	ND
Gilmour et al.,1998	Sulfide (as bisulfide) Amendment Experiment	Surficial Sediments. Florida Everglades, USA	~1	ND	ND	250 uM	NA	decrease (sulfide)	ND

Table 1. Continued: A comparison of methylation and demethylation potentials across studies with nitrogen and sulfur amendments.

Source	Description of Potential Rate Constant Experiment	Environment	kmeth (percent per day)	kdemeth (percent per day)	Sulfate Concentration	Sulfide or Reduced Sulfur	Nitrate Concentration	Amendment' Effect on Methylation	Amendments' Effect on Demethylation
Calvin et al., in prep	Ambient (Control)	Sandy Sediment, Coastal Estuary Santa Cruz, CA, USA	~2- 4.25 (2022)	35-45 (2022)	ND	29.1 mM	BD (0.005) - 163 uM)	NA	NA
Calvin et al., in prep	Nitrate Amendment Experiment	Sandy Sediment, Coastal Estuary Santa Cruz, CA, USA	2.25-3.75 (2022)	5-20 (2022)	ND	29.1 mM	106 mM	no change (nitrate)	decrease (nitrate)
Calvin et al., in prep	Ambient (Control)	Organic-Rich Sediment, Coastal Estuary Santa Cruz, CA, USA	0.1-0.3 (2020)	ND	ND	167 mM	BD (0.005) - 168 uM)	NA	NA
Calvin et al., in prep	Nitrate Amendment Experiment	Organic-Rich Sediment, Coastal Estuary Santa Cruz, CA, USA	0.19-0.21 (2020)	ND	ND	167 mM	106 mM	no change (nitrate)	ND

CHAPTER 2. Improved Total Mercury Analysis in Estuarine Porewaters from Longer Oxidation Times

Abstract

Quantification of aqueous total mercury (HgT) from environmental samples by Cold-Vapor Atomic Fluorescence Spectroscopy (CVAFS) depends upon a complete oxidation of ligands capable of coordinating Hg(II) and preventing its reduction to Hg^0 prior to detection. Dissolved organic matter (DOM) and sulfide are examples of ligands responsible for matrix effects that can be eliminated with oxidative digestion. The standard method, EPA 1631, employs bromine monochloride as an oxidant and recommends digestion durations on the order of hours. However, during the course of research at an estuarine wetland, we found some porewater samples failed to oxidize completely under the established conditions of 2% BrCl and a 12-hour room-temperature digestion. The standard method recommends increasing the amount of BrCl in such cases, however our samples suggest that there exists a subset of brackish porewater samples which have low enough Hg to warrant avoiding the increased Hg blank associated with 5% BrCl (v/v) but that have analytical interference due to recalcitrant DOM. Here we present the results of oxidative digestion trials encompassing a range of BrCl concentrations (0.25-5% v/v) and extended digestion periods (12-24 hours, 2-24 days) designed to reveal conditions that would best support oxidation of organic ligands while minimizing the reagent blank. A 24-day incubation treatment yielded larger observed values of Hg when compared to a 14-day incubation or a heated water bath treatment during the first set of trials (1-8). For subsequent trials 12-16, porewater was treated with 5% (v/v) BrCl and again, a 24 day digestion yielded larger values of Hg compared to EPA Method 1631 or a heated water bath. Therefore, a 24-day room temperature digestion was identified as the most appropriate condition to support complete oxidation of ligands within brackish porewater samples. Furthermore, it was found that 5% (v/v) BrCl was required for complete oxidation of Hg in lagoon porewater samples, which suggests that 5% (v/v) BrCl is

appropriate for some natural waters, which may pose as complex of matrices as wastewater effluent.

2.1 Introduction

Wetland and estuarine water samples frequently pose matrix effect obstacles for the chemical analyst due to high concentrations of dissolved organic matter (DOM), salinity, and sulfide, all potentially capable of interfering with the determination of an analyte of interest. The detection of total mercury (HgT) in saline porewater is no exception. Room temperature bromine monochloride (BrCl) addition is an established technique in routine use with both freshwater and marine samples to both oxidize potential interferants and render organo-mercury species into Hg(II) prior to reduction with $SnCl_2$ and purge-and-trap pre-concentration (Gill and Fitzgerald 1987). The standard method, EPA 1631, employs this approach, indicating that 0.5% (v/v) of stock BrCl reagent is appropriate for clear samples and 1.0% (v/v) BrCl for brown or turbid samples to achieve full oxidation of organic matter with a digestion period on the order of hours (USEPA 2002). In extreme cases, the method suggests using as high as 5% (v/v) BrCl to digest highly organic matrices such as wastewater effluent. Alternatively, the work of Lang et al. (2005) examined the efficacy of BrCl digestion for total Hg in freshwater, under cold and microwave-assisted digestions. The results of the study indicated that 2% (v/v) BrCl and a minimum 2-day cold digestion was optimal, with the increase from 1% to 2% (v/v) BrCl being essential for complete oxidation of samples containing >7.49 mg/L DOC. Furthermore, the results of Lang et al. indicated that heating the samples via microwaves could cause unintended degradation of the analyte. We have found, working in brackish waters with high dissolved organic carbon and sometimes sulfide, that adherence to EPA protocols was insufficient for complete digestion of estuarine porewater samples under the time periods investigated. This was indicated by some samples retaining some of their original coloration or developing a haze following reduction of BrCl with NH_2OH prior to further analysis. The samples encountered during the current work suggest that there

exists a subset of brackish porewater samples which have low enough Hg to warrant avoiding the increased Hg blank associated with 5% (v/v) BrCl but that have analytical interference due to recalcitrant DOM.

Thus, our study explores options for overcoming matrix effects when working with brackish porewater samples that contain both elevated DOM and sulfide. The study aims to provide an effective methodology when processing samples that cannot be subjected to 5% (v/v) BrCl as the HgT concentration of the sample is insufficient to detect above the blank but when the samples still contain complexing ligands that must be oxidized fully prior to HgT determination. We compared the efficacy of 1) increased concentration of BrCl, 2) increased digestion time, and 3) heating the sample after adding BrCl, or a combination. While some authors found UV-oxidative pre-treatment before BrCl addition to be essential for complete Hg recovery in aqueous samples (Olson et al. 1997), our initial study was designed with the goals of eliminating the requirement of a UV-light producing apparatus and limiting the total amount of BrCl used to 2% (v/v). However, it was later found that some natural water samples require the use of 5% (v/v) BrCl to overcome the matrix interference.

A replicate experiment conducted in September-October 2023 was designed to examine the reproducibility of the results from trials 1-8, with all four digestion treatments compared on porewater of the same identity (same day and depth of collection). BZ and EF samples, from 2 different depths each, were treated with 2% (v/v) BrCl and subjected to EPA Standard Method 1631, a heated water bath, or a room-temperature 14-day or 24-day digestion in trials 9-12. A following round of trials (13-16) included porewater from EF 2 cm and 10 cm depths treated with 5% (v/v) BrCl, as 2% (v/v) BrCl was found to be insufficient to fully oxidize the available Hg.

2.2 Methods

Porewater and Surface Water Sample Collection

All samples were waters collected from Younger Lagoon Reserve (YL; 37° 57' 5"_N, 122° 3' 51" W; https://ucnrs.org/reserves/younger-lagoon-reserve/), which includes a 10.1-hectare estuarine wetland in Santa Cruz, California. The Lagoon experiences a brief connection to the ocean during the winter when waves and tides combine to erode its barrier beach. Following this, the beach reforms and the Lagoon receives fresh groundwater and rain that mixes with the entrained seawater, leading to a freshening through the winter and spring. The dry summer and fall then lead to a gradual increase in salinity and lowering of water level through evaporation and groundwater transport to the ocean.

Two sites within YL were selected for Hg biogeochemical studies due to their dramatic differences. The Beach Zone (BZ) site at the southern end of the Lagoon represents locations with sandy, low organic carbon sediments. In contrast, the East Fork (EF) site at the northeast end of the Lagoon possesses clay- and organic matter-rich sediments and is located further inland. Water depths during sampling were never greater than about 1.5 m, and the sites were accessed with waders. At both sites, 1-L surface water grab samples were collected in acid-cleaned Teflon bottles, with each vessel being rinsed 3x before collection. Porewaters were collected through a ¼" stainless steel push piezometer (MHE Products) inserted into the sediment by hand and sampled in 2 cm increments down to 20 cm depth (similar strategy to (Lutz et al. 2008). Acid-washed C-flex tubing was attached to the piezometer and a peristaltic pump was used to draw porewater out of the sediment until about 250 mL was collected. A mesh guard (MHE) was taped around the outside of the piezometer inlet to prevent clogging by plant roots or particulates. Porewater samples were capped and placed in amber bags inside a cooler until transported to the lab. In the lab, the porewater and surface water samples were filtered with a 0.45 um groundwater capsule filter (Millipore Sigma GWSC04501) and acidified to 0.1% (v/v) with 12 M HCl before storage

double-bagged at 4 °C. The capsule filter was rinsed with 2 L of 18 MΩ-cm water before any samples were passed through and was rinsed with 0.5 L 18 MΩ-cm water between each sample.

Experimental Design & Success Criteria

Trials 1-8

The experiments described below were grouped into several different rounds which coincided with seasonal sampling for our broader biogeochemical studies. Within a round, different trials consisting of combinations of our primary variables (time, temperature, oxidant amount) were conducted. For an oxidation trial to be considered an improvement relative to the others in the same round, the concentration of Hg determined in porewater at each depth within a porewater profile needed to be at least as large as the concurrent trials and the sample needed to be clear (not cloudy or colored) upon addition of hydroxylamine hydrochloride following BrCl digestion. Three rounds of trials were conducted to evaluate the effects of BrCl concentration, digestion time, or heat treatment. Round 1, conducted using porewaters collected in December included Trials 1-3, was designed to reveal the minimum concentration of BrCl that supported complete oxidation of porewater for both locations within the lagoon, Beach Zone (BZ) and East Fork (EF). Trial 1 samples were allowed to incubate for a minimum of 12 hours. The dissolved HgT analysis was performed over 3 days which meant that samples later in the analytical queue digested for >12 hours. It was observed that longer incubation times had an effect on the amount of Hg recovered from the samples, thus, the second round of trials (Trials 4 and 5, April porewater) focused on increasing the digestion time to 4 days while comparing two different BrCl concentrations. For December and April trials, samples with digestion periods > 12 hours were double bagged in zip-sealed bags and incubated in a closed plastic chamber to minimize uptake of Hg^0 from laboratory air. The third round of trials (Trials 6, 7 and 8) focused on samples only from EF collected in October with the goal of achieving complete oxidation with a maximum BrCl concentration of

2% (v/v). Samples were treated with 2% (v/v) BrCl and subjected to 14- or 24-day ambient temperature digestions (Trials 6 and 8) in comparison with a 6-hour digestion in a 50 °C water bath (Trial 7) as indicated by EPA Method 1631 for difficult-to-oxidize samples. Not all depths had a representative sample for each of the three trials (i.e., insufficient volume from 2 cm depth for multiple trials), thus depths with missing observations were not available (NA) and could not be included in paired statistical tests. This resulted in a final sample size of n=4 for EF October samples when comparisons were made between the three trial conditions. October samples and associated reagent blanks were prepared in crimp-sealed glass vessels to reduce gas permeability (rather than Teflon bottles as were used previously) in preparation for longer oxidation periods on the order of weeks.

Trials 9-16

Crimp-sealed glass vessels were also used for all replicate trials. EF samples were from 2 and 10 cm depth and BZ samples were from 2 and 20 cm depth. Porewater from 20 cm depth at EF could not be collected due to complete clogging of the piezometer. Trials 9-12 treated EF and BZ porewaters with 2% (v/v) BrCl, and four replicates of each of four treatment conditions (EPA Method 1631, 6-hour digestion in a 50 °C water bath, 14-day or 24-day ambient temperature digestions) were created and analyzed. In trials 13-16, samples were treated with 5% (v/v) BrCl and underwent the same four treatments as for trials 9-12. Trials 13-16 were conducted on EF porewater (n = 4) from each of two depths. A summary of each of the treatment conditions for Trials 1-16 and the identity of the samples subjected to each treatment is shown in Table 2. It was observed that porewaters transitioned from having visible white, flocculated clumps (presumed to be polysulfide) suspended in the porewater to transparent yellow solution after digestion for 24 days. The change in texture and color was used as a qualitative indicator that sulfide had oxidized to sulfate (Hubert and Vourdow, 2007).

Statistical Analysis

Trials 1-8

As the data was not normally distributed and sample sizes were small (n < 30), non-parametric tests were selected to compare trials 1-8. Statistical testing at the 95% confidence level was conducted according to two different workflows depending on if 3 trials were being compared (Workflow 1) or 2 trials were being compared (Workflow 2). Workflow 1 first applied a Friedman test, a rank-sum test for comparing the effect of different treatments on grouped (blocked) data (Conover 1999). A Friedman test was appropriate here because the samples were paired by depth (blocks), meaning water from a given depth was subjected to each of the three treatments (trials) with a single observation (Hg measurement) for each. The test was used to assess whether there were differences between trials, not depths. When significant differences were found between trials, a post-hoc multiple-comparison Nemenyi test, from the R package PMCMRplus (Pohlert and Pohlert 2018), was used to single-out which pair of trials was different (Hollander et al. 2013).

Workflow 2 utilized a Wilcoxon paired-sample signed-rank test, the non-parametric equivalent to the Student's t-test for matched pairs (Conover 1999). The null hypothesis of the Wilcoxon signed-rank test states that the median of the differences between trials is equal to zero while the alternative hypothesis asserts that it is not (King and Eckersley, 2019). Since paired observations are used here, calculated values were included even if they were below the daily LOD. There is a lack of agreement in the literature whether to substitute 0, ½*LOD, or the LOD itself for performing statistical tests when observations are below the LOD, as each would be associated with a particular type of bias. Thus, all three scenarios were tested with the case using values "as calculated," including any negative values. This was applicable to Trials 4 and 5 in April, as well as to October Trials 6 and 8 after inconclusive results of LOD scenarios with Friedman testing. When Workflow 2 was used to compare Trial 6 vs. Trial 8, overlying water was included as the test requires a minimum of

n=5. The test was set up to consider if the median result of all Trial 6 - Trial 8 pairs = 0, where rejection of the null hypothesis suggests differences between trials. The final step of Workflow 2 was to calculate an estimate of effect size to assess the impact of LOD-substitution choice on the magnitude of the difference in medians between trials. The effect size estimate is defined as a correlation coefficient that assumes values from -1 to +1, and when squared and multiplied by 100, represents the percentage of variance in the dependent variable that can be explained by the independent variable. The estimate of effect size is an equivalent metric to Pearson's correlation coefficient (*r*) in a non-parametric setting (Tomczak and Tomczak 2014) and can be directly compared. The formula for calculating the estimate of effect size is: where Z is the Z-score from the Wilcoxon signed-rank test and n is the total number of pairs of observations (Fritz et al. 2012). The effect size estimate was calculated here using the R package rstatix (Kassambara 2021). In criteria outlined by Cohen and used by others, $r >= 0.5$ is considered a large effect (Coolican 2017).

Trials 9-16

For trials 9-16, each treatment had four samples from a given water depth. Therefore, non-NA sample values were averaged by treatment group and means were compared, rather than being compared as individual paired values as was done in trials 1-8, where a single measurement per treatment was available from a given depth. Dixon's Q-test was used to assess potential outliers and extreme values removed were replaced with NA. Values that were below each daily LOD were replaced with 0 pM for calculating means and performing statistical tests. HgT values were plotted by site and depth to determine normality. When conditions for normal distribution were met (visual inspection, Shapiro-Wilk test p-value > 0.05), one-way ANOVA was used to compare sample means by treatment group (Workflow 3). Tukey's Honest Significant Differences (Tukey's HSD) was used as a post-hoc test for multiple comparisons following ANOVA. For BZ 2 cm and 10 cm depth samples, both sets of values were ln-transformed prior to statistical testing with ANOVA so

that conditions of normality were met. EF samples treated with 2% (v/v) BrCl from 2 cm depth were also ln-transformed prior to ANOVA. Means of EF samples treated with 2% BrCl from 10 cm depth were compared with Workflow 4, using a Kruskal-Wallis test, the non-parametric equivalent to a one-way ANOVA, as ln-transformation did not result in normally distributed data. Dunn's test was used as a post-hoc test for multiple comparisons, with p-value adjustment by the Bonferroni method. All statistical testing was conducted at the 95% confidence level.

Porewater BrCl Digestion

Trials 1-8

Following filtering and acidification, aliquots of each sample were prepared for BrCl digestion in acid-cleaned Teflon bottles. We found that while a 20 mL sample was sufficient for dissolved HgT analysis at East Fork, a 40 mL sample was required from Beach Zone to provide enough Hg to be above the limit of detection. Less BrCl (0.25% (v/v); BZ Trial 1) was used initially for BZ samples as the HgT concentration was anticipated to be lower than at EF and there was concern an increased reagent blank could interfere with detection of the sample. Therefore, the focus was to minimize the amount of BrCl added while fully oxidizing organic ligands. Three associated method blanks were prepared for each trial with the corresponding amount of BrCl used for a given trial added to 20 or 40 mL of MilliQ water in either threaded-cap Teflon or crimp-sealed glass bottles. Blanks were incubated under the same time and temperature conditions as the samples to control for the diffusion of Hg into or out of the sample during storage.

The conditions tested within our study included 0.25-5 % (v/v) BrCl, as EPA Method 1631 recommends 0.5% (v/v) BrCl for clear samples and 1.0% (v/v) BrCl for colored or turbid samples. EPA Method 1631 suggests using as high as 5% (v/v) BrCl for highly organic matrices, or as low as 0.2% (v/v) BrCl when trying to lower the LOD. While 1.0% (v/v) ultimately worked well for BZ samples when a minimum of 4-day digestion period was used,

BrCl was increased to 2% (v/v) and 5% (v/v) for colored samples at EF in an attempt to achieve complete oxidation. However, 0.5% (v/v) or less was an insufficient amount of BrCl for BZ samples and less than 2% (v/v) BrCl was insufficient for EF samples, as indicated by the retention of color or cloudiness following the digestion period. While the range of BrCl concentrations tested was within the range suggested by EPA Method 1631, the oxidation times were increased from the suggested 12 hour minimum to 2- and 4-day periods, followed by 14- and 24-day periods.

Trials 9-16

Glass serum jars were acid-washed, rinsed, and pretreated with 1% (v/v) BrCl for 24 hours, which was then neutralized with 30% (w/v) NH_2OH. Jars were then rinsed, returned to 10% 12M HCl overnight, and finally rinsed 5x with 18 MΩ-cm water. Filtered and acidified porewater, collected as described for trials 1-8, was stored in Teflon bottles was kept double-bagged and refrigerated until it was portioned into clean glass serum jars by weight with a Mettler Toledo PB3002-S/FACT balance. BrCl (0.5% w/v solution) was added to reach 2% or 5% (v/v), then jars were capped with septa and crimp sealed before being placed in the dark to incubate. Three method blanks (MB) were created for each treatment type, using 20 or 40 ml of MilliQ water. BrCl 0.5% (w/v) solution and 30% (w/v) NH_2OH solution were added at the same (v/v) percentage as the corresponding treatment, and MB's were incubated along with samples. The cleaning procedure for septa for trials 9-12 was 3 days in 1% (v/v) Solujet and 3 days in 10% (v/v) 12M HCl, with each step followed by a 5x 18 MΩ-cm water rinse, on previously used septa. This protocol yielded septa with a non-zero and variable blank.

The heated water bath was especially susceptible to contamination compared to the other treatment types, as this was the only condition where the formation of steam caused the sample to contact the septa, thus contaminating the porewater in the serum jar after condensing. For room temperature treatments, no steam was generated and serum jars were stored upright for incubation, preventing contact of the porewater with the septa. For

trials 13-16, the cleaning procedure was modified to 3 days in 1% (v/v) Solujet, 3 days in 10% (v/v) 12M HCl, 24 hours in 5% (v/v) BrCl, followed by neutralization with NH_2OH, with 5x 18 MΩ-cm water rinsing after each step, as enough new septa could not be obtained. Septa cleaning and reuse was done out of necessity, however, the BrCl treatment led to visible degradation of the septa material, which may have compromised the gas-impermeability of the serum jars.

Hg Determination

Following BrCl-oxidation, 50 µL (Trials 1-8) or 200 µL (Trials 9-16) of 30% (w/v) NH_2OH was added to remove free halogens that could damage the pre-concentration columns. The samples were mixed and allowed to react for at least 20 minutes. Then, a sample (or subsample) was poured into a "UConn" bubbler that allows for continuous headspace purging and 100 µL of 3% (w/v) $SnCl_2$ solution was added to reduce all Hg species to Hg^0. The bubbler was then switched to purge mode and the liquid was degassed with UHP N_2 at 250 mL/min. for 5 minutes to concentrate the evolved Hg^0 onto the first gold trap of a Tekran 2600 Mercury Analyzer. This first gold trap was then heated to desorb the Hg^0 in a stream of UHP Ar onto a second gold trap which in turn was heated and the Hg determined by Cold-Vapor Atomic Fluorescence Spectrophotometry (CVAFS).

The instrument was calibrated with Hg^0 vapor standard and with Hg(II) aqueous standard each day of analysis. If the vapor curve and aqueous curve slopes were different by more than 10%, the aqueous standard was remade and, in accordance with Method 1631, another series of 5 non-zero standards were run to create the calibration curve. At least three $SnCl_2$ blanks were run each day of analysis, and the average peak area associated with 100 µl of the 3% (w/v) $SnCl_2$ solution was subtracted from the average (n=3) peak area of the reagent blank, to yield the peak area associated with only the amount of BrCl added plus 50 µl of 30% (w/v) NH_2OH. This peak area will be referred to as "adjusted reagent blank ". The average peak area associated with the 100 µl of $SnCl_2$ solution was used as the zero point of

the calibration curve and this area was not subtracted from the peak area of each of the standards. MilliQ water alone used in creating reagent blanks was determined to have an HgT concentration not quantifiable above the signal from BrCl and NH_2OH + BrCl. Raw sample peak areas were corrected by subtracting the adjusted reagent blank peak area before using the calibration curve to solve for pmoles of HgT. The daily LOD was calculated by solving for the pmoles of HgT in each reagent blank (using uncorrected peak area), taking the mean of the daily reagent blanks in pmoles, multiplying the standard deviation by 3, and dividing by 20 or 40 mL, as appropriate for the location.

Modifications for Trials 9-16

For trials 9-16, the entire porewater sample volume of 20 or 40 mL could not be analyzed at once due to foaming in the bubbler, thus aliquots analyzed were smaller than the total volume digested. Therefore, a "prorated" MB value was calculated for the three method blanks by dividing the peak area from each MB by the volume analyzed. The mean of the three MB's was calculated and this value (peak area/mL) was multiplied by each sample volume analyzed for that treatment to determine "prorated method blank peak area" per sample. The average (n=3) daily Sn blank (from 100 uL of 3% (w/v) $SnCl_2$) was subtracted from the prorated method blank peak area per sample to yield "corrected prorated method blank peak area". This value was used to solve for pmoles of methylmercury using the daily calibration curve. The pmole value was then divided by the corrected sample volume to determine HgT in pM. Corrected sample volume, to account for HgT coming from a volume of porewater, but disincluding the increased volume coming from reagents) was calculated using the following equation:

Corrected porewater sample volume = (sample volume analyzed/total sample volume with BrCl and NH_2OH)(sample volume total - volume coming from BrCl and NH_2OH)*

LOD's were calculated as described above,and are reported as both absolute detection limits in pmoles and as concentration LOD's in pM, by dividing the absolute LOD by the average sample volume analyzed. The daily LODs are presented in Table 2.

Table 2. Oxidation Trial Conditions, Sample Identity & Limit of Detection (LOD) Concentration

Trial #	Location	Date Collected	BrCl (µL)	Sample Volume (mL)	BrCl % (v/v)	Oxidation Temp	Oxidation Time	Concentration LOD [pM]
1	EF	Dec. 2019	100	40	0.25	RT	variable (12 hours to 3 days)	0.34
2	EF	Dec. 2019	200	20	1	RT	2 days	2.6
3	EF	Dec. 2019	400	20	2	RT	4 days	4.6
4	EF	Apr. 2020	400	20	2	RT	4 days	4.3
5	EF	Apr. 2020	1000	20	5	RT	4 days	6.4
6	EF	Oct. 2020	400	20	2	RT	14 days	0.88
7	EF	Oct. 2020	400	20	2	Water bath at 50 degrees C	6 hours	3.7
8	EF	Oct. 2020	400	20	2	RT	21-24 days	3.8
0 (data not shown)	BZ	Dec. 2019	50	50	0.1	RT	variable (12 hours to 3 days)	3.1
1	BZ	Dec. 2019	100	40	0.25	RT	variable (12 hours to 3 days)	6
2	BZ	Dec. 2019	200	40	0.5	RT	overnight	3.3
3	BZ	Dec. 2019	400	20	2	RT	4 days	1.4
4	BZ	Apr. 2020	400	20	2	RT	4 days	3.4
5	BZ	Apr. 2020	400	40	1	RT	4 days	2.8
9	BZ	Sept. 2023	800	40	2	RT	12-24 hours	0.29
9	EF	Sept. 2023	800	17	2	RT	12-24 hours	0.68
10	BZ	Sept. 2023	800	40	2	Water bath at 50 degrees C	6 hours	0.66
10	EF	Sept. 2023	800	40	2	Water bath at 50 degrees C	6 hours	1.5
11	BZ	Sept. 2023	800	40	2	RT	14 days	0.08
11	EF	Sept. 2023	800	40	2	RT	14 days	0.19
12	BZ	Sept. 2023	800	17	2	RT	24 days	1.4
12	EF	Sept. 2023	800	10	2	RT	24 days	2.4
13	EF	Sept. 2023	1000	8	5	RT	12-24 hours	1.2
14	EF	Sept. 2023	1000	8	5	Water bath at 50 degrees C	6 hours	2.4
15	EF	Sept. 2023	1000	9	5	RT	14 days	0.77
16	EF	Sept. 2023	1000	8	5	RT	24 days	0.67

2.3 Results

Trials 1-3. December 2019 Porewater

The results of Hg determinations on overlying water and porewater (through 20 cm depth) for the first three trials are shown in Figure 2 as a function of depth. Regardless of treatment, the results show that overlying water at both locations had similar HgT concentrations and that East Fork porewaters were higher in concentration on average than porewaters at Beach Zone. Furthermore, East Fork porewaters tended to increase in concentration with depth while Beach Zone was relatively constant or even decreased with depth. The results from Trials 1-3, shown as box and whisker plots including median values for all December trials at EF and BZ (n=11 for both) are shown in Figure 3.

East Fork

When EF December Trials 1-3 were compared with Workflow 1, at least one of the trials exerted an effect on the Hg measured (Friedman test, $p = 0.02$), with Trial 3 found to be different than Trial 1 (Nemenyi test, $p = 0.015$). It was concluded that a higher median for Trial 3 vs. Trial 1 (38.5 vs. 28.8 pM, respectively) demonstrated the relative success of the trial (Figure 3). Therefore, 2% (v/v) BrCl with a 4-day digestion was selected for future trials at EF. Trial 3 conditions allowed for more HgT to be detected in nine out of eleven samples when compared to Trial 1. Trial 2 had intermediate performance with a median value of 34.9 pM, and this may have been due to insufficient BrCl, digestion time, or a combination. Some Trial 2 samples had a colored or hazy appearance after NH_2OH addition, suggesting that DOC was not completely oxidized.

Beach Zone

Workflow 1 was also used to compare HgT porewater observations from December Trials 1-3 at Beach Zone. The trials compared were not equal (Friedman test, $p = 0.02$), while post-hoc testing revealed that the effect occurred between Trials 2 and 3 (Nemenyi test, $p = 0.02$). Trial 3 conditions of 2% (v/v) BrCl and 4-day digestion time were selected for use with future BZ samples as the median HgT value measured under Trial 3 conditions was greater than that of Trial 2 (22.4 vs. 12.6 pM), respectively). More HgT was measured in ten out of eleven samples under Trial 3 conditions compared to Trial 2. Trial 1 had a median of 13.9 pM, which was similar to that of Trial 2, further supporting the conclusion that Trial 3 conditions were most effective amongst those compared.

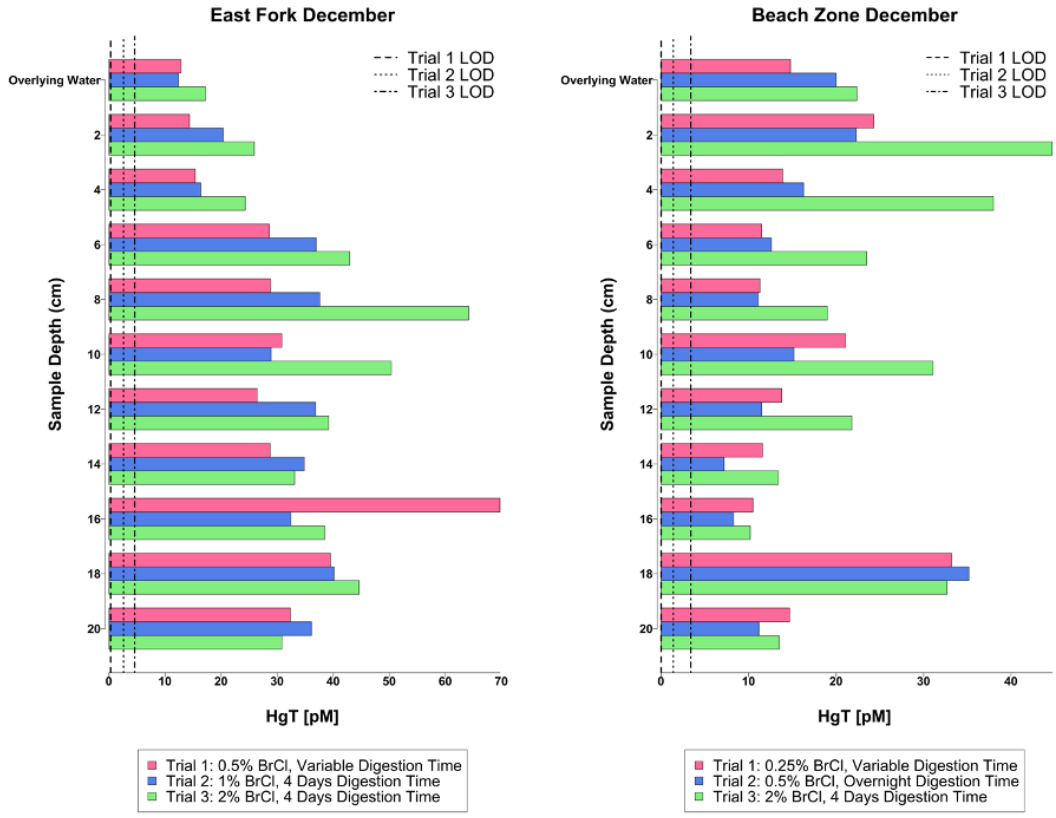

Figure 2. East Fork December samples (left) and Beach Zone December samples (right) oxidized under the conditions of Trials 1, 2 and 3, and presented by depth. East Fork LOD's were 0.34, 2.6, and 4.6 pM for Trials 1, 2, and 3, respectively. Beach Zone LOD's were 3.3 (Trial 1), 1.4 (Trial 2), and 3.4 pM (Trial 3).

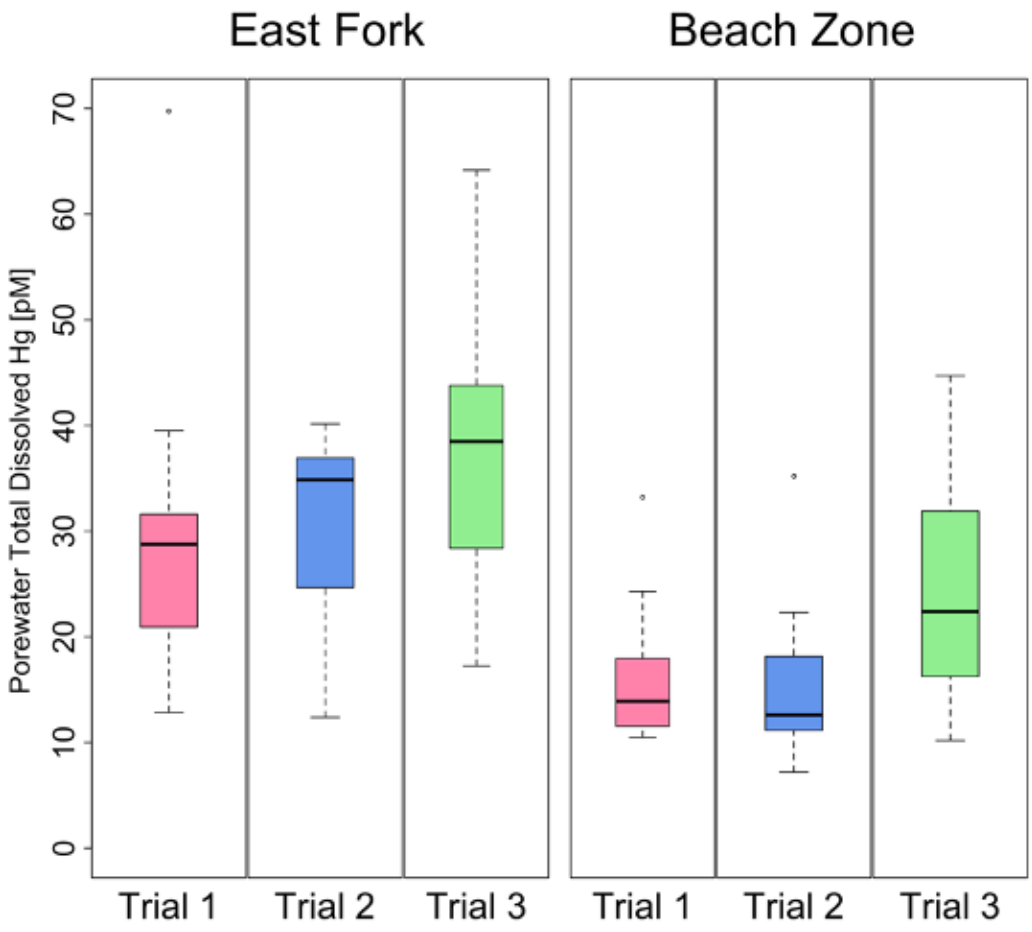

Figure 3. Boxplots of East Fork December samples (left) and Beach Zone December samples (right) oxidized under the conditions of Trials 1, 2 and 3. The center line within the box depicts the median observation from each trial, with the bar of each whisker showing the 1st and 3rd interquartile ranges, and outliers plotted as circles beyond the whiskers. The highest median concentrations of HgT were observed under Trial 3 conditions at both locations.

Trials 4 & 5. April 2020 Porewater

During the April sampling for Trials 4 and 5, surface water concentrations were substantially lower than they were in December, but still essentially the same as each other (Figure 4). Porewater concentrations at EF were similar to those found in December but were generally lower in April than in December at BZ. The vertical profiles were highly treatment

dependent which illustrates the seasonal variability in the difficulty of getting successful HgT digestions at this location.

Workflow 2 was applied to compare Trials 4 and 5, resulting in significant differences between trials at both EF and BZ. The Friedman test p-values were 0.004 and 0.007 for EF and BZ, respectively, for the case using values as calculated. All three LOD substitution scenarios also resulted in significant p-values, indicating the statistical significance of results was not dependent on how data that were below detection were handled. Thus, we are able to conclude that the median HgT measured under Trial 4 conditions was significantly different than that of Trial 5 for both locations (median values shown in Figure 5). The value of *r* was 0.85 at EF (confidence interval 0.73-0.89) and 0.78 (confidence interval 0.48-0.89) at BZ, for the cases using values "as calculated", both values are considered to be large. For EF and BZ April LOD substitution scenarios, all effect sizes were large regardless of the value substituted, with the range of effect sizes being (0.85-0.86) and (0.70-0.78) at EF and BZ, respectively.

While Trial 5 (5% (v/v) BrCl) at EF yielded higher HgT concentrations than did Trial 4 (2% (v/v) BrCl), we were interested in whether changing the length of the incubation could improve a trial's performance when using 2% (v/v) BrCl, as there was interest in keeping the reagent blank low. Therefore, future trials with EF October porewater focused on 2% (v/v) BrCl with varied digestion time and temperature. Overall, more HgT was measured in BZ samples under Trial 5's 1% (v/v) BrCl conditions, with a median value of 8.7 pM vs. a median of 2.0 pM for Trial 4, and so future trials at BZ used 1% (v/v) BrCl and >4-day digestion periods.

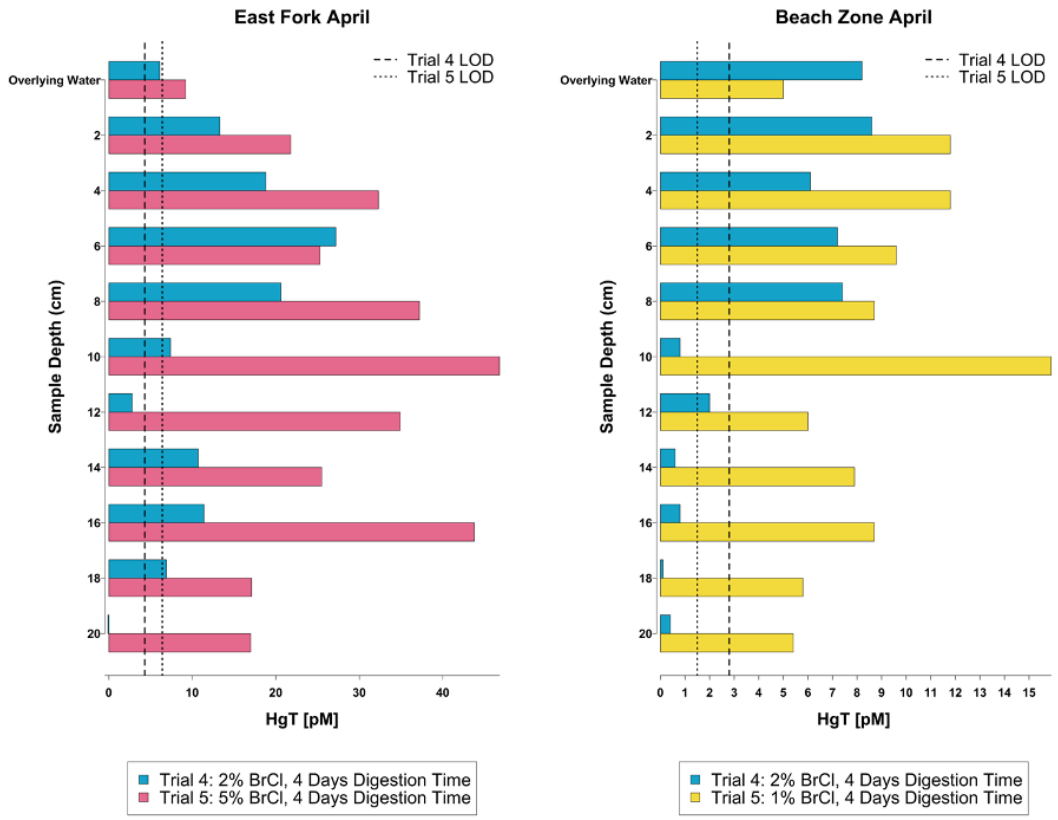

Figure 4. Barplots of April HgT concentrations for all depths (n=11 for both) at East Fork (left) and Beach Zone (right). Values depicted are calculated values, including any BLOD. The LOD for each trial is given by a dashed line for Trial 4 and a dotted line for Trial 5. Trial 4 resulted in two BLOD samples (12 and 20 cm) at EF and six BLOD samples at BZ (10 cm-20 cm). All samples subjected to Trial 5 conditions at either site were quantifiable. East Fork LOD's were 4.3 and 6.4 [pM] for Trials 4 and 5, respectively. Beach Zone LOD's were 2.8 pM (Trial 4) and 1.5 pM (Trial 5).

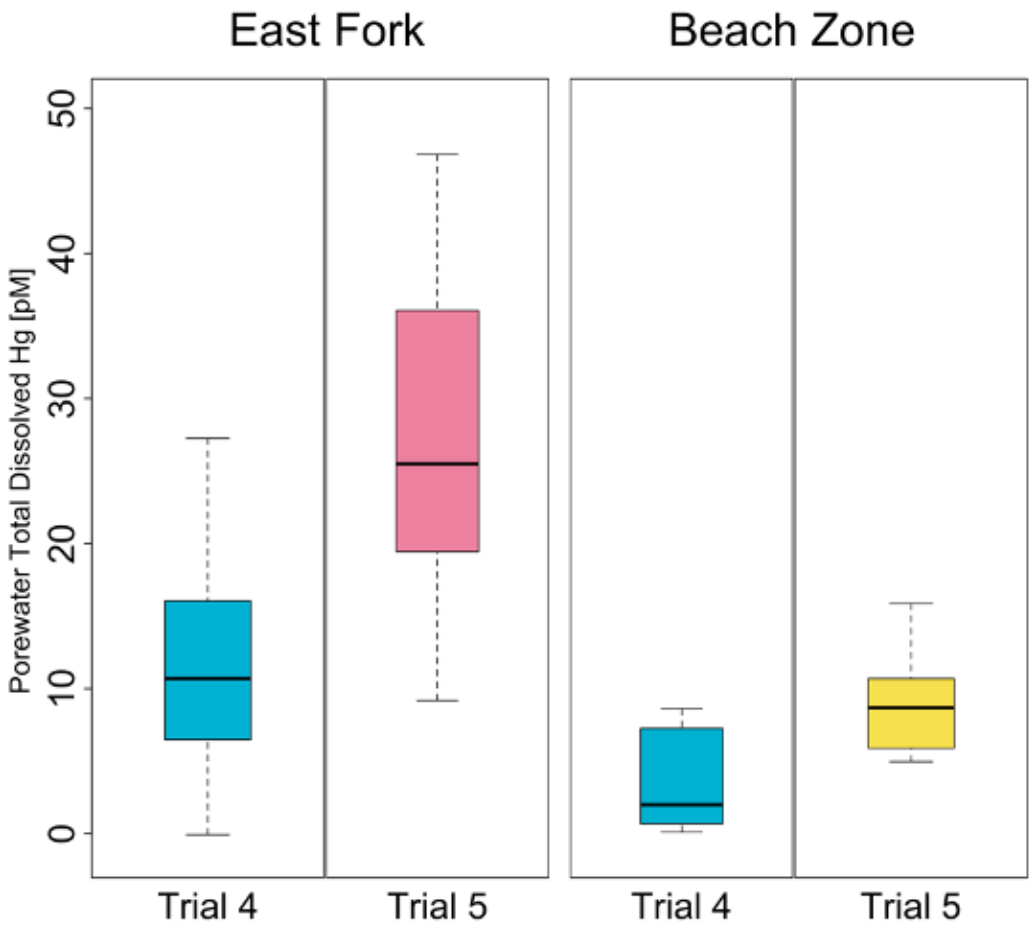

Figure 5. Boxplots showing the median HgT concentration for April porewater samples subjected to Trial 4 vs. Trial 5 conditions at East Fork (left) and Beach Zone (right). The median concentration of Hg at both East Fork and Beach Zone was higher under Trial 5 conditions, and no samples were BLOD. The higher median, along with the results of Wilcoxon signed-rank testing, demonstrate that 1% (v/v) BrCl with a 4-day digestion was a more effective oxidation treatment for BZ samples than was 2% (v/v) BrCl with a 4-day digestion.

Trials 6-8. East Fork October 2020 Porewater

Overlying water HgT concentrations at EF in October were similar to April, and lower than either location in December. There was no apparent trend with depth, as all samples between 6 and 18 cm were < 20 pM (Figure 6). Samples at 4 and 20 cm had notably higher HgT concentrations when compared against any other depth or season. The three trials for

October used 2% (v/v) BrCl so that oxidation times could be compared. Workflow 1 was applied to October "as calculated" values as well as the three LOD substitution scenarios. However, unlike the April trials, each method of substitution did not lead to the same conclusion as to whether the trials had a significant effect. Table 3 shows a summary of the p-values and conclusions associated with each LOD substitution scenario.

Table 3. LOD substitution scenario results for East Fork October Friedman test comparisons

LOD Substitution Value	p-value from Friedman Test	p-value from post-hoc Nemenyi test	Conclusion
N/A (used calculated values)	0.04	0.04	Trial 8 is different than Trial 7
0	0.04	0.06	Trials not significantly different, despite significant p-value from Friedman's test
1/2*LOD	0.02	0.01	Trial 8 is different than Trial 6
LOD	0.02	0.01	Trial 8 is different than Trial 6

For "as calculated" values, at least one of the treatments had an effect on Hg measured (Friedman test, p-value 0.04), while post-hoc testing revealed that the effect occurred between Trials 7 and 8 (Nemenyi test, p-value = 0.04). As Trial 7 had a median concentration that was BLOD and Trial 8 had a median of 16 pM, Trial 8 conditions were identified as the most appropriate for supporting oxidation of DOM in EF samples. Median values (including any negative signs) are shown as boxplots in Figure 7 (n = 4 for each trial). In the LOD scenarios where ½*LOD or full LOD were substituted in place of BLOD values, the effect was found between Trials 6 and 8 (Nemenyi test, p-value = 0.01). During post-hoc testing, no significant difference was found between trials when 0 was substituted for the LOD (Nemenyi test, p-value = 0.06), despite the significant p-value of 0.04 from the

Friedman's test. As the results of the statistical testing were not in agreement depending on the type of LOD substitution made, observations from Trial 6 and Trial 8 were compared using Workflow 2. The results shown in Table 4 demonstrate that while there is disagreement in significance if only the p-value is considered, likely due to the small sample size, the effect size of each type of substitution yields a more consistent conclusion. Regardless of the approach to handling BLOD data, the effect size was large for all LOD scenarios, providing further support that Trial 8 resulted in significantly higher HgT concentrations than Trial 6.

Table 4. LOD substitution scenario results for Trial 6 vs. Trial 8 Wilcoxon testing

Type of LOD Substitution	p-value	Effect size (*r*)	Confidence Interval of *r*
N/A (as calculated values used)	0.03	0.91	0.90 – 0.95
0	0.06	0.78	0.18 – 0.93
½*LOD	0.06	0.78	0.18 – 0.93
LOD	0.03	0.91	0.90 – 0.95

Furthermore, a qualitative conclusion as to the most effective October trial was made by examining the median HgT concentration of each trial and considering the total number of samples in the trial that were BLOD. By this determination, Trial 8 conditions were the most effective, as Trial 8 contained only one BLOD sample (overlying water) and Trial 8 had the higher median value of those compared. As less HgT than contained in the reagent blank was detected in 3 out of 4 samples under Trial 7 conditions resulting in a median value that was BLOD, a heated water bath was found to be the least practical oxidation method, as 75% of the total samples compared were BLOD for this trial. This result suggests that either DOM did not completely oxidize under Trial 7 conditions, or that Hg was lost from the vessel during the heated incubation procedure. It is less likely that it was the latter as reagent blanks were subjected to the same conditions as samples, and if Hg was able to diffuse out of crimp-sealed glass vials under heating conditions, this would have happened to the blanks as well

as the samples. As 2% (v/v) BrCl was used across October trials, digestion time was identified as the variable responsible for an effect, with 24-day digestions providing higher HgT measurements for most samples, as well as a greater median value when compared to either Trial 6 or 7. Figure 6 provides HgT concentrations for all samples subjected to Trial 6-8 conditions, from overlying water to 20 cm depth, at 2 cm increments. While only samples from depths 6-10 cm were included in the Workflow 1 statistical analyses due to the paired sample requirement, Figure 6 shows that under Trial 8 conditions, more HgT was measured in samples from depths 4-20 cm, compared to Trial 6 or Trial 7 conditions.

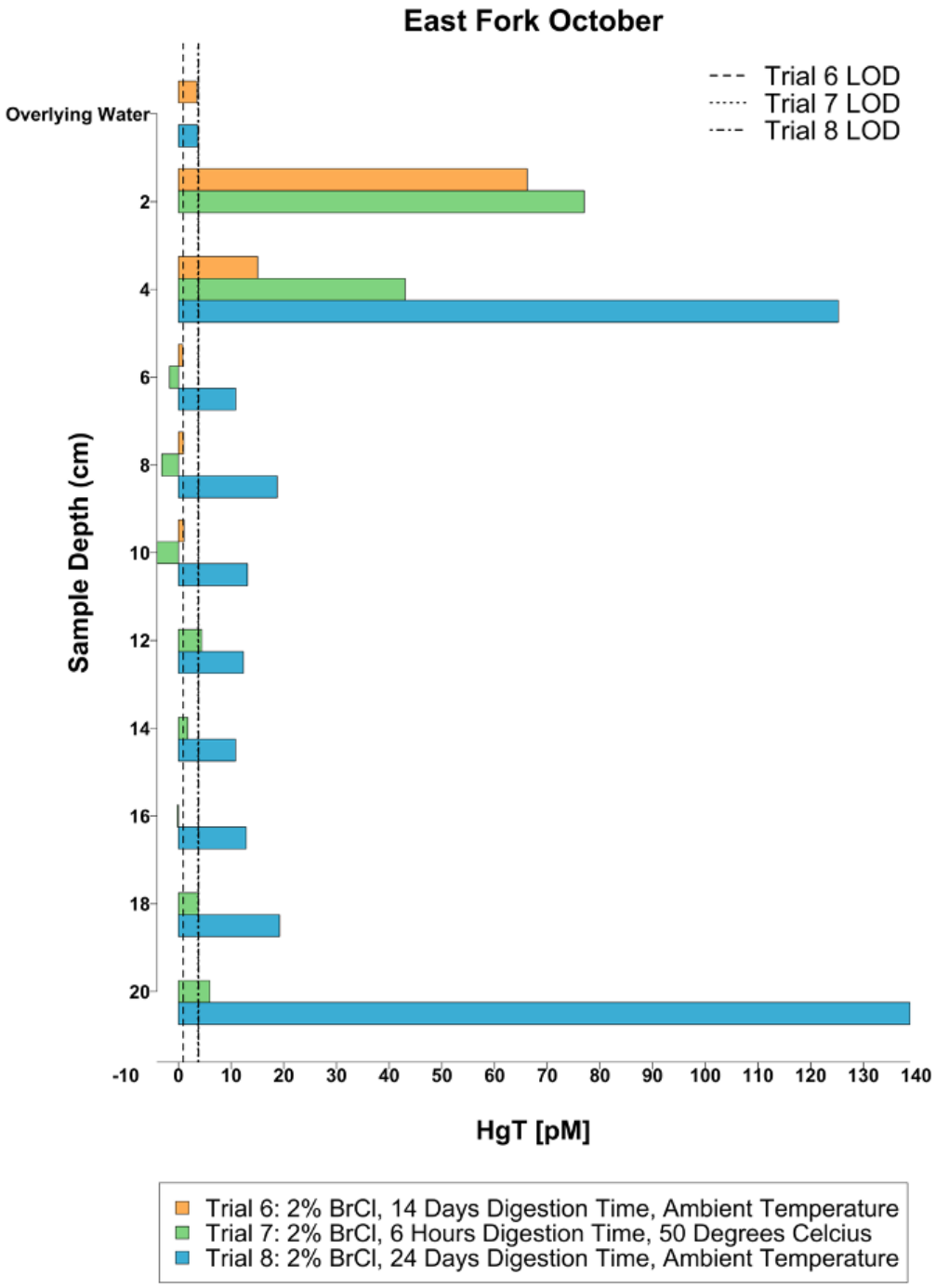

Figure 6. Barplot of HgT concentrations of East Fork samples from October using digestion conditions of Trials 6-8. Note that some values are negative (6-10 cm), under Trial 7 conditions, as less HgT was detected in these samples than the average reagent blank.

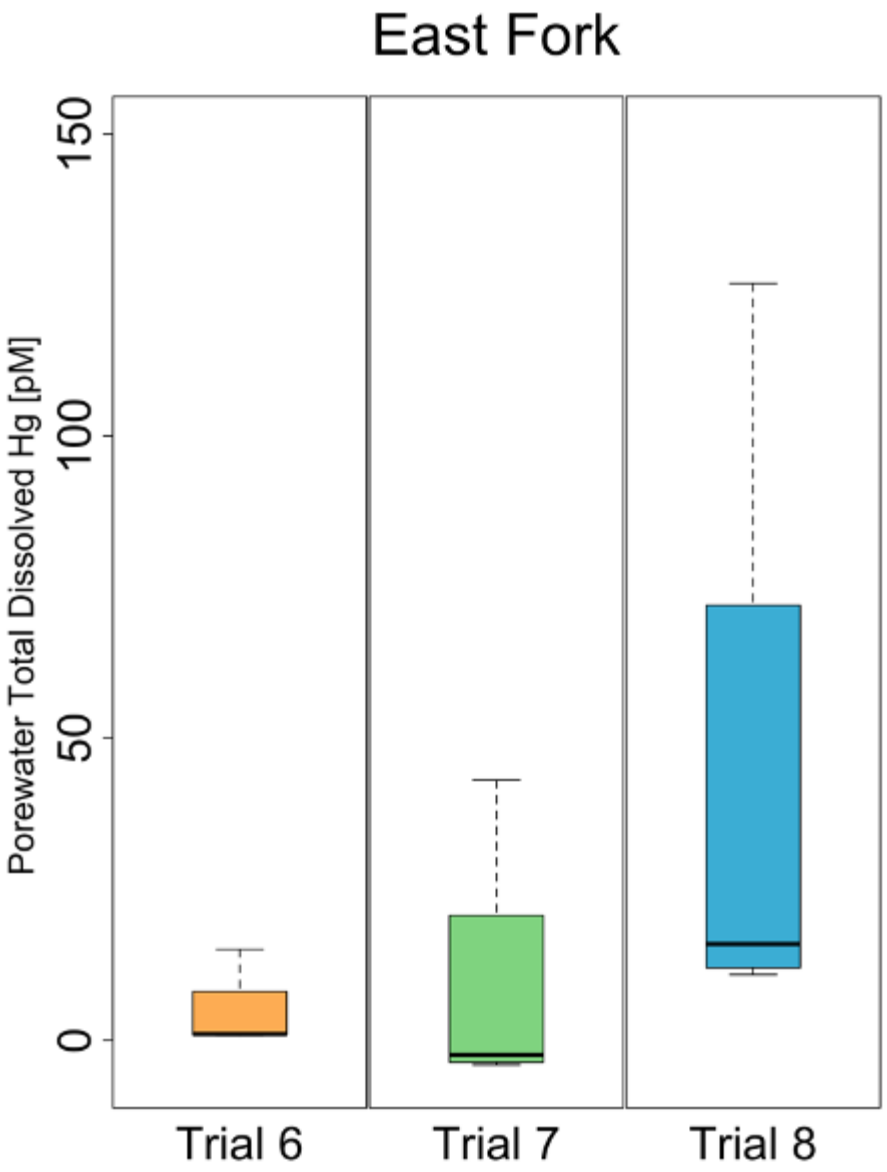

Figure 7. A comparison of trials 6, 7 and 8 for East Fork October samples, depicting the relative success of the extended 24-day oxidation of Trial 8. Values depicted are calculated values from depths 6-10 cm, including any BLOD, as were included in the statistical analyses (n = 4 for each trial).

Trials 9-12. September 2023 Porewater

Mean HgT concentrations at EF and BZ in September 2023 were quantified for two depths at each location, Beach Zone and East Fork (Table 5 and Table 6, respectively). The majority of samples at EF 10 cm were BLOD, indicating insufficient BrCl to oxidize the matrix and prevent the formation of foam in the bubbler. HgT concentrations were greater for 20 cm depth than at 2 cm depth at BZ (Figure 8), whereas the HgT concentrations were more similar between depths at EF (Figure 9) when treated with 2% (v/v) BrCl. The HgT concentration for BZ 2 cm samples was similar to that observed in April 2020 for samples treated with 2% (v/v) BrCl, and lower than December 2019. For BZ 20 cm samples, the September 2023 HgT concentration was greater than was observed previously for April or December.

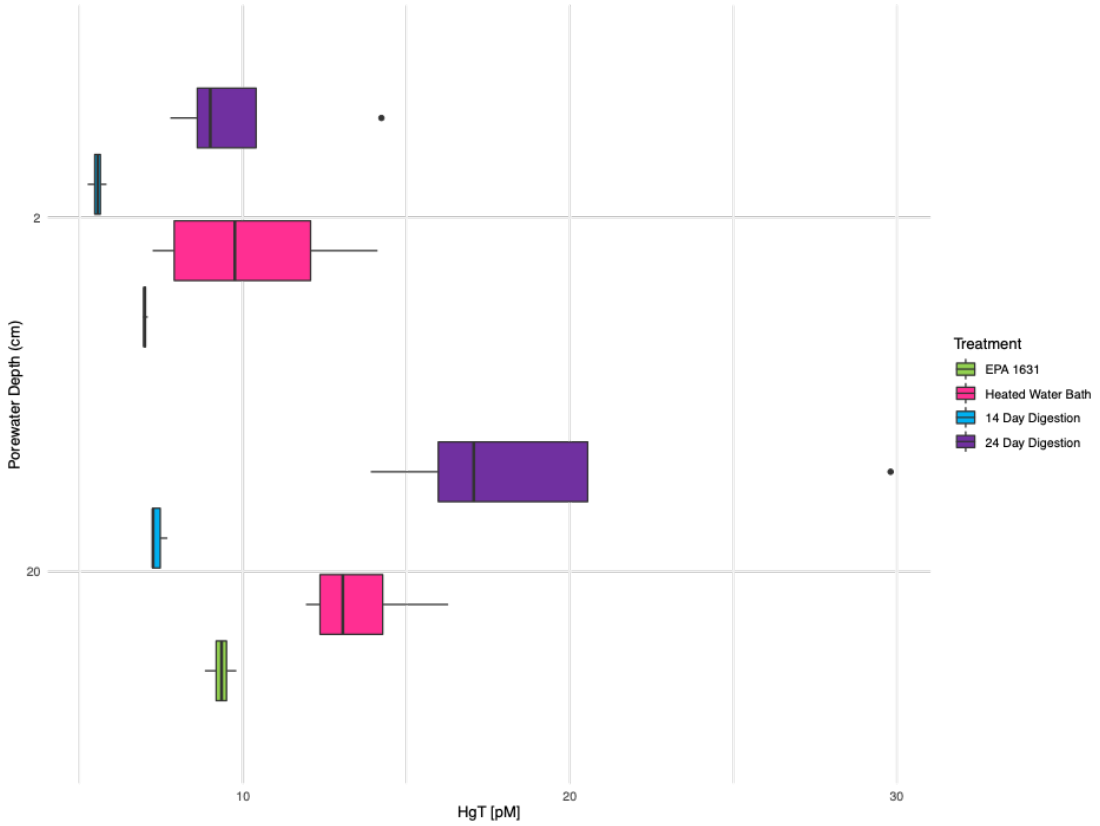

Figure 8. Boxplots by treatment group at Beach Zone (BZ) under 2% (v/v) BrCl with dark black line depicting the median HgT concentration (pM). Depth (cm) is plotted on the y-axis and samples are from 2 and 20 cm depth. For BZ 2 cm samples, a heated water bath was not significantly different from a 24-day digestion nor from EPA Method 1631. For BZ 20 cm samples, the 24-day digestion and heated water bath treatments performed similarly (Table 5) and were both significantly greater than the 14-day digestion, although only the 24-day digestion was significantly different from EPA Method 1631.

Beach Zone, 2% (v/v) BrCl

Workflow 3 was applied to ln-transformed BZ data for the 2 cm and 20 cm samples, and for both there were significant differences between means (one-way ANOVA, $p = 0.004$ and $p = 0.0002$, respectively). Post-hoc testing showed that the mean of the 14-day digestion (5.5 pM) was significantly lower than that of a heated water bath (10.2 pM) (Tukey's HSD, $p = 0.008$) and of a 24-day digestion (10.0 pM) ($p = 0.009$) for BZ 2 cm samples. For the same

samples, the heated water bath and the 24-day digestion performed similarly ($p = 1.0$). As the EPA Method 1631 was not statistically different than any other treatment for the BZ 2 cm matrix, either the EPA Method 1631 or a longer, 24-day oxidation could be used to achieve similar results. It is unclear why a 14-day digestion was not as effective as either the 24-day digestion or heat treatment.

For the BZ 20 cm matrix, heat treatment, with a mean of 13.6 +/- 1.9 pM, and a 24-day digestion, with a mean of 19.5 +/- 7.1 pM, were not statistically different (Tukey's HSD, $p = 0.3$). While the mean of the heated water bath and that of the 24-day digestion were both significantly greater than the 14-day digestion mean of 7.4 +/- 0.3 pM ($p = 0.007$ and $p = 0.0002$, respectively), only the 24-day digestion was significantly different from EPA Method 1631 ($p = 0.001$). This result illustrates how an extended digestion time of 24-days allows for more HgT to be detected than with EPA Method 1631.

Table 5. Mean & standard deviation of HgT concentrations at Beach Zone by digestion treatment with 2% (v/v) BrCl

Treatment	Depth (cm)	n	Mean HgT (pM)	Standard Deviation
EPA Method 1631	2	4	7.0	0.1
Heated Water Bath	2	4	10.2	3.2
14 Day Digestion	2	4	5.5	0.2
24 Day Digestion	2	4	10.0	2.9
EPA Method 1631	20	4	9.3	0.4
Heated Water Bath	20	4	13.6	1.9
14 Day Digestion	20	3	7.4	0.3
24 Day Digestion	20	4	19.5	7.1

East Fork, 2% (v/v) BrCl

Ln-transformed data from EF 2 cm porewater had a significant difference between means (one-way ANOVA, p = 0.03) when compared with Workflow 3. The mean of the 14-day digestion (14.4 pM) was significantly different than that of the heated water bath (64.7 pM) (Tukey's HSD), p = 0.02). The means of EPA Method 1631, a 14-day digestion, and a 24-day digestion were not significantly different from one another, and all three treatments failed to fully oxidize available Hg, as the average HgT of these three treatments (18.9 +/- 4.0 pM) is lower than the average value of 48.0 +/- 1.9 pM revealed for EF 2 cm samples under 5% (v/v) BrCl (14-day and 24-day digestions). The results suggest that 2% (v/v) BrCl was insufficient for complete oxidation of EF samples. The average HgT from the heated water bath (64.7 +/- 16.6) was higher than the average (48.0 +/- 1.9 pM) from EF 2 cm under 5% BrCl (14-day and 24-day digestions), suggesting that contamination of the septa caps may be responsible for the higher values observed during heat treatment.

For the EF 2% (v/v) BrCl samples at 10 cm depth, Workflow 4 indicated there was a significant difference between means (chi-squared = 11.6, p =0.009). The means of the 14-day digestion and of the 24-day digestion were both BLOD, and significantly different than that of the heated water bath (29.4 pM) when pairwise comparisons were made with Dunn's test (adjusted p = 0.009 for both comparisons). No other means were significantly different at

alpha = 0.05. For EF 10 cm depth samples, the results of EPA Method 1631, 14-day and 24-day digestions were complicated by values below the limit of detection (BLOD). Two samples from the 14-day digestion could not be analyzed due to the amount of foam generated in the bubbler, repeatedly wetting the soda lime trap and interfering with detection of Hg, thus 2 observations are missing from 10 cm depth. Incomplete oxidation of the matrix as a result of insufficient BrCl is likely responsible for this outcome. Under the heated water bath treatment with 2% (v/v) BrCl, the mean HgT was 29.4 +/- 0.7 pM, which is very similar to the mean of 29.8 +/- 2.7 pM from EF 10 cm with 5% (v/v) BrCl (EPA Method 1631, 14 Day and 24 Day Digestions). It appears that the heated water bath was effective in completely oxidizing Hg under the 2% (v/v) BrCl treatment for EF 10 cm samples, as a similar HgT value was achieved under heat and 2% (v/v) BrCl as with room temperature and 5% (v/v) BrCl. EPA Method 1631, 14-day and 24-day digestions were not effective as the majority of HgT values from these treatments were BLOD or could not be analyzed.

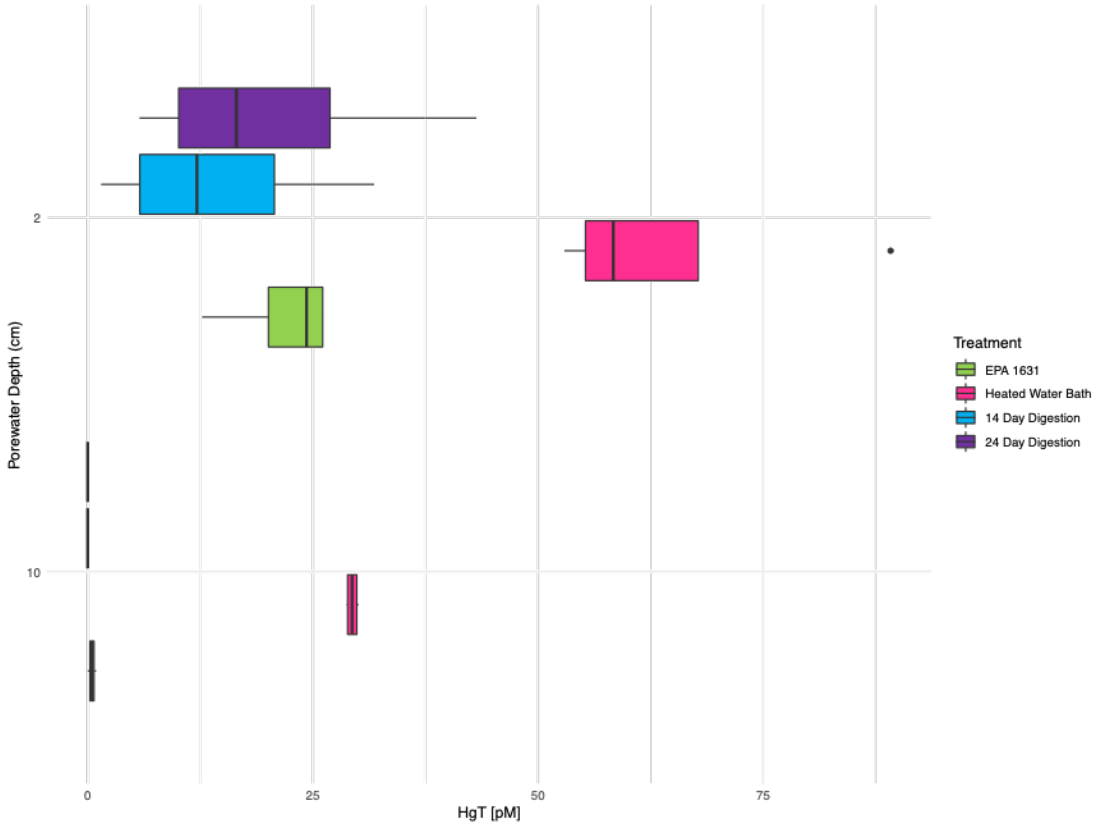

Figure 9. Boxplots of HgT concentrations by treatment group, with 2% (v/v) BrCl at East Fork with dark black lines depicting the median HgT (pM) for each group. Depth (cm) is plotted on the y-axis and porewater samples are from 2 and 10 cm depth. For 2 cm samples, EPA Method 1631 performed similarly to a 14-day digestion and a 24-day digestion, though these values were lower than when 5% (v/v) was used, indicating incomplete oxidation under 2% (v/v) BrCl. Higher HgT values for the heated water bath treatment were likely a result of contamination. For EF 10 cm samples, a heated water bath was found to be significantly different than the other three treatments, and the mean of the 2% (v/v) BrCl heat treatment (Table 6) was in agreement with the mean HgT concentrations for EF 10 cm samples treated with 5% (v/v) BrCl (Table 7).

Table 6. Mean & standard deviation of HgT concentrations at East Fork by digestion treatment with 2% (v/v) BrCl

Treatment	Depth (cm)	n	Mean HgT (pM)	Standard Deviation
EPA Method 1631	2	4	21.9	6.3
Heated Water Bath	2	4	64.7	16.6
14 Day Digestion	2	4	14.4	13.3
24 Day Digestion	2	4	20.5	16.5
EPA Method 1631	10	2	0.5	0.7
Heated Water Bath	10	4	29.4	0.7
14 Day Digestion	10	4	BLOD	NA
24 Day Digestion	10	4	BLOD	NA

Trials 13-16. September 2023 Porewater

EF porewater HgT concentrations were greater at 2 cm depth than at 10 cm depth, when samples were treated with 5% (v/v) BrCl (Figure 10). For EF 2 cm, the mean HgT concentration was greater than it was under 5% (v/v) BrCl in April 2020. EF 10 cm samples from September 2023 had a mean HgT concentration less than that observed in April 2020.

East Fork, 5% (v/v) BrCl

Workflow 3 was applied to EF 2 cm samples, and at least one significant difference between means was found (one-way ANOVA, $p < 0.001$). The means of the 14-day digestion (46.6 pM) and 24-day digestion (49.3 pM) were significantly greater than that of the heated water bath (34.3 pM) (Tukey's HSD, $p = 0.006$ and $p = 0.001$, respectively). The mean of EPA Method 1631 (32.1 pM) was also significantly different than that of the 14-day and 24-day digestions ($p = 0.001$ and $p = 0.0004$, respectively). There was no significant difference between the mean of EPA Method 1631 and that of a heated water bath ($p = 0.83$) nor was there a significant difference between a 14-day digestion and a 24-day Digestion ($p = 0.77$). The results of trials 12-16 suggest that once sufficient BrCl has been added to oxidize a given matrix, digestion times > 12-24 hours are beneficial in supporting complete oxidation.

For EF 5% (v/v) BrCl samples from 10 cm depth, there was a significant difference between means (ANOVA, $p = 0.00004$). Subsequent testing indicated that the mean of the heated water bath treatment (16.6 pM) was significantly different from that of EPA Method 1631 (32.8 pM), 14-day (27.5 pM), and 24-day digestions (29.2 pM) (Tukey's HSD, $p = 0.00003$, $p = 0.002$, and $p = 0.0002$, respectively). The 14-day and 24-day Digestions were not different from one another ($p = 0.85$) nor from EPA Method 1631 ($p = 0.12$ and $p = 0.31$, respectively). For this matrix, EPA Method 1631, 14-day, and 24-day digestions all resulted in similar means. The heated water bath treatment had the lowest mean pM value, which was significantly lower than the other three treatments, suggesting that Hg^0 may have been lost from the sample under the heated condition, despite the use of glass serum jars. Therefore, while a heated water bath appears to have merit under the EF 2% (v/v) BrCl condition (10 cm samples), it resulted in apparent loss of Hg^0 under the 5% (v/v) BrCl condition (10 cm samples). Additionally, a heated water bath was less effective than a 14-day or 24-day digestion under 5% (v/v) BrCl for EF 2 cm samples. Therefore, the use of a heated water bath for oxidation of porewaters is not recommended.

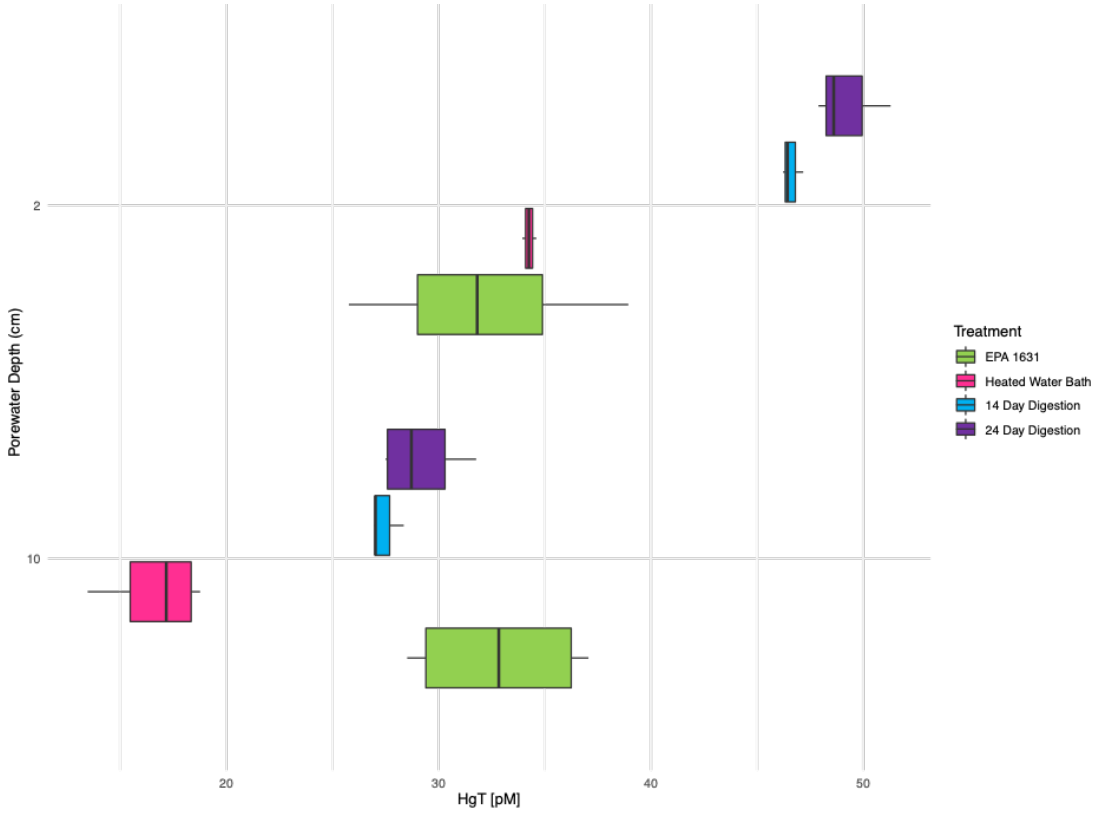

Figure 10. Boxplots by treatment group under 5% (v/v) BrCl at East Fork (EF) with dark black lines depicting the median HgT concentration (pM) for each group. Depth (cm) is plotted on the y-axis and samples are from 2 and 10 cm depth. At EF 2 cm, the 14-day and 24-day digestions performed similarly, and had significantly greater mean HgT concentrations than did EPA Method 1631 or a heated water bath (Table 7). More Hg detected after longer digestion times suggests incomplete oxidation under EPA Method 1631. Incomplete oxidation or loss of Hg^0 are potentially responsible for less Hg detected within the heated water bath. For EF 10 cm samples, the mean of the heated water bath was lower than that of the other three treatments. For this matrix, results were not significantly different for room temperature digestion periods from 12 hours to 24 days.

Table 7. Mean & standard deviation of HgT concentrations at East Fork by digestion treatment with 5% (v/v) BrCl

Treatment	Depth (cm)	n	Mean HgT (pM)	Standard Deviation
EPA Method 1631	2	4	32.1	5.6
Heated Water Bath	2	3	34.3	0.3
14 Day Digestion	2	3	46.6	0.5
24 Day Digestion	2	3	49.3	1.8
EPA Method 1631	10	4	32.8	4.3
Heated Water Bath	10	4	16.6	2.4
14 Day Digestion	10	3	27.5	0.8
24 Day Digestion	10	4	29.2	2.0

2.4 Discussion

The results of our trials demonstrate that 2% (v/v) BrCl with a minimum of 24-days digestion at ambient temperature was optimal for achieving DOM-oxidation prior to HgT analysis. The work conducted here was not intended to suggest that the EPA 1631 method is flawed. Instead, it was conducted to expand upon the oxidative digestion work with freshwater samples conducted by Lang et al. and provide options for researchers attempting to overcome analytical hurdles when working with brackish or seawater samples that may possess a combination of characteristics (i.e., relatively high DOM and low HgT) limiting the effectiveness of previously proposed oxidative digestion techniques. Trials 9-16 were conducted as a means to address limitations of the initial investigation, including a lack of replication within a given treatment, direct comparison of treatments with the same concentration of BrCl on water of the same identity, and an evaluation of using 2% vs. 5% (v/v) BrCl on water of the same identity. The follow-up trials supported the original finding suggesting that a minimum of 24-days digestion is the most dependable method to achieve DOM-oxidation prior to HgT analysis.

When conducting total Hg analyses on porewater, some general guidelines may be helpful in achieving complete oxidation of interferences. First, use sufficient BrCl. Using 5%

(v/v) BrCl was necessary for complete oxidation of Hg for natural lagoon water samples containing OM and S. While EPA Method 1631 suggests increasing BrCl to 5% (v/v) for "highly organic matrices such as sewage effluent", the present study has indicated that some natural lagoon waters may also require this concentration of BrCl. Creating a pilot test with 2%, 5%, and 10% (v/v) BrCl may be beneficial in targeting an appropriate concentration of BrCl for a given matrix, prior to consideration of digestion time. Second, use a long (24-day) oxidation time when possible. It may result in the same HgT concentration as EPA Standard Method 1631 for some matrices, but for others, the longer oxidation time results in the detection of more Hg. Thirdly, avoid heat treatment as a means of accelerating digestion. A heated water bath invites apparent loss of Hg0, and can increase the risk of contamination from the septa caps. Fourthly, use acid-washed, 18 MΩ-cm water- rinsed septa that have not been previously used for research, as neither cleaning procedure used in the present study was entirely sufficient to ensure low-Hg septa while maintaining integrity of the septa material. Lastly, use glass serum jars for incubations to avoid issues related to gas-permeability. While glass jars did not prevent a loss of Hg0 under the heated water bath condition (loss may have occurred through the septa), avoiding gas-permeable Teflon bottles is a recommended precaution. Furthermore, it is advisable to prepare method blanks that experience the same conditions as the samples, as a control on Hg invasion or evasion from the sample, so that sample peak areas can be corrected for Hg gained or lost from the method.

The results of the porewater digestions highlight how longer (24-day) digestions at room temperature) can be beneficial in overcoming matrix effects for certain types of interferences. Future work may consider analyzing the concentrations of DOM and total S present in samples alongside HgT. For example, EF 2 cm samples had more brown pigment than did EF 10 cm samples. While the EPA Method 1631 worked similarly to the 14-day and 24-day digestions for EF 10 cm, this was not true for EF 2 cm samples. For the same amount of BrCl (5% (v/v)), samples at EF 2 cm only revealed higher HgT when incubated for

14 or 24 days. Quantifying the concentration of DOM and S may allow for an understanding of whether there is a threshold concentration of OM, S, or OM and S together, that is indicative of the need to oxidize longer than 12-24 hours.

CHAPTER 3. The Influence of Nitrogen and Reduced Sulfur on Microbial Mercury Methylation at a Coastal Estuarine Wetland

Abstract

Methylation of mercury (Hg) by microbes is of critical concern, as the organometallic form of this neurotoxic element, methylmercury (MeHg), more readily bioaccumulates within marine food webs than does the inorganic form. Prior research on the impact of eutrophication on microbial Hg methylation has provided inconsistent answers as to whether addition of nutrients would have a positive or negative relationship with methylmercury production. Thus, the impacts of nitrogen (nitrate and ammonium) and reduced sulfur on Hg biogeochemistry were examined at an estuarine wetland (Younger Lagoon) in close proximity to agricultural sites. Trends in MeHg production in the field were positively correlated with nitrate across all seasons in the organic-rich sediments of the East Fork site (EF) but not at the sandy Beach Zone site (BZ). Interestingly, addition of nitrate to sediment microcosms stimulated the methylation of Hg(II) at BZ yet had no effect at EF. Measured rates of methylation were limited under molybdate addition. These two findings were interpreted as reflective of a sulfate-reducing bacteria (SRB) dominated methylating community that is able to switch terminal electron acceptors when available. This was borne out in finding Proteobacteria and Chloroflexi to be the dominant bacterial phyla at both locations, and in finding Desulfobacterota to be a top phylum at BZ. Members of iron-reducing *Geobacter* and nitrite-oxidizing *Nitrospina* were notably absent from 16S sequences, though two sequences from nitrate-reducing sulfide-oxidizing bacteria (NR-SOB) *Sulfurospirillum* were found at BZ. While interactions between NR-SOB and SRB may be at least partially responsible for the increase in methylation under nitrate amendment at BZ, it is more likely that the greater prevalence of members of the Desulfovibrionaceae phylum are responsible, as the percentage of sequences belonging to this phylum was roughly double at BZ compared to EF (0.32% and 0.15%, respectively). A higher concentration of porewater acid-volatile sulfide

(AVS) may have also contributed to the lack of increased methylation seen under nitrate amendment at EF. Replicate methylation assays, investigating low and high nitrate amendments at BZ only, revealed no change to k_{meth} while k_{demeth} was suppressed in parallel demethylation assays under both nitrate conditions. These results were hypothetically attributed to facultative, heterotrophic SRB capable of respiring nitrate when available, and competing with denitrifiers who may have otherwise contributed to demethylation.

3.1 Introduction

While all forms of mercury (Hg) are toxic, methylated mercury (MeHg) poses the greatest health risk to humans, animals and ecosystems (Boening, 2000). This is due to the propensity of this Hg species to bioaccumulate in terrestrial, freshwater and marine foodwebs (Driscoll et al. 2007) and biomagnify with each trophic transfer (Chen et al. 2008). Mercury is biotically methylated by microbes, though the reasons for this behavior are yet unknown. Current hypotheses have established that methylation is formed as a metabolic side-product (Choi et al. 1994a, Choi et al. 1994b), hence, a general trend is to observe more methylation under conditions that would stimulate microbial metabolic activity (i.e., increased temperatures, availability of oxidizable substrates, and/or terminal electron acceptors; Bravo and Cosio, 2020). Sulfate-reducing bacteria (SRB), microorganisms who oxidize organic matter (OM) for electrons and use sulfate as a terminal electron acceptor, were first implicated as methylators by Compeau and Bartha (1985) which led to a focus on obligate anaerobes as responsible for Hg methylation. While SRB are indeed key players, more recent work has revealed additional clades of microorganisms capable of contributing to the production of MeHg.

Microbes with alternative metabolisms, such as iron-reducing bacteria (FeRB) (Gilmour et al. 2013) and methanogens (Hamelin et al. 2011) have since been identified as participants in the process. Furthermore, the identification of the *hgcA* and *hgcB* gene pair as genes encoding two proteins which confer methylation capability (Parks et al. 2013) has

allowed current researchers the ability to assess novel environments for the presence of methylating genes through metagenome assemblies. Such work has revealed that the environments in which methylation putatively occurs, as suggested by the presence of *hgcA-like* genes in oxic marine water, may be more diverse than previously understood (Bowman et al. 2019).

While neither *hgcA* nor *hgcB* have yet to be amplified from marine water column samples (Podar et al. 2015) or sea ice, amplified sequences from these environments revealed similarity to a conserved region of the protein encoded by the *hgcA* gene. Translated sequences matching an HgcA-like protein have been found in the oxygen minimum zone of the Equatorial North Pacific (Podar et al. 2015), in the North Atlantic, and in Antarctic sea ice (Gionfriddo et al. 2016), and were aligned with *hgcA*-like sequences belonging to the bacterial genus *Nitrospina*. This finding is notable in that *Nitrospina* are microaerophilic bacteria,and are primarily responsible for nitrite oxidation in the ocean (Levipan et al. 2014), while all confirmed mercury methylators are obligate anaerobes (Gilmour et al. 2013), as are most known *hgcA* carriers. *Nitrospina*'s presence in environments without other identifiable culprits contributing to methylmercury production suggests that methylation capability may be more widespread than just *hgcA*-possessing microbes or obligate anaerobes. The aforementioned studies provide justification for expanding research into oxic or partially-oxic environments, as well as those anticipated to be nitrogen impacted, so that the potential involvement of N-cycling microbes can be further investigated.

Prior research on mercury methylation in environments with elevated nutrient concentrations has revealed paradoxical results. For example, the "Driscoll hypothesis", a conceptual model, formulated upon observations from coastal ecosystem case studies, suggests that increased nutrient loading may have unintended effects for Hg-cycling, namely decreasing bioavailability and trophic transfer, which would in turn reduce methylmercury production (Driscoll et al. 2012). Following this logic, efforts to reduce eutrophication would

be expected to enhance methylmercury production via increased bioavailability of Hg(II) and lead to increased trophic transfer of MeHg. Work in the Great Sippewissett Marsh, a salt marsh with a history of receiving sewage-sludge based fertilizer, found results consistent with the Driscoll hypothesis. Control plots had the highest percentage of Hg in the form of MeHg compared to plots receiving the highest dose of fertilizer which had the lowest percentage of Hg as MeHg, as well as lowest sediment sulfide (Lamborg et al. 2019). Similarly, Todorova et al. (2009) found that nitrate additions to eutrophic, freshwater Onondaga Lake reduced the accumulation of MeHg in anoxic water and that MeHg concentrations were diminished when nitrate was present above the sediment-water interface.

Conversely, work in fertilized agricultural wetlands and unfertilized non-agricultural wetlands in Yolo County, CA revealed that the former exhibited higher MeHg concentrations than the latter (Marvin-DiPasquale et al. 2014). Though calculations of methylmercury potential production rate suggested that the system was dominated by SRB, the study established that enhanced methylation was not due to stimulation by sulfate addition. Rather, microbial activity, and therefore potential Hg methylation, was concluded to be controlled by access to labile organic carbon (Marvin-DiPasquale et al. 2014). Agricultural plots received fertilizer in the forms of ammonium sulfate and urea, and higher concentrations of MeHg were observed in agricultural plots, though as the focus of the study was not on the effect of nitrogen inputs, it is unclear whether ammonium or urea was directly influential on the process of Hg methylation.

For studies that found a positive relationship between fertilizer loading and MeHg, the question remains whether the fertilizer had an effect on microbial community composition or if changes in MeHg come as a result of increased supply of OM for respiration, as increased respiration by methylating microbes would be expected to correlate with increased MeHg. Work conducted by Schartup et al. (2013) suggests that it is OM quality, not quantity, that has the potential to influence methylation, findings further supported by Eckley et al. 2021). To

further complicate matters, the influence of OM may be observed via coordination of Hg(II), impacting its bioavailability for methylation, which could ultimately limit MeHg production.

To address these interrelated questions, we designed incubation experiments to test the impacts of the fertilizer species nitrate and ammonium, as well as molybdate (a sulfate-reduction inhibitor), and molybdate + nitrate over a 48 hour period. In this way, we could directly examine the effect of nitrate or ammonium on methylation without the interaction of increased OM from additions or from photosynthetic production, as microcosms were incubated in the dark. Seasonal monitoring was conducted to provide information on the *in situ* relationships between MeHg, nitrate and ammonium, and sediment and porewater sulfides (acid-volatile sulfide and chromium-reducible sulfide, AVS and CRS, respectively.) Sequencing and classification of bacterial 16S rRNA sequences were used to characterize the microbial community within Younger Lagoon (YL) sediment, and to confirm the presence or absence of SRB and other relevant clades of bacteria.

3.2 Methods

Site Selection Rationale

Younger Lagoon Reserve (YL; 37° 57’ 5”N, 122° 3’ 51” W; https://ucnrs.org/reserves/younger-lagoon-reserve/) was chosen as the wetland in which to conduct seasonal monitoring and to collect sediment samples for laboratory incubation experiments. The Lagoon experiences a brief connection to the ocean during the winter when waves and tides combine to erode its barrier beach. Following this, the beach reforms and the Lagoon receives fresh groundwater and rain that mixes with the entrained seawater, leading to a freshening through the winter and spring. The dry summer and fall then lead to a gradual increase in salinity and lowering of water level through evaporation and groundwater transport to the ocean.

Two sites within YL were selected for Hg biogeochemical studies due to their dramatic differences (Figure 11). The Beach Zone (BZ) site at the southern end of the

Lagoon represents locations with sandy, low organic carbon sediments. In contrast, the East Fork (EF) site at the northeast end of the Lagoon possesses clay- and organic matter-rich sediments and is located further inland. The lagoon's seasonal dynamics in salinity, proximity to agricultural fields, partially oxic conditions, and the variability of sediment OM concentrations within the site made YL an ideal location in which to conduct our investigation.

Figure 11. Younger Lagoon Reserve site map with Beach Zone marked with a blue star and East Fork marked with a teal star.

Acid-Washing of Equipment

All Teflon tubes, vessels and bottles, glass microcosm chambers, and C-flex tubing were washed in accordance with a trace metals clean protocol. First, each container was filled with 1% Solujet solution and allowed to sit for 3 days, before being rinsed 5x with MilliQ (>18 MΩ-cm resistivity) water. Bottles were then filled with 10% HCl and allowed to sit for 3 days, followed by three rinses with MilliQ water. For methylmercury sampling, the bottles were then capped tightly and double-bagged for storage in zip-sealed bags. If containers

were to be used for total mercury digestion only (during porewater oxidation) they were again filled with MilliQ water and BrCl was added to create a 0.5% solution. Containers were allowed to sit for 24 hours under BrCl oxidation to degrade any remaining OM and leach any Hg adsorbed to the vessel walls. Next, 50 µL of hydroxylamine hydrochloride was added to terminate the oxidation reaction by neutralizing any remaining bromine. The bottles were then rinsed 5x with MilliQ and again filled with 10% HCl for 24 hours before being rinsed 3x with MilliQ, then capped and double-bagged for storage.

Porewater Collection

Water depths during sampling were never greater than about 1.5 m, and the sites were accessed with waders. At both sites, 1-L surface water grab samples were collected in acid-cleaned Teflon bottles, with each vessel being rinsed 3x with ambient water before collection. Porewaters were collected through a ¼" stainless steel push piezometer (MHE Products) inserted into the sediment by hand and sampled in 2 cm increments down to 20 cm depth (similar strategy to Lutz et al. 2008). Acid-washed C-flex tubing was attached to the piezometer and a peristaltic pump was used to draw porewater out of the sediment until about 250 mL was collected. A mesh guard (MHE) was taped around the outside of the piezometer inlet to prevent clogging by plant roots or particulates. Porewater samples were capped and placed in amber bags inside a cooler until transported to the lab. In the lab, the porewater and surface water samples were filtered with a 0.45 um groundwater capsule filter (Millipore Sigma GWSC04501) and acidified to 0.1% (v/v) with 12 M HCl before storage double-bagged at 4 °C. The capsule filter was rinsed with 2 L of 18 MΩ-cm water before any samples were passed through but used without further preparation. A handheld YSI water quality meter (Yellow Springs Instruments, Yellow Springs, Ohio, USA) was used in the field using a flow-through chamber to collect salinity, O_2, temperature, and pH measurements during each of the three seasonal sampling events (December 2019, April 2020, and October

2020). Dissolved oxygen values were corrected for oxygen diffusing through the tubing during pumping by subtracting the lowest O_2 value from each of the other values.

BrCl Digestion for Porewater Total Hg

Aliquots of each sample were prepared for BrCl digestion as detailed in EPA Method 1631 (US EPA, 2002). An exploration into the conditions that would support full oxidation of the dissolved organic matter (DOM) matrix ensued, guided by the methods of Lang et al. (2005). The conditions tested within our study included 0.25-5 % (v/v) BrCl. EPA Method 1631 suggests using as high as 5% (v/v) BrCl for highly organic matrices, or as low as 0.2% (v/v) BrCl when trying to lower the limit of detection (LOD). While 1.0% (v/v) ultimately worked well for BZ samples when a minimum of 4-day digestion period was used, BrCl was increased to 2% (v/v) and 5% (v/v) for colored samples at EF in an attempt to achieve complete oxidation. However, less than 2% (v/v) BrCl was insufficient for EF samples, as indicated by the retention of color or cloudiness following the digestion period. While the range of BrCl concentrations tested was within the range suggested by EPA Method 1631, the oxidation times were increased from the suggested 12 hour minimum to 2- and 4-day periods, followed by 14- and 24-day periods. The full details of the porewater digestion method are available in Calvin et al. (in prep*).*

Hg Determination

Following BrCl-oxidation, 50 µL of 30% (w/v) NH_2OH was added to remove free halogens that could damage the pre-concentration columns. The samples were mixed and allowed to react for at least 5 minutes. Then, a sample (or subsample) was poured into a "UConn" bubbler that allows for continuous headspace purging and 100 µL of 3% (w/v) $SnCl_2$ solution was added to reduce all Hg species to Hg^0. The bubbler was then switched to purge mode and the liquid was degassed with UHP N_2 at 300 mL/min. for 5 minutes to concentrate the evolved Hg^0 onto the first gold trap of a Tekran 2600 Mercury Analyzer (Tekran

Corporation, Ontario, Canada). The first gold trap was then heated to desorb the Hg^0 in a stream of UHP Ar onto a second gold trap which in turn was heated and the Hg determined by Cold-Vapor Atomic Fluorescence Spectrophotometry (CVAFS). The instrument was calibrated with Hg^0 vapor standard and with Hg(II) aqueous standard each day of analysis. If the vapor curve and aqueous curve slopes were different by more than 10%, the aqueous standard was remade and, in accordance with Method 1631, another series of 5 non-zero standards were run to create the calibration curve. At least three $SnCl_2$ blanks were run each day of analysis, and the average peak area associated with 100 µl of the 3% (w/v) $SnCl_2$ solution was subtracted from the average (n=3) peak area of the reagent blank, to yield the peak area associated with only the amount of BrCl added plus 50 µl of 30% (w/v) NH_2OH. This peak area will be referred to as "adjusted reagent blank". The average peak area associated with the 100 µl of $SnCl_2$ solution was used as the zero point of the calibration curve and this area was not subtracted from the peak area of each of the standards. MilliQ water alone used in creating reagent blanks was determined to have an HgT concentration not quantifiable above the signal from BrCl and NH_2OH + BrCl. Raw sample peak areas were corrected by subtracting the adjusted reagent blank peak area before using the calibration curve to solve for fmoles of HgT. The daily LOD was calculated by solving for the fmoles of HgT in each reagent blank (using uncorrected peak area), taking the mean of the daily reagent blanks in fmoles, multiplying the standard deviation by 3, and dividing by 20 or 40 mL, as appropriate for the location. The daily LODs ranged from 0.34 to 6.4 pM.

Sediment Total Hg Quantification

Sediment cores were collected by hand in triplicate (at both locations) following the December sampling event which did not yield sufficient sediment for all analyses from a single core. Core tubes were stored in black plastic until they were brought back to the lab following the sampling event and were processed the same day as collected. Sediment cores were sectioned at 1 cm resolution and each depth segment was transferred to a 50 mL

Falcon tube so that fractions from each replicate core could be pooled together. Samples were vortexed, frozen away at -80°C until solid, and lyophilized on a Freezone 4.5L benchtop freeze dry system (Labconco, Kansas City MO, USA) until completely dry (as determined by constant weight), then stored in the dark until analysis. Samples were crushed by hand and homogenized with a clean spatula after freeze drying. Aliquots of ~0.1 g of dry sediment were accurately weighed into quartz boats (previously blanked through heating to 550°C in a muffle furnace) using a Mettler Toledo analytical balance with a minimum of three replicates for each depth. Samples were analyzed for total mercury on a DMA 80 Direct Mercury Analyzer (Milestone Corporation, Shelton, CT, USA) with internal calibration. Reference standard IAEA-158 was used to ensure concentration measurements were within 10% of the reference standard. Measurements were averaged and two additional replicates were performed for those with standard deviation >10% of the total concentration. For samples with more than 3 replicates, Dixon's Q-test was used to eliminate significant outliers before the values were averaged.

Sediment and Porewater Methylmercury Distillations

Sediment

Lyophilized sediment samples (~0.3-1.0 g from East Fork and ~1.0-2.0 g from Beach Zone) were distilled following the methods described in Hammerschmidt and Fitzgerald (2006). The dry material was weighed into a tared Teflon distillation vial and ~40 mL of MilliQ water was added atop the sediment followed by 400 µL of 2 M sulfuric acid, 400 µL of 1 M copper sulfate, and 200 µL of 20% (w/v) KCl solution. The distillation vessels were placed in a hot block on a hot plate set at 140°C. A collection vessel for each distillation vessel was prepared by adding ~5 mL of MilliQ water into a Teflon vessel and placing it in an ice bath. Distillation caps and tubing were used to connect the distillation vessels within the hot block to the receiving vessels in the ice bath. The tubing was placed below the water level and N_2

gas was bubbled into the distillation side samples for the duration of the distillation, approximately 5 hours. Samples were distilled until ~60-70% of the liquid on the distillation side had transferred. To distill past this point led to interference from the matrix during the subsequent ethylation step and also increased the likelihood of the formation of artifact methylmercury. Therefore, distillations were terminated when they had distilled to 70% or had distilled for 5 hours, whichever came first. Samples were stored refrigerated and in the dark for no longer than 48 hours prior to ethylation and analysis on Tekran 2700.

Two distillation reagent blanks were prepared along with each set of 6 environmental samples. A reagent blank was prepared by adding ~40 mL of MilliQ water to a distillation vessel, then adding 400 µL of 2M sulfuric acid, 400 µL of 1M copper sulfate, and 200 µL of 20% (w/v) KCl solution as was done for a sediment sample and subjecting the vessel to the distillation procedure within the hot block. Two reagent blank peak areas were averaged together for each day of analysis, and the average blank peak area was subtracted from the sample peak area before the slope of a calibration curve (disincluding the y-intercept) was used to solve for pg of MeHg in a 10 mL sample of distillate. The total amount of MeHg in the whole volume of distillate for each sample was calculated based on the concentration of the analyzed aliquot and the total volume of distillate produced for a given depth. The total mass of sediment was used to calculate the concentration of MeHg in pg/gram dry sediment. For days where one reagent blank had a peak area of zero, the reagent blank with a non-zero value was used to correct the sample peak area. For days where an ethylation blank had a peak area greater than or equal to the reagent blanks, or when both reagent blanks had peak areas of zero, the peak area of the ethylation blank was used to correct the sample peak area. A five-point standard curve, generally from 1.6-32 pg of MeHg (as Hg) or as was appropriate to the concentration range of the samples, was prepared along with each set of samples analyzed on the Tekran 2700. Acetate buffer was prepared fresh when the ethylation blank was determined to have >1.9 pg MeHg per 10 mL sample. The limit of detection was set at 3x the standard deviation of the reagent blank average, with all reagent

blank peak areas converted to pg of MeHg by the curve pertaining to the day of analysis, and the standard deviation of reagent blanks was calculated for pooled reagent blanks across all days of sediment analysis. The concentration of reagent blanks (~10 ml volume) was 0.36 +/- 0.33 pg/ml when averaged across all days of analysis, which resulted in a limit of detection (LOD) of 1.0 pg/ml. The average excluded reagent blank values that had peak areas of zero.

Porewater

Porewaters were distilled following the method of Horvat et al. (1993). A minimum of 50 mL of porewater was needed to quantify MeHg following distillation. As the distillation vessels had a maximum volume of 60 mL, adding the entire 50 mL sample led to unacceptable foaming once heating and purging with N_2 gas began. The foam caused components of the porewater matrix to distill over to the collection side. Therefore, after 889 µL of 8 M sulfuric acid, 400 µL of 1 M copper sulfate, and 200 µL of 2 M potassium acetate buffer was added, the sample was shaken to mix and ~25 mL volume of liquid was transferred into the distillation vessel. Once the liquid level of the distillation vessel had dropped to ~15 mL (approximately 2 -2.5 hours of distillation), the gas was left on but the distillation vessel was removed from the hot block and placed in the ice bath until cool enough to open. The remaining sample was transferred from the amber vial, the vessel recapped and returned to the hot block, and the distillation continued. For porewaters, an average reagent blank across all days of analysis was calculated to be 1.0 +/- 0.9 pg/ml which resulted in a LOD of 0.3 pg/ml for a ~ 10 ml aliquot.

Ethylation and Analysis on Tekran 2700

Subsamples (~10 mL volumes) of distillates were placed in septum-sealed amber vials, buffered with 40 µL of 2 M potassium acetate solution, treated with 20 µL of 2.5% (w/v) ascorbic acid and ethylated with 20 µL of 1% (w/v) sodium tetraethyl borate (NaTEB). An

ethylation blank of 10 mL MilliQ water and the same quantities of reagents was prepared. Upon incubating for a minimum of 17 minutes, samples were purged for 8 minutes with Ar using a Tekran Model 2621 autosampler and the volatile methylethylmercury was collected on a Tenax trap within a Tekran 2700 instrument. The Hg derivative was thermally desorbed from the trap and determined as Hg^0 by CVAFS following in-line pyrolysis.

Loss-on-Ignition Organic Matter Quantification

Aliquots of dry sediment (~2 g) were added to tared ceramic crucibles in duplicate for each depth. The samples were combusted at 550°C for 4 hours in a preheated muffle furnace and allowed to cool inside the furnace until they could be handled for weighing following the methods of Heiri et al. (2001) for determination of organic matter (OM) content. Percentage of OM (w/w) in dry sediment was calculated as mass lost during combustion at 550°C as shown in the following equation: LOI = ((DW - CW)/DW)*100. In the equation, LOI represents the mass of organic matter lost via combustion as a percentage of total sediment mass, DW represents the mass of lyophilized sediment, and CW represents the mass of sediment after combustion at 550°C, the latter two values having units of grams. The samples were not oven dried prior to combustion at 550°C and therefore could have contained clay water or hygroscopic water that was also lost on ignition, which possibly biased the LOI data high. Ex post facto drying tests constrained that bias to, at most, 14% of total LOI at EF and 7% of total LOI at BZ .

Enriched Isotope Spiking Solution Preparation

Following the methods of Martin-Doimeadios et al. (2002) and Filipelli and Baldi (1993), isotopically enriched $Me^{198}Hg$ and $Me^{199}Hg$ were synthesized for use in the 2022 microcosm experiments from ^{198}HgO and ^{199}HgO sourced from Oak Ridge National Labs. A solution of $^{200}Hg(II)$ in 0.1% HCl and deionized water was prepared using isotopically enriched $^{200}HgCl_2$ from Oak Ridge National Labs for both the 2020 and 2022 microcosm

experiments. A Thermo Element XR Inductively Coupled Plasma Mass Spectrometer (ICPMS; ThermoFisher Scientific, USA), hyphenated to a Tekran 2700 Methylmercury Analyzer, was used to determine the isotopic composition of all three enriched-isotope solutions. The Thermo Element XR was also used to determine the concentrations of the isotopically enriched $Me^{198}Hg$ and $Me^{199}Hg$ solutions by reverse isotope dilution (Hintelmann and Evans, 1997).

Microcosm Experimental Design, October 2020

At both BZ and EF in October 2020, sediment was collected from the upper 5 cm of depth, sealed into separate clean plastic tubs, and immediately stored away in a dark cooler until it was brought back to the lab and stored in a refrigerator. Every effort was made to minimize exposure to the air. Overlying water (2 L) from each location was collected and returned to the lab where a ~20 mL aliquot was spiked with isotopically enriched ^{198}MeHg and ^{202}Hg(II) and allowed to equilibrate overnight at 4°C. The following day, sediment was placed in a nitrogen-flushed glove bag, homogenized by stirring, and spiked with overlying water that contained ^{198}MeHg and ^{202}Hg(II) for final enriched concentrations of 1.4 pg ^{198}MeHg /g wet sediment and 3.4 ng ^{202}Hg(II) /g wet sediment. The spiked sediment was stirred until homogeneous. The remaining overlying water (~1.5 L) was divided into 6 aliquots of ~250 mL each, and each 250 mL volume received either no treatment (two controls), or spikes of nitrate, ammonium, molybdate, or molybdate and nitrate. The six treatments and the corresponding concentration of amendments within the overlying water are given in 81. N=3 for each condition at each location.

Table 8. Location & concentrations of amendments for microcosms, October 2020

Treatment	Concentration at EF (mM)	Concentration at BZ (mM)
Molybdate	39	37
Nitrate	117	106
Ammonium	107	99
Nitrate + Molybdate	107, 39	106, 37
48 hour control	Overlying water only	Overlying water only
Instantaneous control	Overlying water	Overlying water

***When two numbers are given, the first refers to the nitrate concentration and the second to the molybdate concentration.**

Within a nitrogen flushed glove bag, ~20 g of wet ^{198}MeHg- and ^{202}Hg(II)-spiked sediment was added to each glass microcosm chamber through an acid-washed funnel. Treatment and control overlying water solutions were bubbled with nitrogen for 30 minutes within the glove bag to deoxygenate prior to 70 mL being added atop the sediment. The headspace of each chamber was flushed with nitrogen gas before being crimp-sealed and inverted to mix. Microcosm chambers were then removed from the glove bag and stored at ambient laboratory temperature in the dark for 48 hours after which the reaction was terminated by placing the chambers in the -80°C freezer until solid. At both EF and BZ, three replicates of each of 4 treatment conditions were prepared. An instantaneous control was prepared to determine changes in MeHg concentration that occurred as a result of perturbing the system with Hg(II) and MeHg spikes that increased the amount of available HgT. The instantaneous control was prepared in triplicate. Vessels were crimp-sealed in the glove bag and moved to the -80°C freezer immediately after preparation. Three replicates of the 48-hour control were incubated for the same time period as the treatment conditions before freezing. Following incubation and freezing, samples were lyophilized as was done for environmental samples and (0.3-2.6 g) aliquots from each treatment replicate were distilled to concentrate MeHg and release it from the matrix per the distillation methodology as described above.

Microcosm Experimental Design, October 2022

As initial microcosm had limited replication (n=3), additional microcosm experiments were conducted in October 2022 at Beach Zone, with a 337 uM nitrate solution ("Low Nitrate"), intended to simulate double the highest ambient concentration of nitrate observed at YL, and a 106mM nitrate solution ("High Nitrate"), replicating the nitrate amendment used in 2020. Sediment and surface water from Beach Zone were field sampled in the same manner as in 2020. Five microcosms of each condition were prepared, with the details presented in Table 9. Samples were spiked with ^{200}Hg(II), used to track methylation, and ^{198}MeHg, used to track demethylation. ^{200}Hg(II) and ^{198}MeHg enriched isotope solutions were added to overlying water and bubbled with nitrogen gas for 30 minutes within a glove bag (COY Lab Products) to deoxygenate. Final concentrations of ^{200}Hg(II) and ^{198}MeHg were 5.1 and 2.0 ng/g dry sediment, respectively.

Table 9. Concentrations of nitrate amendments for October 2022 microcosms

Treatment	Concentration within BZ Porewater
Low Nitrate (micromolar)	337
High Nitrate (millimolar)	106
48 hour control	Overlying water only
Instantaneous control	Overlying water only

ICPMS Analysis & Isotope Calculations

We measured the isotopic composition of MeHg in the incubations by connecting the output gas from a Tekran 2700 to an Element XR (Thermo) ICPMS. Subsamples (~10 mL) of the microcosm sediment distillate were ethylated and Hg was determined as described above for native sediment samples.Prior separation of species by the GC column allowed for distinct peaks corresponding to Hg0, MeHg, and Hg(II). Peak areas were integrated within the internal software of the Element XR for each Hg isotope and a curve specific to each of ^{200}Hg and ^{202}Hg was created for each day based on calibration standards prepared from bulk MeHg

standard with a concentration of 1.51 pg Hg/µL. The isotope-specific calibration curves were applied to the integrated peak areas to solve for MeHg in pg of Hg for that isotope. The pg values were used in the linear algebra matrix calculations of Ouerdane et al. (2009) following the technique of Hintelman and Evans (1997) for separating the signal from $Me^{202}Hg$ produced from the spike from that of the background pool of $^{202}Hg(II)$ in the sediment.

The bulk MeHg standard calibration curve consisted of 6 points, including an ethylation blank, and 5 standards ranging from 5-300 µL of standard. The pg quantity from each of the two sample replicates was corrected by subtracting the pg's coming from the daily average reagent blank (2 reagent blanks per day, with 2 technical replicates of each measured). The resulting "corrected pg value" was used to calculate the average MeHg concentration in pg/g dry sediment of a given sample. Next, pg/g concentrations were averaged across all three replicates of the same treatment and standard deviation was calculated. Following that, the resulting average concentration value was divided by the spiked concentration for each site (4460 pg/g dry sediment at BZ and 8420 pg/g dry at EF), as was the standard deviation calculated from the average of the three treatment replicates. Finally, the proportion of the spike methylated was converted to a rate by dividing by the number of days and multiplied by 100 to express as a percent. The error bars depict one standard deviation of the mean of each group of replicates. Plots show the 48-hour control specific methylation rate (as a percentage of the $^{202}Hg(II)$ spike methylated per day) so that treatments' specific methylation rates can be compared. Typical reagent blanks had a mean of 5.8 +/- 4.6 for 10 mL of reagent blank distillate, and resulted in a limit of detection (LOD) of 1.4 pg/mL.

Modifications to ICPMS method & calculations for microcosm experiment, October 2022

$^{199}MeHg$ was used as an internal standard, with ~100 ul spiked into distillate vessels prior to distillation, and used to track MeHg recovery and ethylation efficiency. The isotope-

dilution method described in Hintelman and Ogrinc (2009), was used rather than the calibration curve approach described above. The two techniques were compared, and found to agree within 8% for final reported concentrations of isotopically enriched Hg(II) converted to MeHg. Peak areas by isotope were integrated using a Python script available at https://github.com/chlamborg/HgICPPeakIntegration (Lamborg, 2023). Matrix algebra (Ourdane et al., 2009) was used to resolve the signal from $Me^{200}Hg$ produced from the spike from that of ambient $^{200}Hg(II)$ in the soil. Matrix output was used to calculate the ratio of the peak areas of $Me^{200}Hg$ to $Me^{199}Hg$. The ratio of $Me^{200}Hg/Me^{199}Hg$ was used to solve for the final amount of excess $Me^{200}Hg$ by multiplying the ratio times the known amount of $Me^{199}Hg$ spiked into the distillation.

Macronutrient Analysis

Sample Preparation

A 50 mL subsample of 0.45 µm-filtered water (unacidified) from each sampling depth was frozen at -80°C in preparation for nutrient analysis. Samples were removed from the freezer and thawed at ambient temperature the day of analysis. To precipitate Fe(III) that could oxidize the Cd column, 5 µL of $CaCl_2$ solution (40 g/L) was added to a 10 mL porewater sample in a 15 mL Falcon tube, following the methods of F. Birgand (personal communication, November 16, 2020). The tube was centrifuged for 15 min. to flocculate and precipitate solid iron chloride. Care was taken to keep pump sampler tubing above the level of precipitate during sample injection with a Gilson 222XL autosampler. Samples with notable sulfidic odor or visible polysulfides at the surface were diluted 1/5 before introduction into the instrument (E. Grande, personal communication, November 24, 2020).

NOx and Nitrite Analysis

NO_x and nitrite were measured separately on a 1 channel Lachat 8000 FIA+ system following method 10-107-04-1-C (Wendt, 2000). Sulfanilamide and N-(1-Naphthyl)

ethylenediamine (NED) were used to react with the sample prior to either determination, though a Cd reducing column is placed in line for NO_x analysis to reduce nitrate to nitrite. Nitrite was determined from the same sample without the Cd column in line. Nitrate was then determined by subtracting NO_2^- from NO_x. The detection limit for the method was 5-50 µM and samples were diluted 1/5 or 1/10 when they measured above this range. Samples with visible red or yellow pigment were preemptively diluted 1/5 to avoid colorimetric interference at 520 nm from the matrix (Fishman and Friedman, 1985), as were those with sulfide odor. When October samples were diluted by 1/5, NOx was below the limit of detection (BLOD). All nitrite data for all seasons was also BLOD.

Ammonium Analysis

Ammonium was determined on the Lachat 8000 FIA+ by method 11-107-06-2-A for seawater (Lachat Group, 2015). The analyte detection limit was from 0.7-36 uM. Salicylate, hypochlorite, and sodium nitroprusside (NaFeCN) were used to react with the sample to produce an emerald green color that could be measured at 660 nm. The same practices for diluting pigmented samples or those with sulfide odor were followed as above.

Color Interference Correction

An aliquot of each porewater was run through the instrument along with DI water in place of reagents as an additional colorimetric blank technique. Any peak area that may have resulted in absorbance from matrix pigment rather than analyte reacting with colorimetric reagents could in this way be quantified and subtracted from the true absorbance as a correction. However, none of the samples had quantifiable colorimetric interference detected during this procedure and the original absorbance values were used along with a calibration curve to solve for concentration.

Sediment and Porewater Sulfide Analysis

The acid-volatile sulfur (AVS) and chromium reducible sulfur (CRS) fractions were released from the sediment during a two-step distillation following the assay described by Marvin-DiPasquale (2007) in the SOP USGS-MP #5 protocol. For this study, sediment cores were processed outside of a glove bag and frozen at -80 °C without addition of ZnAc. No radiotracing was used. All reagents and water were degassed with N_2 for at least 30 minutes before contacting sediment. All distillation steps took place under a continuous flow of N_2 gas at a rate of 130 +/- 5 ml/min. Lyophilized sediment (~1 g) was added to a round bottom flask and 6 mL of anoxic water was used to rinse the sample tube and sides of the flask to ensure all of the sample aggregated at the bottom of the flask. The sediment and water within the flask were flushed with N_2 gas for 5 minutes and then 20 mL of 0.35M $TiCl_3$ in 8.4 M HCl was added atop the water and sediment. The mixture was stirred magnetically without heating for 45 minutes to release the AVS fraction from the sediment matrix. Next, 20 mL of 0.6M $CrCl_3$ in 4M HCl solution (pre-reduced with Zn) was added to the same aliquot of sediment in the round bottom flask and was stirred for 60 minutes while heating to release the CRS fraction. The heat was set just hot enough so that steam formed but then quickly condensed on the tubing on the way to the ZnAc trap. If Cr reagent began to enter the steam, as evidenced by a greenish color in the condensed liquid within the tubing, the heat was reduced. Both AVS and CRS fractions of distillate steam (sulfur as H_2S gas) were trapped separately in aliquots of 20 mL of 10% (w/v) ZnAc solution.

ZnAc traps were vortexed prior to subsampling, and a 0.1 to 1 mL aliquot (as appropriate to the range of the curve) was transferred to a cuvette with 6 mL MilliQ water and 1 mL Cline's reagent (Cline, 1969). Color was allowed to develop for 15 minutes before the samples were analyzed with a OceanInsight FLAME miniature spectrophotometer connected to an OceanInsight UV-Vis Sampling System light source set at 670 nm. A standard curve (0.1 to 1.6 mmol/L) prepared from a stock solution of sodium sulfide and zinc acetate (final

sulfide concentration ~8.6 mmol/L) was used to solve for the concentration of sulfide in the distilled AVS and CRS fractions. A reagent blank was prepared by distilling reagents ($TiCl_2$/HCl for AVS and $CrCl_3$/HCl reduced with Zn metal for CRS) in 6 mL of MilliQ water without sediment in the same glass distillation set-up as the sediment samples. The reagent blank was associated with values of 0-0.1 absorbance (typical = 0.01), and for days with a non-zero absorbance, the sample absorbance was corrected by subtracting the value of the reagent blank before the curve was used to solve for the concentration within the sample tube.

Porewater AVS Analysis

A 50 mL porewater sample was subsampled in the field into a 50 mL Falcon tube prepared with 5 mL of 10% ZnAc solution to immediately precipitate dissolved sulfide as ZnS solid. These tubes were transported to the lab in a cooler and frozen at -80 °C until they were thawed on the benchtop the day of analysis. The thawed aliquot was vortexed and a 1 mL subsample was reacted with Cline's reagent and porewater AVS was measured spectrophotometrically as described for sediment AVS.

Genomic DNA Extraction

Sediment from the upper 4 cm of each location was collected in October 2020 during the same sampling event as the sediment taken for microcosms. Sediment was scooped into a plastic box while the box remained under the surface of the water such that the overlying water served as a cap on exposure to air during the sampling. The plastic box was tightly capped and placed in a dark cooler until transported to the lab. Once at the lab, the overlying water and the top 2 cm of sediment was removed, and subsamples were placed in Falcon tubes and stored at -80 ºC for DNA extraction. Samples were thawed on ice and four subsamples (0.36-0.81 g wet sediment) from BZ (BZ 1-4) and four subsamples (0.37-1.06 g wet sediment) from EF (EF 1-4) were weighed out into the bead beating tubes of a Qiagen

DNEasy PowerLyzer PowerSoil Kit. DNA was eluted into nuclease-free water rather than buffer,and stored at -20 ºC until amplification.

We were unable to successfully extract DNA from the frozen sediment from EF. The sample was used up in the first attempt, and a second attempt to extract DNA at EF sampled the microcosm instantaneous control as this was prepared from the same sediment on the same day as the failed samples and was frozen immediately upon microcosm preparation. Though not identical in sample handling as the sediment from BZ, the lyophilized sample was the best representative available for the EF October sediment, after initial attempts to extract DNA were unsuccessful. Lyophilized sediment was washed with "Poulain Magic Buffer" (0.5 M EDTA, 1 M Tris-HCl, 0.5 M sodium phosphate heptahydrate, pH=8) (Poulain et al. 2015) to remove inhibiting substances and then centrifuged to separate the supernatant. This process was to be repeated until the supernatant ran clear, however after 4 rounds the process was terminated despite color still present in the supernatant. Wet washed sediment (0.12 - 0.3 g), previously frozen and lyophilized, was used for the second round of extractions at EF, called EF A-D. The second extraction used a modified version of the Qiagen kit which added a proteinase K digestion step to the extraction procedure. Proteinase K (0.5 mg per sample) was combined with solution C1 in step 2 prior to bead beating for 40 seconds at 4000 (M/s) in a Fast Prep-24 bead beating system (MP Biomedicals, LLC. Irvine, CA, USA) and allowed to incubate at 55 °C for 30 minutes. The regular protocol was resumed upon completion of the incubation step.

Amplification with Polymerase Chain Reaction (PCR)

Three of the genomic DNA (gDNA) samples from BZ (samples 2-4) amplified successfully using Bakt_341F and Bakt_805R primers for the hypervariable V3/V4 regions of the 16S rRNA gene (Herlemann et al. 2011; Turk-Kubo et al. 2018). A Qiagen PowerClean DNA Clean–Up Kit was used on Sample BZ-1 and following this procedure it amplified successfully. The same kit was used on all four extracted gDNA samples from EF (samples

A-D), but the target region failed to amplify even after cleaning. A dilution series was created from cleaned gDNA to reduce the concentration of inhibitors and we found that EF gDNA diluted 1/8 with nuclease-free water could be amplified. PCR reaction mixtures were run in a Peltier Thermal Cycler PTC-200 (MJ Research, Quebec, Canada). The conditions used for the PCR are shown in Table 10 and the reagent volumes used are given in Table 11 (Shilova et al. 2017). All PCR products were cleaned using a Qiagen MinElute PCR Purification kit before quality assessments with Nanodrop and Qubit. Sodium acetate (10 µL, 3M, pH =5.2) was added to each PCR product to adjust the pH as required by the kit to facilitate column binding. Nanodrop 260/280 ratios should be ~1.8 for "pure" DNA and 260/230 ratios should be between 2.0-2.2. Sample 260/280 ratios ranged from 1.76-1.90 and 260/230 ratios ranged from 1.27-1.94. Sample EF-A was excluded from sequencing due to its low 260/230 ratio of 1.27 and as the final quantity was less than 500 ng which was the minimum required by the sequencing service.

Table 10. PCR thermocycling program

Step	Description	Degrees Celcius	Duration (seconds)
1	Initial denaturation	95	300
2*	Denaturation	95	40
3*	Anneal	53	40
4*	Elongation	72	60
5	Final Elongation	72	7
6	Hold Temperature	4	hold

***Steps 2-4 are repeated for a total of 25 cycles.**

Table 11. Volumes of reagents used in PCR

Reagent	Initial Concentration	Final Concentration	Units	Per Reaction (µL)
Water	-	-	-	19.5
CoralLoad Buffer	10	1	x	2.5
MgCl2	In buffer	1.5	mM	In buffer
dNTP Mix	10,000	200	µM	0.5
341_F	10	0.2	µM	0.5
805_R	10	0.2	µM	0.5
Invitrogen Platinum Taq	-	-	-	0.5
Template DNA	-	-	-	1.0

DNA Sequencing

Amplicons from the same gDNA template were pooled following repeated PCR reactions until >500 ng of DNA was present in each sample as determined by Qubit or Picogreen fluorescence assay. Concentrations were normalized to ~20 ng/µL and samples were sent to Azenta Services for sequencing (Plainfield, NJ, USA). BZ samples 1-4 and EF samples B-D were sent, as EF-A had an insufficient quantity even after the products from four PCR reactions were pooled. Illumina MiSeq with 2x250 configuration was used to sequence the PCR amplicons resulting in reads that had a ~20 bp overlapping region. Primers and proprietary multiplexing adapters were trimmed from the sequences by the commercial service.

Bioinformatic Analysis

Sequencing produced .fastq files that were loaded into RStudio running R statistical computing language. The 'dada2' package (Callahan et al. 2016) was used to calculate the sequencing error rate and remove sequences with a statistically high chance of existing due to sequencing error, filter the reads to remove those shorter than 20 nt or longer than 475 nt, and merge forward and reverse reads into "contigs". Reads were not merged if the overlap

region was less than 12 bases in length or if the reads failed to have 100% sequence identity in the overlap region. Contigs were dereplicated with multiple instances of the same sequence binned together as amplicon sequence variants (ASV's), identical sequence reads. Chimeras were removed from the final dataset leaving 59% of the prior ASV's. Finally, ASV's <200 or >475 were removed, as these sequences were likely the result of nonspecific priming. The remaining sequences (7924) were aligned to the SILVA NR training set (v.138.1; McLaren et al. 2021) to assign taxonomy to the genus level (Quast et al. 2013; Yilmaz et al., 2014). Species could not be assigned using 16S amplicon sequences due to limitations described by Wright and Baum (2018).

The 'phyloseq' package (McMurdie and Holmes, 2013) was used for downstream analysis of determining abundance by taxonomic level. 'BiocManager' (Morgan, 2021) was used to access 'Bioconductor' (Gentleman et al., 2004) and the 'DESeq2' package. 'DESEq2' allows for the quantification of changes between experimental conditions while accounting for variation that arises within a single treatment or control condition (Love et al. 2014). It has been proposed as a superior tool for normalizing abundances of libraries of different sizes so that statistically valid comparisons can be made (McMurdie and Holmes, 2014). An alternative, but inferior technique is to "rarefy" data, which means to subsample randomly from larger libraries to equalize them in size to smaller libraries. However, this procedure potentially eliminates rare taxa of interest and introduces the possibility of not detecting a difference between samples when one exists (Type II errors). DESeq2 was used to estimate dispersions based on a model of independent and dependent variables and to calculate log2 fold change between conditions. P-values were calculated within the DESeq2 algorithm, based on the Wald test and were adjusted using the Benjamini-Hochberg method of correction for multiple inferences (Love et al. 2014). A confidence level of 99% was used for the creation of the model that is depicted in the log2 fold change plot. The log2 fold change (LFC) is calculated using EF as the reference, such that LFC=log2(BZ/EF), with positive values indicating that a sequence is more abundant at BZ and negative values indicating a

less abundant sequence. Additional detail about all R package versions and the RStudio environment in which they were used is provided in Appendix A: Supplementary Table S1.

Methods of Statistical Testing, 2020 Microcosms

Methylmercury production rates from the microcosm experiment were grouped by site (n =18) and subjected to normality tests, including plotted histograms and a Shapiro-Wilk test from the 'stats' package (R Core Team, 2023). Normality was assessed across all samples by site (n=18), not by treatment replicate. The test results suggested the methylmercury production rates at BZ had marked deviations from normality while EF did not (p-value = 0.015 and 0.49 for BZ and EF, respectively, Shapiro-Wilk test). Therefore, an analysis of variance (ANOVA) test was used for EF data and the equivalent non-parametric test, Kruskal-Wallis, was used for BZ data. The tests allowed us to check for significant differences among group means.

Following the ANOVA test, the residuals of the EF ANOVA fit model were checked for independence, normal distribution, and homogeneity of variance, and none of the plots led us to be suspicious about the normality of the distribution. A Shapiro-Wilk test and a Kolmogorov-Smirnov test from the 'stats' package were applied to check for normality of the residuals (R Core Team, 2023). For all statistical testing, the confidence level was 95%. A Brown-Forsyth test from the 'car' package (Fox and Weisberg, 2019) is a test of differences from the median of each group. The test was conducted to check homogeneity of variance (homoskedasticity) as equal variances among groups compared is an assumption of an ANOVA. The results gave no indication the residuals had unequal variances (p-value 0.59, Brown-Forsyth test for EF). Finally, eta squared (η^2), the effect size metric for an ANOVA, was calculated using a function from the 'lsr' package (Navarro, 2015) and the effect size is given in Table 13 along with the p-value and F-statistic. The effect size metric for the Kruskal-Wallis test, epsilon squared (ε^2), was calculated as $\varepsilon^2=H*(n+1)/(n^2-1)$ where H was the chi-squared statistic from the Kruskall-Wallis test and n was the total number of observations

(Tomczak and Tomczak, 2014). As the omnibus tests' results did not indicate any means were significantly different at either location, post-hoc testing was conducted only to reveal which groups had the greatest likelihood of being different, as indicated by smallest p-values within comparisons of means. A post-hoc Dunnett's test from the 'DescTools' package (Signorell et al. 2021) was used to reveal which group(s) had a mean significantly different than that of the control following ANOVA at EF. A Dunn's test from the 'FSA' package (Ogle, et al. 2022) was used for non-parametric BZ data after Kruskal-Wallis. The Dunnett's test only compares each treatment against the control whereas the Dunn's test makes all possible comparisons of means between all groups.

Methods of Statistical Testing, 2022 Microcosms

For the 2022 microcosm samples, the final number of analyzed samples for each treatment was: instantaneous control (n=5), 48 hour control (n=4), Low Nitrate (n = 3), and High Nitrate (n=5). Dixon's outlier test was used to remove data from 48 hour control microcosm E. k_{meth} and k_{demeth} were examined using an unbalanced design (type = "III"), 1-way ANOVA with treatment as a factor. Tukey's Honest Significant Differences test (Tukey's HSD) was used as a post-hoc test of multiple comparisons. The 'Anova' function from the 'car' package and the 'TukeyHSD' function from the 'stats' package of R statistical computing language were used (Fox and Weisberg, 2019; R Core Team, 2023). The 'ggplot2' package (Wickham, 2016) was used along with the color palette package 'wesanderson' (Ram and Wickham, 2018) to produce plots.

3.3 Results

Seasonal Field Observations

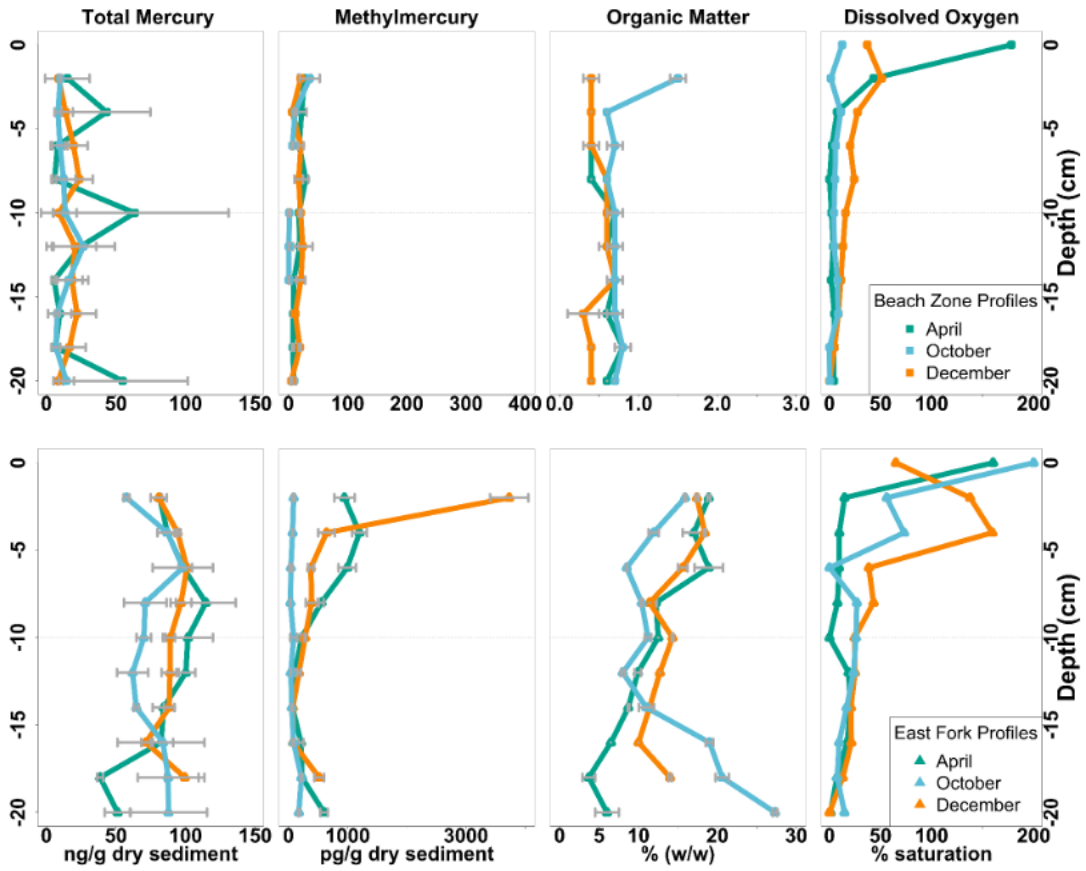

Figure 12. Depth profiles of HgT concentration, MeHg concentration, organic matter percentage, and dissolved oxygen percent saturation for sampling conducted in April, October, and December for Beach Zone (top row) and East Fork (bottom row). Error bars depict standard deviation of mean values for data with replicates. Missing values at BZ for methylmercury are NA for 16,18, and 20 cm and is BLOD for 8 cm depth.

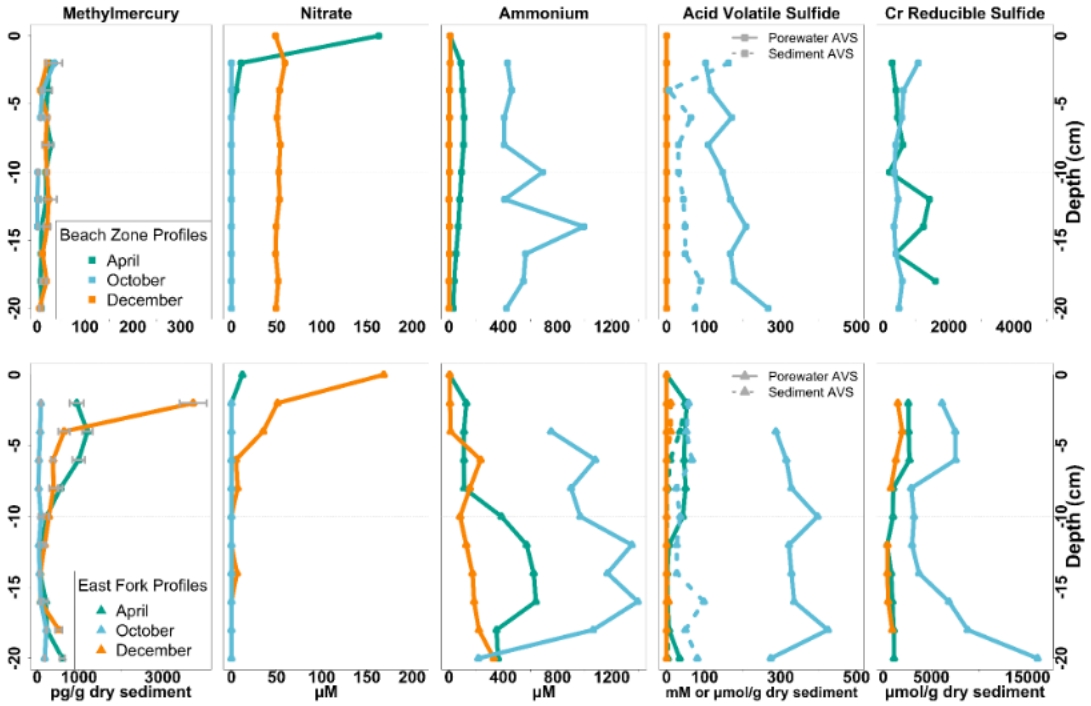

Figure 13. Depicts depth profiles for MeHg concentration, nitrate concentration, ammonium concentration, AVS concentration and CRS concentration for sampling conducted in April, October, and December. Data shown is for Beach Zone (top row) and East Fork (bottom row). Error bars depict standard deviation of mean values for data with replicates. Properties listed as per gram are sediment and per liter are porewater. Missing values at BZ for methylmercury are NA for 16,18, and 20 cm and is BLOD for 8 cm depth. Porewater AVS concentration is BLOD for April at BZ and for both sites in December. Sediment AVS and sediment CRS concentrations are NA for BZ December. Sediment AVS concentration is BLOD for BZ in April.

Table 12. One-predictor models for East Fork and Beach Zone

Predictor	Estimate of Coefficient at EF	R^2 at EF	Estimate of Coefficient at BZ	R^2 at BZ
Depth (cm)	**-0.46**	**0.21**	**-0.42**	**0.18**
Sed. HgT (ng/g dry)	0.06	0.00	0.04	0.00
LOI %	0.31	0.09	0.11	0.01
Ammonium (µM)	**-0.46**	**0.21**	**-0.43**	**0.18**
Porewater AVS (mM)	-0.32	0.11	**-0.49**	**0.24**
Porewater O2 % saturation	**0.50**	**0.25**	0.28	0.08
Porewater HgT (pM)	-0.09	0.01	0.21	0.04
Nitrate (µM)	**0.77**	**0.60**	0.22	0.05
pH	-0.03	0.00	-0.32	0.10
Salinity (ppt)	-0.37	0.14	-0.20	0.04
Temp. (Celcius)	-0.34	0.11	-0.27	0.07

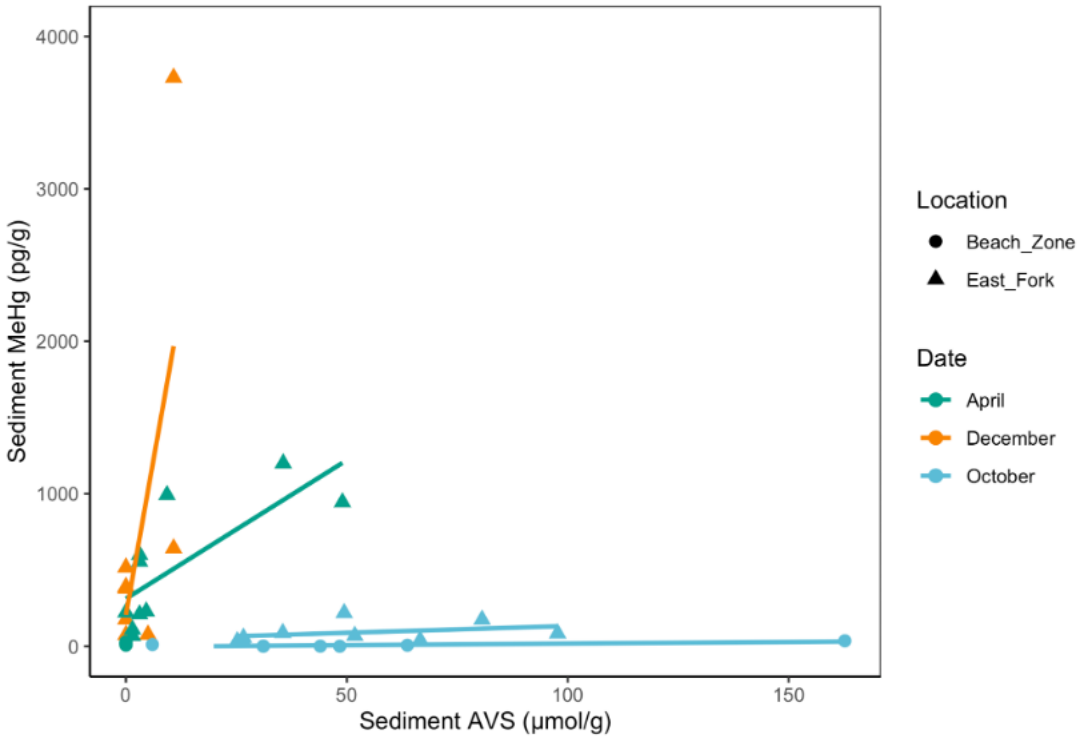

Figure 14. Sediment AVS concentration plotted against sediment MeHg concentration for all seasons, at both EF and BZ. Regression lines shown in the same color as used for group month. Sediment AVS and MeHg had a positive relationship until sediment AVS reached ~50 µmol/g dry sediment. After this point, all observations of sediment MeHg concentration measured <1000 pg/g. MeHg concentrations are generally limited in October, when many sediment AVS values were >50 µmol/g. The maximum MeHg concentration was seen at EF in December, when sediment AVS were ~11 µmol/g. Sediment AVS is NA for BZ in December and is BLOD for BZ in April. The regression lines are not shown for December nor April at BZ.

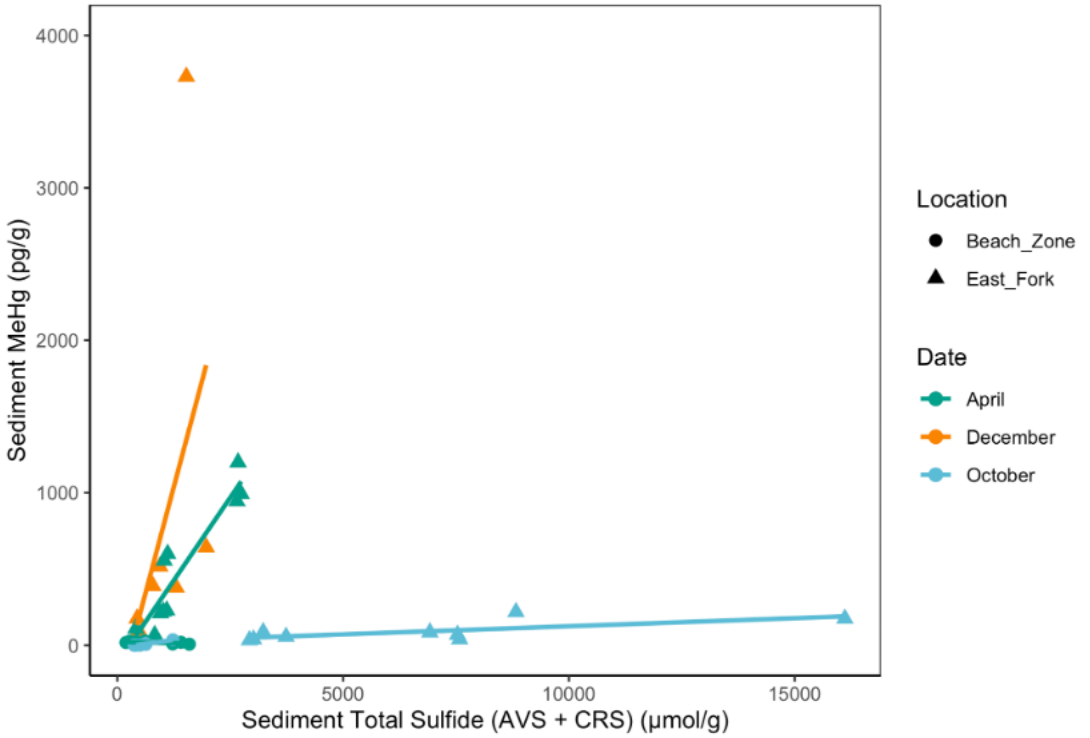

Figure 15. Sediment total sulfide (AVS + CRS) concentration plotted against MeHg concentration for all seasons, at EF and BZ. Regression lines shown in the same color as used for group month. Sediment total sulfide (as the sum of sediment AVS and CRS) in µmol/g dry sediment, at concentrations >~2800 µmol/g were associated with limited MeHg concentration. All of the observations above ~2800 µmol/g total S concentration were from EF in October. Sediment total S was ~1500 µmol/g when the highest MeHg concentration was observed. Sediment AVS and sediment CRS concentrations are NA for BZ December and sediment AVS concentration is BLOD for BZ in April. The regression lines are not shown for December nor April at BZ.

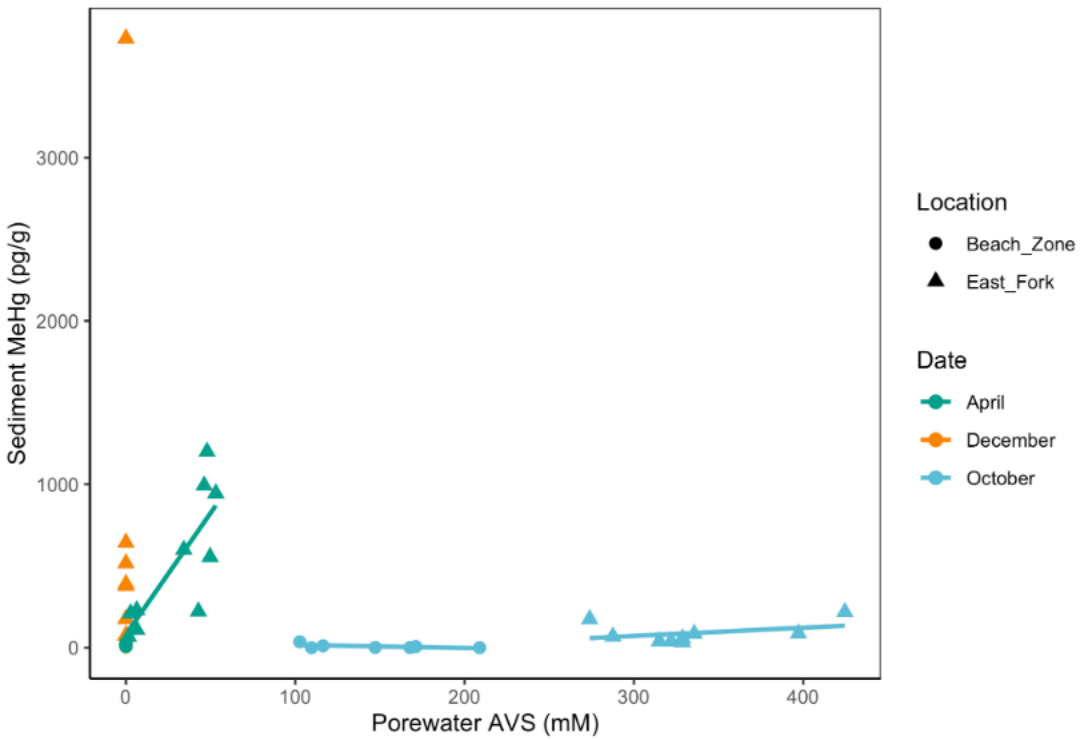

Figure 16. Porewater AVS concentration plotted against sediment MeHg concentration for all seasons at EF and BZ. Regression lines shown in the same color as used for group month. Porewater AVS concentration and MeHg concentration had a positive association in April for EF data. In October, no such relationship was present at either location. Porewater AVS concentrations >100 µmol/ml appeared to limit MeHg concentration, with an October maximum MeHg concentration at EF of 2.18E+2 pg/g compared to 1.20E+3 pg/g in April or 3.73E+3 pg/g in December. No regression lines are shown for BZ in April nor at either site for December, as porewater AVS concentrations were BLOD.

Table 13. Results of Analysis of Variance (ANOVA) test at EF & Kruskal-Wallis test at BZ

Location	Test	Test Statistic	Degrees of freedom	p-value	Effect Size
Beach Zone	Kruskal-Wallis	7.47 chi-squared	4	0.11	0.57 ε^2
East Fork	ANOVA	3.33 F-value	4, 10	0.06	0.57 η^2

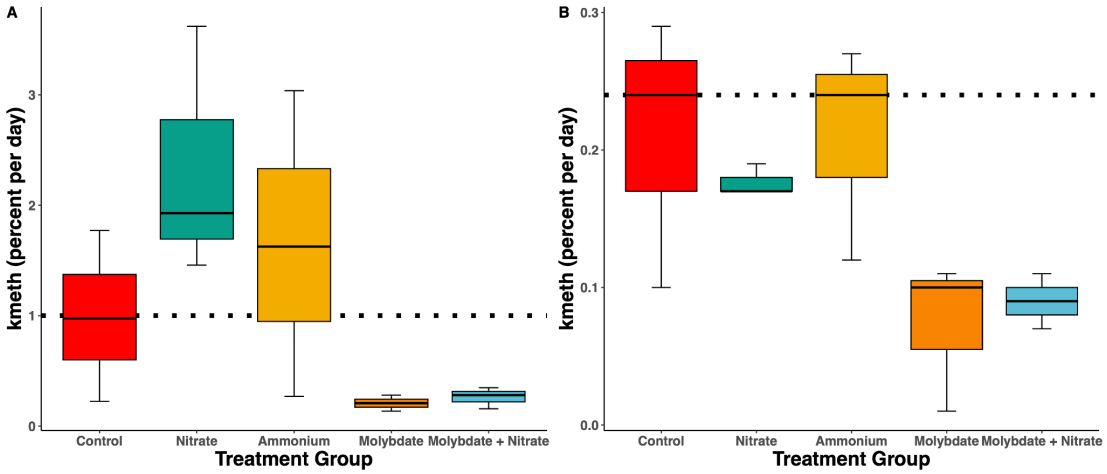

Figure 17. Boxplots of k_{meth} at Beach Zone (A) and East Fork (B) from microcosm experiments amended with nitrate, ammonium, molybdate, and molybdate plus nitrate in October 2020. Mean k_{meth} value for the 48 hour controls is depicted as a black line within each box. 1st and 3rd quartiles from each of the microcosm experiment treatment groups and the control are shown as box edges. Whisker edges portray the data's maximum and minimum for a given condition. Note the difference in scale of the y-axis between locations. Horizontal black dotted lines indicate the median of each control.

Table 14. k_{meth} (percent per day) averaged by treatment group

Treatment Group	Location	Group Mean k_{meth} (% per day)	Standard Deviation (% per day)	Number of replicates
Control	Beach Zone	1.0	0.8	3
Nitrate	Beach Zone	2.3	1.1	3
Ammonium	Beach Zone	1.6	1.4	3
Molybdate	Beach Zone	0.2	0.1	2*
Molybdate + Nitrate	Beach Zone	0.3	0.06	3
Control	East Fork	0.2	0.1	3
Nitrate	East Fork	0.2	0.01	3
Ammonium	East Fork	0.2	0.08	3
Molybdate	East Fork	0.07	0.06	3
Molybdate + Nitrate	East Fork	0.09	0.02	3

***One outlier was removed after Dixon's Q-test.**

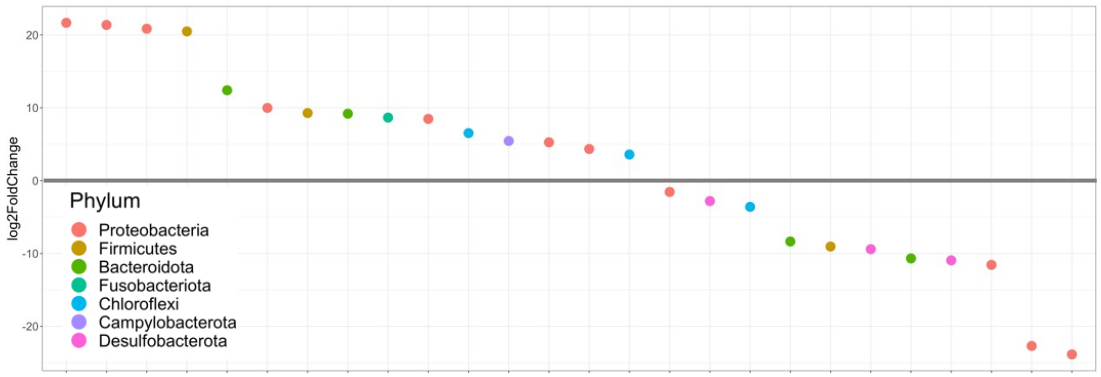

Figure 18. A log2 fold change plot used to reveal differences in bacterial genera between BZ and EF from environmental sediment samples. A horizontal gray line indicates the 0 point of the y-axis. Above the gray line (positive) log2 fold change indicates more prevalence at BZ than EF, whereas negative values indicate less prevalent sequences.

Table 15. k_{meth}, MeHg concentrations, percent MeHg and salinity across studies, freshwater lakes, rivers, and wetlands.

Location	Source	Substrate Type	k_{meth} (percent per day)	Ambient Sediment MeHg (pg/g dry sediment)	Percent MeHg	Salinity
Freshwater Lakes, Rivers & Wetlands						
East Fork Poplar Creek, Oak Ridge, Tennessee	Christensen, et al., 2018.	River sediment upstream of Hg contamination	0.021 +/- 0.011	310 +/- 11	0.025-0.027	Fresh
East Fork Poplar Creek, Oak Ridge, Tennessee	Christensen, et al., 2018.	River sediment downstream of contamination	0.045 +/- 0.007	2,700 +/- 250	0.07-0.09	Fresh
Lake 658, Experimental Lake Area, Canada	Achá et al., 2012.	Water column of a stratified oligotrophic lake	0.5 – 1.7	Ambient Porewater conc: 160 - 1300 pg/L	NA	Fresh
Yolo Bypass, California	Marvin-DiPasquale et al., 2014.	Agricultural Wetland Sediment	0.06 – 9.0	1800 - 2980	0.5 - 1	Fresh (0.17 - 0.28) (Fields fertilized with ammonium sulfate & urea)
Florida Everglades	Gilmour et al, 1998.	Everglades Nutrient Removal Area & Water Conservation Areas Sediment	0 - 12	< 100 - 5000	<0.2 - 2	Fresh (contained agricultural runoff)
Yolo Bypass, California	Marvin-DiPasquale et al., 2014.	Non-Agricultural Wetland Sediment	7.0 – 43	1300 - 2350	0.9 - 1.42	Fresh (0.08 - 0.16)
San Francisco Bay Delta	Windham-Myers et al., 2009.	Yolo Bypass Ag. Wetland Sediment	1.4 -15.6	400 - 1400	0.1 -0.9	Fresh
San Francisco Bay Delta	Windham-Myers et al., 2009.	Yolo Bypass Non-Ag. Wetland or Cosumnes River Floodplain Sediment	0 - 51	400 - 9600	0.3 - 9.1	Fresh (0.006 - 0.74)

Table 15. Continued: k_{meth}, MeHg concentrations, percent MeHg and salinity across studies, estuarine and salt marsh sediment.

Location	Source	Substrate Type	k_{meth} (percent per day)	Ambient Sediment MeHg (pg/g dry sediment)	Percent MeHg	Salinity
Estuarine and Salt Marsh Sediment						
New Jersey Salt Marsh	Blum and Bartha, 1980.	Sediment Slurry under N2	0.015	NA	NA	30
EF Nitrate amended	this study	Muddy Estuarine Sediment, Nitrate amended	0.17 – 0.19	33 – 218	0.04 - 0.25	33.3 -39.8
EF Younger Lagoon	this study	Muddy Estuarine Sediment	0.1 – 0.3	33 – 3730	0.04 - 4.6	33.3 -39.8
BZ Younger Lagoon	this study	Sandy Estuarine Sediment	0.2 – 1.8	BLOD - 36	BLOD - 0.5	34.3 - 38.4
BZ Nitrate amended	this study	Sandy Estuarine Sediment, Nitrate amended	1.5 – 3.6	BLOD - 36	BLOD - 0.4	34.3 - 38.4
Öre River Estuary, Sweden	Liem-Nguyen et al., 2016.	Estuarine Sediment, amended with N + P	1.0 – 5.0	280 - 323	0.63 - 0.84	3.86
Kirkpatrick Marsh, Maryland	Mitchell and Gilmour, 2008.	Estuarine Marsh Soil	0.2 – 7.0	200 – 5000	0.2 - 4.6	1.8 - 32.5
San Francisco Bay Delta	Windham-Myers et al., 2009.	Petaluma River or Alviso Marsh Sediment	0.1 – 14.2	300 - 5200	<0.1 - 1.9	17.2 - 33.4

Table 15. Continued: k_{meth}, MeHg concentrations, percent MeHg and salinity across studies, estuarine and salt marsh sediment.

Location	Source	Substrate Type	k_{meth} (percent per day)	Ambient Sediment MeHg (pg/g dry sediment)	Percent MeHg	Salinity
Marine Sediment						
Mid-Atlantic Continental Shelf	Hollweg et al., 2010.	Marine Sediment	0.2 – 5.3	8-96	0.9 - 1.4	31 - 35
Long Island Sound	Hammerschmidt and Fitzgerald, 2004.	Marine Sediment	1.4 – 8.2	200 - 3200	0.5 - 1.1	53.7
New England Continental Shelf	Hammerschmidt and Fitzgerald, 2006.	Marine Sediment	2.0 – 21	11 - 334	0.4 - 1	33.6 - 34.4

***The tabled rates are ordered from lowest to highest within a given subsection (Fresh, Estuarine, Marine). When a range is given, the maximum was used to order the values. Entries are italicized when the site was either experimentally amended with nutrients or if the site description indicated the presence of agricultural fertilizer. When salinity values were given in ppm [Cl^-], conversions to ppt were made by multiplying the ppm value by 0.00187 (Mitchell and Gilmour, 2008). NA is for not available data.**

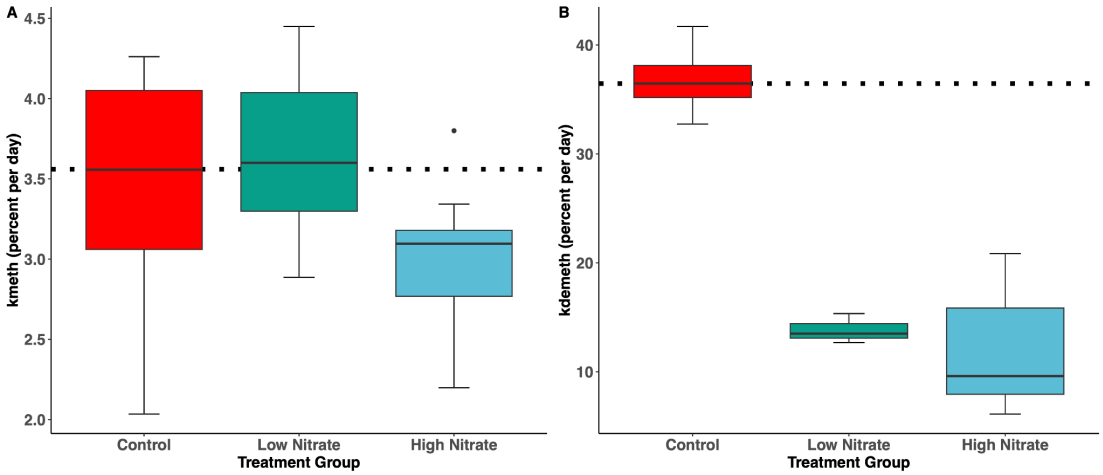

Figure 19. Boxplots of k_{meth} (A) and k_{demeth} (B) from microcosm experiments amended with nitrate in October 2022. Low nitrate treatment corresponds to a nitrate concentration of 337 µM and high nitrate treatment corresponds to a 106 mM nitrate concentration. No significant difference was seen in methylation potential (k_{meth}) with nitrate treatment, though demethylation potential (k_{demeth}) was significantly suppressed by either nitrate amendment. Black dashed line indicates the median k_{meth} or k_{demeth} of the control for each assay.

Table 16. k_{meth} and k_{demeth} averaged by treatment group for Beach Zone October 2022 microcosms

Treatment Group	Methylation Group Mean (% per day)	Standard Deviation (% per day)	Demethylation Group Mean (% per day)	Standard Deviation (% per day)	Number of replicates
Instantaneous control	BLOD	NA	1.1	0.17	5
48 hour control	3.4	0.81	37	3.7	4
Low Nitrate (micromolar)	3.7	0.53	14	1.4	3
High Nitrate (millimolar)	3.0	0.45	12	6.1	5

***Control Treatment E was removed as an outlier after Dixon's Q-test.**

Table 17. Results of Analysis of Variance (ANOVA) test for Beach Zone October 2022 demethylation assay microcosms

Location	Test	Test Statistic	Degrees of freedom	p-value
Beach Zone	ANOVA	35.924 (F)	2	p< 0.001

3.4 Discussion

Ambient MeHg Concentrations at Younger Lagoon

The greatest concentrations of MeHg at YL were measured in the upper 0-5 cm of sediments, which is consistent with the observations of others (Krabbenhoft et al. 1995; Gilmour et al. 1998). MeHg as a percentage of HgT was on average 0.5% at EF and 0.13% at BZ. MeHg as a percentage of HgT across all seasons ranged from 0.04 - 4.6% (w/w) at EF and from BLOD - 0.5% (w/w) at BZ (Table 15). Ambient MeHg concentration ranged from 33 - 218 pg/g at EF and from BLOD to 36 pg/g at BZ in October. Across all seasons, ambient MeHg ranged from 33 - 3.73E+3 pg/g at EF and from BLOD to 36 pg/g at BZ. For seasons when nitrate was above the LOD, the greatest MeHg concentrations were also measured in the overlying water and within the top 4 cm of sediment.

Dissolved Oxygen

The upper 5 cm region was also the most oxygenated at YL, where dissolved oxygen concentrations were >100% (w/w) at EF in December and October. EF was more oxic than BZ in December and October. DO profiles were of similar shape and concentration at both locations in April (Figure 12).

Organic Matter at Younger Lagoon

Driscoll et al. (2012) and Lamborg et al. (2019) found a negative association with nutrient loading and MeHg, by way of nutrients stimulating increased production of organic matter, which in turn reduced bioavailability of Hg(II) to methylators. The results from YL were in contrast to those studies. OM was not significantly correlated with MeHg at either YL location for pooled data but was positively correlated with MeHg for October only at BZ ($p = 0.004$). The coefficient was 0.92 and OM explained 81% of the variability in MeHg for this season. Attempts to explain limitation of MeHg production at YL by coordination with

particulate OM can be discounted, as increased OM would be anticipated to have a negative relationship with MeHg and would be in contrast to the observed results. Thus, we can consider the presence of sulfide in porewater or sediment as a possible alternative control.

Reduced Sulfur at Younger Lagoon

Porewater AVS was found to be the best predictor for explaining variability in MeHg at BZ for pooled data, with an adjusted r^2 of 0.21 ($p = 0.01$; Table 12). The relationship between the variables is negative, suggesting that as porewater AVS concentrations increase, MeHg production is suppressed. A negative relationship between MeHg and porewater or sediment sulfide has been found by other researchers (Craig and Moreton, 1983; Gilmour and Henry, 1991; Gilmour et al. 1998; Benoit et al. 2001a). Research in the Everglades revealed that as porewater sulfide concentrations were increased from ambient (~200 µM) to ~250 µM, methylation was limited in sediment microcosm experiments (Gilmour et al. 1998). In comparison, the porewater sulfide at YL in October had concentrations higher than 250 µM at both locations, with means of 335 +/- 48 mM and 146 +/- 39 mM for EF and BZ, respectively. At both BZ and EF, elevated porewater AVS concentrations in October (>100 mM) was associated with low sediment MeHg concentrations and no trend was observed (Figure 16) for this season. A positive relationship between porewater AVS concentration and sediment MeHg concentration was observed at EF in April when porewater AVS concentrations were below ~100 mM.

A positive relationship also exists between sediment AVS concentration and sediment MeHg concentration at EF in April and December, but no trend exists in October when sediment AVS surpasses ~ 50 µmol/g (Figure 14). A similar positive relationship is observed for sediment total sulfide (AVS + CRS) and MeHg concentration at EF in December and April. Again, in October, when sediment sulfide concentrations exceed ~2800 µmole/g, sediment total sulfide concentration fails to have a trend with MeHg concentration (Figure 15). The Gilmour curve hypothesis states that while readily available sulfate stimulates SRB

and therefore methylation, an accumulation of sulfide from SRB metabolic activity limits methylation (Gilmour and Henry, 1991). In fact, when sulfide was increased from uM to mM concentrations in the water of a culture experiment, methylation of Hg decreased. (Benoit et al. 2001a). This relationship was also observed in river sediment, where MeHg and sediment sulfide had a positive relationship up to 1.8 mg sulfide/g sediment, whereas above that level MeHg concentrations declined with increased sulfide (Craig and Moreton (1983). A proposed mechanism for this relationship suggests that increased porewater sulfide concentrations favor the formation of charged Hg-S complexes, rather than neutral complexes, which are more likely to occur under lower sulfide conditions (<10 μM) (Benoit et al. 2001b). Charged complexes render the Hg biologically less available for methylation, as small and uncharged species, such as HgS^0 more readily cross the cellular membranes of SRB (Benoit et al., 2001a).

At YL in October, sediment sulfide as AVS was about 1.8 mg sulfide/g sediment (~56 μmol/g) at either location, with a mean of 55 +/- 50 μmol/g at BZ and a mean of 52 +/- 25 μmol/g at EF (Figure 13). However, when total sulfide was considered (sum of AVS and CRS), the mean was and 591 +/- 301 μmol/g at BZ and 6603 +/- 3993 μmol/g at EF. These sediment sulfide concentrations are ~10x and ~100x those found to inhibit MeHg production by Craig & Moreton (1983). The negative relationship between MeHg and porewater AVS across all seasons at BZ and the maximum ambient MeHg concentration's occurrence at EF in December, when sediment AVS was about 11 μmol/g and porewater AVS was BLOD, suggest that sulfide exerts control on MeHg production at YL. However, sulfide concentrations from both locations are in the range expected to favor hinder methylation and only go so far to help explain the difference observed in ambient MeHg concentrations and in methylation potentials (Figure 17) between BZ and EF.

Nitrogen Species at Younger Lagoon

Nitrate was BLOD in October at both EF and BZ. Nitrate was 11 µM at BZ in April at 2 cm depth and 5 µM at 4 cm, while the rest of the profile was BLOD. Nitrate ranged from 49-59 µM at BZ in December. At EF, nitrate was BLOD in April and ranged from 5-51 µM in December (Figure 13). Porewater ammonium was higher in October than in other seasons with means of 9.9E+2+/- 3.5E+2 µM and 5.43E+2 +/- 2.2E+2 µM, at EF and BZ respectively. In April, mean concentrations of porewater ammonium were 3.4E+2 +/- 2.2E+2 µM at EF and 7.7E+1 +/- 2.8E+1 µM at BZ. In December, EF had a mean porewater ammonium concentration of 1.3E+2 +/- 8.3E+1 and BZ had a mean of 4 +/- 2 µM.

Single-predictor linear regression models for pooled data revealed nitrate to explain the most variability in MeHg concentration, ~58% at EF with a positive correlation, while nitrate was not a significant predictor of MeHg at BZ for pooled data nor in any individual season. Nitrate was also positively associated with MeHg at EF in December ($p = 0.004$) with an adjusted r^2 of 0.68. While nitrate explained over half the variability of MeHg at EF, and had a positive correlation with MeHg, the trend in field data is in contrast to that of the microcosm results.

Acknowledgment of Limitations of Microbial Characterization Pilot Study at Younger Lagoon

It is important to note that the microbial results reported are from a limited number of DNA extraction replicates ($n = 4$) per YL site. It is best practice to consider the data and interpretations as a pilot study characterization of the microbial community at YL and rely on the findings only as qualitative descriptions. As only surface sediment was sampled (0-4 centimeters depth) and only in October 2020, the microbial community was not characterized for deeper than 4 cm into the sediment nor in 2023. It is also important to note that the microbial sequences identified and reported are from environmental sediment sampling and do not represent shifts in the microbial community as a result of amendments within

microcosms. Comprehensive analyses and descriptions of how chemical inputs shift microbial community composition in regards to carbon amendment and *hgcA* expression are reported in Christensen et al. (2018). Carrell et al. (2021) and Chen et al. (2023) provide data on the effects of nitrate amendments on *hgcA* expression and the work of Li et al. (2022) details the shifts in expression of genes related to nitrogen reduction under conditions of varied forms of reduced sulfur species. Efforts to amplify and visualize an amplicon of *hgcA* from DNA recovered at Younger Lagoon yielded results with DNA fragmentation that obscured the ability to interpret the gel electrophoresis data. Characterization of the *hgcA*-possessing community at YL will require method development to support sufficient amplification of a gene product for sequencing to be successful, so that the identities of *hgcA*-possessing microbes can be revealed.

Microbial Community Composition at Younger Lagoon

The most abundant microbial phyla at BZ included Chloroflexi, Desulfobacterota, and Proteobacteria, while at EF the most abundant phyla were Chloroflexi and Proteobacteria. At the family level of taxonomic classification, Anaerolinaceae, Desulfobacteraceae, Desulfocapsaceae, Desulfosarcinaceae, and Rhodobacteraceae were most abundant at BZ. Anaerolinaceae, Hydrogenophilaceae, and Rhodobacteraceae were the most abundant families at EF. When the communities were compared using the DESeq2 algorithm, genera that had a positive log2 fold change at BZ compared to EF included three members of Proteobacteria and one of Firmicutes (Figure 18). Curiously, three members of the Desulfobacterota phyla were more abundant at EF than BZ, despite Desulfobacterota being a top phylum at BZ though not at EF.

Effect of Amendments on Microcosm Methylation Rates Constants October 2020

K_{meth} values at Beach Zone under nitrate treatment were approximately double that of the control. However, at the 95% confidence level, no significant differences were found

among means of methylation rate between experimental groups at BZ nor at EF. The ANOVA and Kruskal-Wallis test results are shown in Table 13. Box and whisker plots depicting the mean and interquartile range of microcosm k_{meth} values for each treatment show the spread of the data for each group and allow for visual comparison of groups (Figure 17).

As the omnibus tests' results did not indicate any means were significantly different at either location, post-hoc testing was conducted only to reveal which groups had the greatest likelihood of being different. A complete table of results from the Dunnett's test at EF and the Dunn's test at BZ is provided in Appendix D: Supplementary Table S4. These results show that at BZ, the control and the nitrate treatment mean methylation rates were most different of the comparisons made against controls, with the nitrate treatment having the higher mean methylation rate. At EF, the molybdate treatment was the most different from the control, with the molybdate treatment having a lower mean methylation rate. The mean k_{meth} values and standard deviation from all controls and treatments from 2020 microcosm assays are presented in Table 14. A small sample size (n=3) for each treatment likely contributed to the lack of significance despite mean methylation rates differences detectable by visual inspection of the box plots. Indeed, calculations verified that if the experiment were to be repeated with an n of 4 for each group, and had the additional replicates been in the same range as was observed for each group, the results of the Kruskal-Wallis test at BZ and the ANOVA at EF would have both been significant at the 95% confidence level. H or F test statistic values calculated with n = 3 are presented in Appendix E: Supplementary Table S5 along with the relevant critical values and H or F statistic values recalculated with a theoretical n = 4 for each group. Demethylation potential could not be determined as the $Me^{198}Hg$ spike was too low and resulting MeHg concentrations were BLOD.

Effects of Nitrate on Hg Transformation within Microcosm Assays

When nitrate was added to BZ October 2020 sediment in microcosm experiments, the specific methylation rate increased roughly two times relative to the control, though

changes were not statistically significant at alpha = 0.05. In follow up work with microcosm experiments of Beach Zone October 2022 sediment, where both potential methylation and demethylation were tracked (Table 16), nitrate treatments resulted in no statistically significant change in methylation potential relative to the control (one-way ANOVA, type “III”, $p = 0.05$) (Figure 19). However, nitrate addition of 106 mM or 337 uM significantly suppressed demethylation (one-way ANOVA, $p < 0.001$, Tukey’s HSD, $p < 0.001$ for both) (Table 17). Provided a similar effect were to happen at EF, the 2023 microcosm results could help to explain positive correlations between nitrate and ambient methylmercury concentrations at EF, as sustained conditions of nitrate enrichment could lead to unabated methylation and lessened demethylation allowing MeHg to accumulate.

SRB Abundance May Explain Differences in Methylation Potentials at YL

When the bacterial communities at EF and BZ were compared, three members of the SRB Desulfobacterota phyla were less prevalent at BZ than EF, which was unexpected given that Desulfobacterota was in the top ten most abundant phyla at BZ but not at EF. However, the abundance of certain genera of Desulfobacterota being more prevalent at EF does not preclude the presence of any Desulfobacterota at BZ, nor does it suggest members of this phylum are not abundant when grouped collectively. In fact, when sequences belonging to the Desulfovibrionaceae family were quantified, they were found to represent 0.32% of total unique sequences and 0.52% of classifiable (family level) unique sequences at BZ. At EF, Desulfovibrionaceae represented 0.15% of total unique sequences and 0.25% of classifiable (family level) unique sequences. Members of the Desulfovibrionaceae family were noted by Carrell et al. (2021) as having a strong relationship with methylation in their study of methylation rates in periphyton, and were mentioned by Achá et al. (2012) as important methylators in the water column. When 16S rRNA sequences from two main families of SRB were extracted from oligotrophic Lake 658 and quantified with qPCR, researchers found

Desulfovibrionaceae represented < 0.01 – 1.12 % of gene copies and that Desulfobacteraceae represented 0.05 - 33% of gene copies (Achá et al. 2012). It appears that while SRB from the Desulfovibrionaceae family are associated with methylation and appear at both EF and BZ, these sequences are roughly twice as abundant at BZ as EF. Relative abundance of Desulfovibrionaceae being greater at BZ than EF is one reasonable explanation for why a higher methylation rate was observed at BZ in microcosm control experiments than at EF.

Comparison of Potential Methylation Rate Constants (k_{meth}) Across Studies

Other incubation experiments with Hg(II) spikes to sediment or overlying water have been conducted both *in situ* and in laboratory microcosms (Table 15). K_{meth} values for spiking experiments tend to be higher than those expected to naturally occur, as adding Hg(II) spikes increases Hg(II) concentrations above ambient levels, and therefore the amount of bioavailable mercury to be methylated. Freshwater rivers and lakes had the lowest potential methylation, while freshwater wetlands included the highest k_{meth} values amongst the studies compared. Marine systems had potential methylation as high as 21% day^{-1}, which is greater than the maximum k_{meth} of 14.2% day^{-1} observed at estuarine systems though lower than the 51% day^{-1} maximum seen within a freshwater system. Potential methylation at EF, including those amended with nitrate, were amongst the lowest k_{meth} values observed for estuarine systems. K_{meth} values at BZ were within the range from estuarine systems, and even when increased by nitrate amendment, were still lower than the maximum k_{meth} values observed at estuarine locations Kirkpatrick Marsh, Petaluma River or Aviso Marsh.

BZ nitrate treatment k_{meth} values of 1.5 - 3.6% day^{-1} (Table 15) were similar to those for nitrate (and phosphate) amended sediment at Öre River Estuary, Sweden, which had k_{meth} values of 1.0 - 5.0% day^{-1} (Liem-Nguyen et al. 2016). For locations which received ambient fertilizer due to agricultural applications, k_{meth} values ranged from 0-12% day^{-1} in the Everglades, from 0-15.6% day^{-1} in the SF Bay Delta, and from 0.06 - 9% day^{-1} in Yolo Bypass

agricultural wetlands. Interestingly, Yolo Bypass agricultural sites had lower potential methylation (0.06 – 9.0% day^{-1}) than non-agricultural sites (7.0 – 43% day^{-1}), while MeHg accumulation at the former was greater (1800 - 2980 pg/g dry sediment) than at the latter (1300 - 2350 pg/ g dry sediment). A similar phenomenon was observed at YL, where methylation rates at BZ were higher (0.2 – 1.8% day^{-1}) than at EF (0.1 – 0.3% day^{-1}), though EF had higher ambient MeHg concentrations (33 – 218 pg/g dry sediment) than did BZ (BLOD - 36 pg/g dry sediment). Such findings highlight the inherent risk of using MeHg concentration as a proxy for methylation rate, as MeHg concentrations depend both on rates of methylation and demethylation. Thus, percent MeHg (MeHg/HgT*100) was calculated as an index of how much of the total Hg in a system is being stored as MeHg, to provide an estimate of MeHg residence time for a given system (Table 15).

In general, the locations evaluated contained ~1-2% total Hg as MeHg, similar to the average values of ~0.5-2% MeHg given in Hollweg et al. (2010). Notable exceptions include 9.1% MeHg at Cosumnes River Floodplain in the San Francisco Bay Delta, the maximum %MeHg value observed here, and 4.6% MeHg at both Kirkpatrick Marsh, Rhode River, MD, and at Younger Lagoon site EF. In contrast, at BZ, the maximum value was 0.5% MeHg. Ambient concentrations of MeHg at BZ were some of the lowest observed amongst the studies compared, and % MeHg values were generally lower than average, though its maximum value was not atypical when compared to other systems. Values of %MeHg were lower in October at YL (the season sediment was collected for microcosms) in comparison to other seasons. In October, the maximum value of 0.4% MeHg was found at BZ, whereas the highest value at EF was 0.2% MeHg.

Contrasting Beach Zone with Nitrate Amendment in Other Sediments

Previous work has found suppression of Hg methylation under nitrate addition (Gilmour 1998, Todorova et al., 2009; Hines et al., 2012; Chen et al., 2023) and also suppression of demethylation with nitrate (Marvin-DiPasquale and Oremland, 1998; Chen et

al., 2023). What was seen at Beach Zone was in contrast to what was seen in freshwater lake sediment, where methylation was suppressed and demethylation enhanced under nitrate treatment (Todorova et al., 2009). It was also in contrast to the work in rice paddies where both potentials were suppressed with nitrate (Chen et al., 2023). Furthermore, the results at BZ are unlike those at Marado and Grado lagoons, where nitrate addition suppressed methylation potential, and stimulated demethylation potential (Hines et al., 2012). The results at BZ possibly help to explain unresolved trends observed in fertilized agricultural fields, with higher MeHg burdens than unfertilized fields. To interpret the results at Beach Zone is challenging because no change to methylation potential was observed, yet demethylation potential was suppressed. To invoke an argument of SRB and/or methanogens getting outcompeted by NRB would require that both methylation and demethylation potentials move in concert. Invoking an argument of abiotic control on demethylation would help explain a disconnect between the potentials, but the argument put forth by Todorova et al., enhanced MeHg degradation under increased nitrate concentration via an abiotic mechanism described by Zepp (1987), only helps to explain *increased* demethylation potential. Three potential mechanisms are presented, with caveats, to guide future work on the topic. If we consider that SRB and methanogens can both methylate and demethylate, and that both would be expected to be outcompeted for carbon sources by NRB, we would have also expected suppressed methylation potential. The fact that we did not suggests that one of the following may be possible:

1) Nitrate-cycling microbes may also be contributing to methylation, although Mo treatments conducted in Oct. 2020 showed that SRB were the primary methylators at BZ. No difference was seen between Mo alone and Nitrate + Mo, indicating that a group of organisms other than SRB was not poised to utilize nitrate and also methylate.

2) Some evidence exists that sulfur-reducing organisms are capable of utilizing nitrate (Greene, 2003) and while it is possible that methylation could continue

unabated under this alternate metabolic pathway, the Oct. 2020 results do not suggest this is so.

3) The result of lessened demethylation could come about due to SRB and methanogens being outcompeted for carbon, which would also lead to methanotrophic bacteria being robbed of CH_4, their required substrate from which to gain electrons.

Methanotrophs have been implicated in a type of demethylation, methanotrophic demethylation (MD), different than oxidative demethylation that is performed by SRB and methanogens. Methanotrophic demethylation occurs once a ligand, methanobactin, helps import MeHg into the cell (Yu and Barkay, 2022). Methanotrophic microbes confirmed to be involved in this type of demethylation are, thus far, anaerobic (Lu et al. (2017) and Kang-Yun et al. (2022). Sequences classified as *Methylarcula*, a facultative methylotrophic organism (Doronina et al. 2000), were present at BZ, but no sequences associated with methanotrophic bacteria were identified. Under this scenario, we would have to assume that SRB and methanogens were only partly responsible for demethylation, along with a large contribution by methanotrophs. These organisms would be unable to contribute to demethylation if their CH_4 source was absent, as methanogens would produce CH_4 for methanotrophs from longer carbon chains. However, this explanation still fails to address a lack of suppression in methylation potential, which would be expected if SRB and methanogens were indeed outcompeted.

If changes under nitrate addition came about as a result of microbial community changes not dependent on carbon competition, we might anticipate that nitrogen-cycling chemotrophs would be relevant players. For example, if nitrite-oxidizing *Nitrospira,* whose presence was detected at BZ, were to methylate, but not demethylate, the behavior of this organism (or others like it) could explain the results observed at BZ with nitrate addition. Another mechanism that could lead to metabolic shifts in microbes or in community

composition might involve the dynamics of nitrate reduction under sulfidic conditions. Sulfur/sulfide oxidizers that reduce nitrate could become active under nitrate treatments, while not activated in the control, and if such organisms contribute to a larger portion of demethylation than methylation at BZ, results like those seen in 2023 could be observed.

The Effects of Nitrate on Sulfate-Reducing Bacteria

If it is indeed SRB who are primarily responsible for methylating Hg at BZ, as suggested by low production of methylmercury (0.2 +/- 0.1% day^{-1}) when molybdate was added to the microcosms, the results suggest that some subset of SRB organisms may be capable of using nitrate as a terminal electron acceptor, or that other microbial clades are active in Hg methylation, though at lower rates than SRB. This finding is contrary to the expectation that SRB are obligate anaerobes as the addition of nitrate increases redox potential, which inhibits the growth of strictly anaerobic SRB's (Widdel, 1988). Furthermore, dissolved oxygen had a significant positive relationship with MeHg at EF when all observations were pooled ($p = 0.01$), though the trend was fairly weak ($r^2 = 0.22$). As most methylators, and all known *hgcA* carriers, are obligate anaerobes (Gilmour et al. 2013), finding dissolved oxygen to be positively correlated with MeHg is somewhat surprising. The results suggest there may be micro-environments within the sediment that allow for SRB and other anaerobic microbes to be active even when overall porewater oxygen concentrations are greater than zero, and/or that some SRB have flexible metabolisms and can utilize alternative electron acceptors.

As the addition of nitrate and molybdate did not result in rates greater than that of molybdate alone, it is possible that it was still sulfate-reducers who utilized the nitrate at BZ, rather than a different clade of organisms. Indeed, some SRB are capable of dissimilatory reduction of nitrate or nitrite to ammonia (Widdel and Pfennig, 1982) and the work of Seitz and Cypionka (1986) suggests the use of nitrate as a terminal electron acceptor, rather than sulfate, results in a higher growth yield. SRB with facultative metabolisms can yield higher

biomass in the presence of nitrate (Marietou et al. 2009), and as MeHg is a metabolic side product, more growth by methylating organisms might lead to more MeHg. Furthermore, a review of the literature by Cypionka (2000) suggests that not only are some species within the SRB genus *Desulfovibrio* tolerant of oxic conditions, others even respire oxygen! This is consistent with our results where methylmercury appears to be produced by SRB but in a partially-oxic system. It seems broadly anoxic conditions are not required for the presence of SRB nor does the presence of oxygen prevent methylation of Hg. However, it is unknown whether SRB methylate Hg when using nitrate as an electron acceptor.

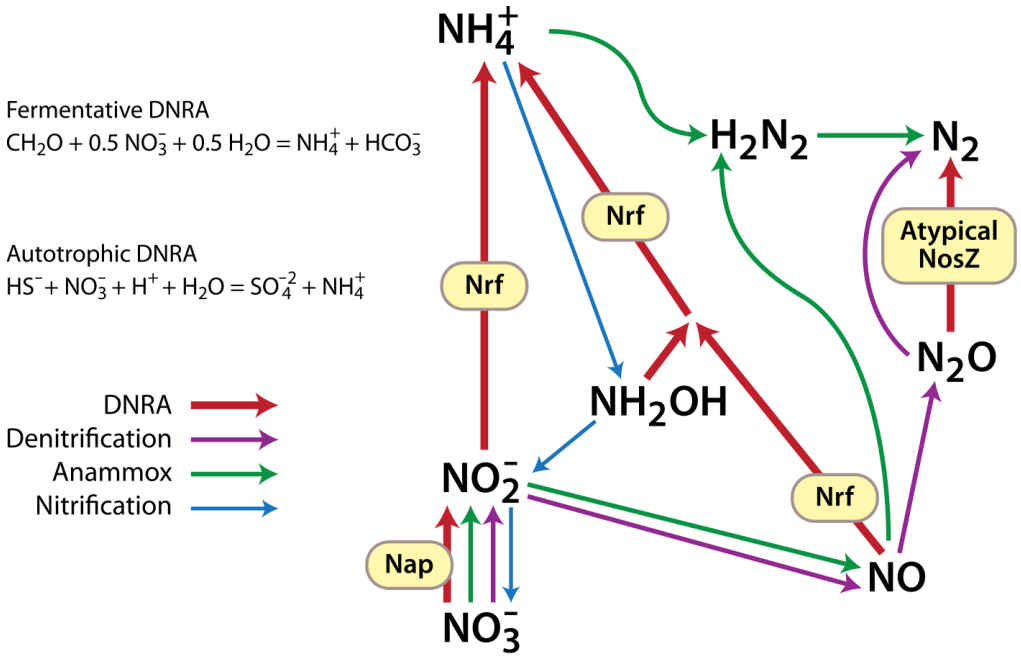

Figure 20. From Giblin et al.(2013). Steps of different nitrogen cycling pathways are shown with colored arrows. Three processes, denitrification, DNRA, and Annamox contribute to nitrate reduction to nitrite. Key enzymes known to be involved in the process of DNRA are in yellow ellipses. Nap = Periplasmic nitrate reductase. Nrf = Cytochrome C nitrite reductase. NosZ = Nitrous oxide reductase.

Nitrogen-Reducing Bacteria and Sulfate-Reducing Bacteria: Interactions

As the microbial consortium could be anticipated to have both methylating and demethylating members, the identity and abundance of specific microbes, as well as their

metabolic rates, would collectively contribute to or subtract from MeHg accumulation. Additionally, metabolites from one organism may feed another, or organisms may compete for the same substrate such as OM, allowing for availability of electron acceptors and donors to control the relative abundance of clades within microbial populations. Denitrifying bacteria reduce nitrate or nitrite to nitrous oxide or nitrogen gas, removing it from a system (Figure 20). Nitrate-reduction can be coupled to oxidation of other substrates, limited to OM and sulfur species for the discussion here. Heterotrophic nitrate reducing bacteria (hNRB) compete with SRB, as they both require OM as an electron donor (Bentzen, 1995; Hubert and Voordouw, 2007; De Gusseme et al. 2009). SRB consume organic matter and utilize sulfate as a terminal electron acceptor (Muyzer and Stams, 2008), a process energetically favorable where sulfate is in ample supply (Widdel and Hansen, 1991; Okabe, 2007) and where more energetically efficient nitrate reduction is unfavorable as a competing process (Laverman et al. 2012). Nitrite reducing sulfur oxidizing bacteria (NR-SOB) would be expected to help SRB, by alleviating accumulated sulfide (Nica, 2000; Greene et al. 2003), which can lead to SRB toxicity. Assisting SRB, through more favorable conditions, and through HgS bioavailability, as previously discussed, would be supportive of methylation.

Nitrate addition has been found to stimulate growth of NR-SOB organisms (Garcia-de-Lomas, 2006) and the presence of NR-SOB has been demonstrated to inhibit SRB in co-culture, even though these organisms may rely on one another in anaerobic environments (Greene et al. 2003). The *Sulfurospirillum* genus contains organisms that oxidize carbon or sulfur, coupled to nitrate reduction, and some *Sulfurospirillum* species even have flexible metabolisms Hubert and Vourdow, 2007). Two sequences classifiable within *Sulfurospirillum* were found, only at BZ. We do not know if these were heterotrophic or sulfur-oxidizers, so cannot say whether they would negatively or positively influence SRB. Organisms confirmed to oxidize sulfur coupled to nitrate reduction (NR-SOB) include two genera found at BZ, *Thioalkalimicrobium* (now reclassified to *Thiomicrospira*) and *Thioalkavibrio* (Hubert and Voordouw, 2007; Tikhonova et al., 2006), though it is not known if these microbes

participates in Hg transformations. Organisms with genes related to nitrate-reduction via denitrification, from genera *Burkholderiaceae* and *Sulfurovum*, were also at BZ.

Sulfur-oxidizing organisms with functional genes for dissimilatory nitrate reduction to ammonia (DNRA) were present at BZ, as sequences from the genera *Lentimicrobium*, *Hydrogenophaga*, and *Nocardioides* were found. DRNA is a process that keeps nitrogen within a system. DRNA organisms can be hetrotrophic or chemotrophic also, and accordingly would have the ability to compete with or assist SRB, were they to oxize OM or sulfur, respectively. No DRNA-performing microbes have been conformed to methylate, though Sonke et al. (2023) report that 11% of organisms with a complete set of genes for conducting Hg methylation (termed *hgc*+ microbes) also are capable of performing dissimilatory nitrate reduction to ammonia (DNRA). Denitrification would be expected to be the dominant nitrogen reduction process (as opposed to DNRA) under conditions of higher nitrate availability and relatively lower availability of electron donors (organic carbon at BZ) ((Kraft et al., 2014; Yoon et al., 2015). However, experiments with different forms of sulfur addition revealed that DNRA becomes the primary nitrogen-reduction pathway when sulfide concentrations are enhanced (Li et al., 2022).

Microcosms from BZ 2023 can be assumed to have enhanced sulfide concentrations, based on porewater and sediment sulfide data from the previous round of experimentation in Oct. 2020, along with the qualitative observations of characteristic sulfide odor during field sampling in 2023. The presence of sequences with functional genes for DRNA, along with evidence that ammonia accumulates (Figure 13), especially deeper in the sediment where reduced sulfur concentrations are greatest, were found at BZ, suggesting that the DRNA process is happening at YL. Sequences from ammonia oxidizing *Nitrosopumilus* were identified at BZ, suggesting that this is one way ammonia is transformed within the system.

SRB Metabolic Flexibility and Speculative Mechanisms to Explain Suppressed k_{demeth}

Results of the 2022 microcosm assays show that k_{meth} decreased with nitrate addition, however k_{demeth} was unchanged. If SRB were responsible for both Hg methylation and demethylation, we would anticipate k_{meth} and k_{demeth} to move in concert were SRB outcompeted by nitrate reducers. So what can help explain a disconnect between the methylation and demethylation potentials? One possibility could be that SRB switch to respire nitrate when it is available, via participation in a portion of the DNRA pathway. The work of Bourceau et al. (2023) has shown that under fluctuating redox conditions with pulses of nitrate availability, microbes traditionally classified as sulfate reducers switch to nitrate reduction when nitrate is available, and that SRB may even become more abundant under conditions of intermittent nitrate. A marker gene for DNRA (nrfA) was found to be associated with the transcripts of sulfur reducing microbes, rather than sulfur oxidizing microbes, as was hypothesized (Bourceau et al. 2023). While we cannot say with certainty that SRB at YL have flexible metabolisms, evidence in support of the presence of SRB, such as sulfide accumulation and DNA sequences classifiable within the Desulfovibrionaceae phylum, exists. An accumulation of ammonium at YL also suggests that some microbes there are capable of DNRA. SRB employing a different metabolic strategy is one possible mechanism to help explain the results observed in the 2022 microcosm assay.

It is possible that MeHg is both produced and degraded by SRB, and that MeHg is also demethylated by denitrifiers. Within the microcosms, methylation observed in the control may have arisen due to SRB activity, as did methylation observed in the nitrate treatments. Even if SRB are not capable of performing all steps of DNRA, the 2022 microcosm results suggest that SRB may be poised to utilize nitrate and would still be able to methylate Hg while utilizing an alternate terminal electron acceptor. Under this condition, heterotrophic denitrifiers could be outcompeted by SRB for organic carbon, which would suppress their

contribution to demethylation. Correspondingly, we can see an effect within the demethylation assay that may be due to competition between microbes.

One plausible explanation is that denitrifiers and SRB contribute to demethylation at YL. With added nitrate, an increase in denitrification would be expected along with an increase in demethylation, based on the work of Hines et al. (2012). What was seen was a decrease in demethylation under nitrate treatment. If SRB switched to nitrate-reduction and were, or became, more abundant in the sediment than denitrifiers, the anticipated effect would align with what was seen in the demethylation essay. If heterotrophic DNRA-performers who are not sulfate reducers were the ones in competition with denitrifiers for organic carbon, we would have expected to see the effect of competition in both the methylation and demethylation assays, assuming heterotrophic DNRA performers also do not methylate. However, in the methylation assay, no decrease in MeHg production was observed, suggesting it was not heterotrophic DNRA performers who accessed the carbon, as there was a lack of evidence for methylating SRB being outcompeted. This speculative conclusion depends on the assumptions that: 1) SRB are the main methylators at YL; 2) heterotrophic DNRA-performers who are not sulfate reducers are also not capable of Hg methylation; and 3) heterotrophic denitrifiers demethylate, but do not methylate.

An explanation for why SRB could not benefit from the nitrate plus molybdate treatment in the 2020 microcosms was because the mechanism of action of molybdate causes sulfate reducers to get stuck in the first step of sulfate reduction, leak ATP from the cell, and eventually lyse (Kögler, 2021). Therefore we could see no evidence of a switch in respiratory strategy as the molybdate addition likely killed sulfate reducers, disallowing them to take advantage of any metabolic flexibility. Finally, it must be noted that the molybdate treatment was not combined with the demethylation assay in the 2022 microcosms. Therefore, the assumption that SRB are the primary methylators at YL may be invalid and a portion of the methylation observed in 2022 could have been attributable to a different clade of microbes. The work presented here would be best interpreted as preliminary findings that

warrant further exploration into whether or not sulfate reducers at YL participate in one or more steps of the DNRA pathway, and whether sulfate reducers still participate in Hg methylation, were they to switch respiratory strategy. Furthermore, identifying a genetic basis that directly confers demethylation capability to denitrifiers would be beneficial to the study of Hg cycling.

Comparing the Demethylation Assay At YL to Nitrate Amendments in Rice Paddies

Under conditions that inhibited sulfate reduction, such as nitrate addition, methanogenesis would also be expected to be unfavorable (Kögel-Knabner et al. 2021). Indeed, Drake et al. (1996), found that demethylation by methanogens was suppressed with nitrate addition, and work in rice paddies found similar results (Chidthaisong and Conrad, 2000). Thus, an effort to explain the finding of suppressed demethylation in paddy soils by way of a microbial mechanism relied on inhibition of the role of methanogens in demethylation (Chen et al. 2023). The work of Yu et al. (2013) confirms methanogens as Hg demethylators and a role for competition between types of methanogens that have implications for net methylation or demethylation have been suggested (Hao et al. 2024). However, stimulation of demethylation has also been demonstrated (Hines et al., 2012) with nitrate addition to lagoon sediment, with the effect ascribed to nitrate-reducing bacteria. Why then, if SRB and methanogens were outcompeted in favor of nitrate-reducers in rice paddies, was demethylation not stimulated by denitrifiers? One possibility is that the type of N-reducers present in rice paddies did not have a contribution to demethylation as was seen in lagoon sediment, whereas the methanogens in rice paddies did participate in demethylation.

N-Cycling Microbes and Demethylation

While there is evidence that denitrifiers participate in demethylation (Hines et al. 2012), less is known about the role of organisms capable of DRNA in demethylation. Further complicating an understanding of how these pathways may affect demethylation is the fact

that denitrification can be based on sulfur oxidation (chemotrophic) or organic matter oxidation (heterotrophic). If organic matter is the substrate getting oxidized, competition between microbes can be induced, ultimately affecting demethylation potentials. However, if sulfide is getting oxidized, it is less clear how a removal of reduced sulfur species would affect MeHg demethylation. Though the topic of how reduced sulfur phases and OM affect MeHg solubility has received preliminary research attention (Skyllberg et al. 2021: Barrouilhet, 2021), open questions remain in modeling these interactions, and how MeHg solubility influences demethylation remains a knowledge gap. Until these processes have been better characterized, it is not possible to speculate on how sulfur oxidation would affect demethylation.

Fe-Reducing Bacteria at Younger Lagoon

The putative presence of FeRB was also investigated via taxonomic classification of 16S rRNA sequences, as some members of this clade are capable of methylating Hg. *Geobacter metallireducens,* an FeRB that can also use nitrate as a terminal electron acceptor (Kerin et al. 2006) and a confirmed methylator (Fleming et al. 2006) is one such bacterium, but the 16S rRNA sequencing results gave no indication that any members classifiable within the *Geobacter* genus were present at YL. It does not appear that FeRB are a notable part of the methylating community at YL.

Future Work at Younger Lagoon

Future work at Younger Lagoon could include BES and Mo along with demethylation assays, in attempt to reveal contributions to Hg transformation mediated by methanogens, or by syntrophy between SRB and methanogens. Studies could also track transformations of N and S species along with Hg cycling within microcosms, and pair this data with how the microbial community composition has changed along time points. In this way, the threshold concentrations of nutrients or metabolites that lead to the regulation of microbial processes

could be better understood. Investigations could pursue whether methanogens are sensitive to nitrite that results from N-reduction coupled to S-oxidation, and if this limits their ability to perform demethylation. The presence of *Sulfurospirillum* sequences at BZ along reinforce the need for more research on NR-SOB *in situ* interactions with SRB, along with an investigation into putative NR-SOB methylation capabilities. These questions deserve attention in the future, as it is likely that both denitrifiers and organisms performing DRNA affect ecological niches which in turn affect the metabolisms of methylators and demethylators.

Single-Predictor Models

Linear models with single predictor variables were constructed for each variable of interest with MeHg as the dependent variable, and applied to pooled seasonal data. Multivariate models were examined, but problems with overfitting arose and the general "rule of thumb" for the number of observations needed per predictor variable was estimated by the "*m*/15 rule" as discussed in Harrell (2015), where *m* represents the number of observations required for a reliable model. With 27 observations, we lacked the data to include more than one predictor. Thus, the p-values and r^2 (Table 12) values from single predictor models were inspected and used to identify models of interest.

Nitrate explained 58% of the variability in MeHg at EF (p = 2.2E-6), the most of any predictor, and had a positive coefficient of 0.77 , indicating a positive relationship between nitrate and MeHg. A limitation of EF models is that none had residuals that were normally distributed (p-values of models and of residuals are given in Appendix B: Supplementary Table 2 (EF) and Appendix C: Supplementary Table 3 (BZ)). In contrast to the positive relationship between nitrate and MeHg found at EF, the greatest amount of variability in MeHg at BZ was explained by porewater AVS, at 24% (p = 0.01). The coefficient of the slope was -0.49 indicating an inverse relationship between MeHg and porewater AVS. However, here also the residuals of the model were not normally distributed (p = 0.04, Shapiro-Wilk

test). Porewater AVS was not a significant predictor of MeHg at EF ($p = 0.1$) and nitrate was not significant at BZ ($p = 0.27$). Oxygen saturation explained about 25% of the variability in MeHg at EF, and was significantly positively correlated at EF ($p = 0.01$) though not at BZ ($p = 0.16$). Ammonium had a significant negative correlation with MeHg at both sites for pooled seasonal data ($p = 0.03$ BZ; 0.02 EF). The percentage of variability explained was fairly low, 18% and 21% at BZ and EF respectively, and the residuals were not normally distributed for either site. Depth explained a similar amount of variability in MeHg, 18% at BZ and 21% at EF, and was significantly negatively correlated with MeHg at both sites, $p = 0.03$ and 0.01, respectively. Temperature was found to have a negative relationship with MeHg at both locations, though p-values were insignificant for both sites (0.09 and 0.18 for EF and BZ, respectively). Models with significant p-values ($p < 0.05$) are in bold text. For the Shapiro-Wilk test of residuals, p-value > 0.05 indicates no marked deviations from normal distribution.

Conclusion

Nitrate addition led to no change to k_{meth} and significant suppression of k_{demeth} within anaerobic microcosms and therefore suggests that eutrophication has the potential to increase net methylmercury production in coastal estuaries, though the conditions under which this occurs may be additionally influenced by dissolved oxygen, sulfide, or the presence of certain microbes, and has spatial variability that contrasts greatly within a single site. The positive association observed between ambient MeHg concentrations and ambient nitrate concentrations is concluded to be as a result of the combination of these conditions under sustained nitrate allowing for MeHg to accumulate. In previous studies, nitrate amendments have been shown to suppress both methylation and demethylation potentials by SRB, due to competition for OM by nitrate reducers. Why k_{meth} and k_{demeth} did not vary together with nitrate addition at YL is unknown, though findings were hypothetically attributed to heterotrophic SRB capable of respiring nitrate when available, and competing with denitrifiers who may have otherwise contributed to demethylation.

CHAPTER 4. Geochemical Controls on Mercury Methylation Rates in Sulfur-Enriched Agricultural Soils

Abstract

Agricultural cropland receives sulfur (S) applications for a variety of functions, as a soil conditioner, pH regulator, fertilizer, and fungicide. To investigate the effect of fungicidal elemental S applications on the production of the toxic and bioaccumulative monomethylmercury (MeHg) species from mercuric ion (Hg(II)) in upland soils, we measured the potential rate of methylation and demethylation in agricultural and non-agricultural site types of the Napa River Watershed. Soils cores were collected from forests, grasslands, and vineyards in the dry and wet seasons. Methylmercury (MeHg) production does occur in upland soils, though not rapidly, with potential, pseudo-first order methylation rate constants (k_{meth}) ranging from below detection (BD) to 0.56 %/day in forests, BD to 0.37 %/day in grasslands, and BD to 0.62 %/ day in vineyards. These rate constants were of similar magnitude to those of upland boreal forest soil (0.011 %/day). k_{meth} values in the wet season were higher on average at all site types compared to the dry season, with the most dramatic increase in k_{meth} occurring between dry and wet season vineyards ($p < 0.001$), with average k_{meth} values of 0.02 +/- 0.03 %/day and 0.13 +/-0.17 %/day, respectively. Sulfate concentration was significantly higher in dry vineyards than in non-agricultural sites, though k_{meth} values at vineyards were not higher than forests in either season. Elevated sulfate was not associated with enhanced k_{meth}, instead, similar to previously investigated aquatic systems, concentrations of sulfate exceeding 20 mg/L (0.2mM) were found to suppress potential methylation. LOI (as a proxy for % organic matter) was not significantly correlated with k_{meth} ($p = 0.3$). Other geochemical variables were investigated as possible controls on MeHg production in upland soils, and while HgT concentration and percent moisture (w/w) content were useful in explaining some of the variability in k_{meth} across all site types, these variables had low adjusted r^2 values of 0.44 and 0.11, respectively. Another biogeochemical

factor not investigated in this study may be responsible for the larger k_{meth} values observed in forests.

4.1 Introduction

Hg is a toxic element that is naturally present in the Earth's crust and atmosphere, though the amount of Hg in the global cycle has increased due to anthropogenic activities (Mason et al. 1994). Inorganic mercury, Hg(II), can become methylated abiotically (Celo et al. 2006) or, more commonly, biotically via a microbially mediated process, converting Hg into an organo-metallic form, methylmercury (MeHg) (Jensen and Jernelöv, 1969). Once methylated, MeHg has the propensity to enter food webs in the terrestrial (Weiss-Penzias et al. 2019; Cristol et al. 2008), freshwater (Watras et al. 1998) and marine (Zhang et al. 2020) environments, where biomagnification (Chen et al. 2008) and bioaccumulation (Driscoll et al. 2007) occur (Gentès et al. 2021; Mason et al. 1996) leading to adverse human and environmental health (Crump et al. 2000; Tan et al. 2009; Wu et al. 2024). Understanding the geochemical processes that lead to the production of MeHg warrant attention.

Hg deposition, sulfur, and dissolved organic matter (DOM) have previously been identified as controls on MeHg production in wetland systems (Aiken, 2004). Research supporting a connection between sulfate-enrichment of sediments and enhanced MeHg production has been conducted in the Florida Everglades Agricultural Area (EAA) (Orem et al. 2019; Pollman, 2015; Gilmour et al. 1998). In these water-saturated, lowland soils and sediments, sulfate was found to be the primary control on MeHg-production (Corrales et al. 2011). Agricultural crops receive S as a soil conditioner, pH regulator, fertilizer, or fungicide, and sulfate is known to stimulate Hg-methylation by stimulating the metabolisms of heterotrophic sulfate-reducing bacteria (SRB) (Griffith et al. 2015). When SRB grow and divide MeHg is produced as a metabolic side product (Choi et al. 1994b). While not the only microbes capable of Hg-methylation, SRB were the first specific clade to be implicated in the process (e.g., Compeau and Bartha, 1985) and are primarily responsible for MeHg

production in most anoxic sediments (Heyes et al. 2006). Brackish and marine systems have ample sulfate available to support SRB metabolisms, while freshwater systems, like the Everglades, only have sufficient sulfate when it is introduced by anthropogenic activities such as agricultural applications. Thus, anthropogenic sulfate has the potential to stimulate MeHg production by SRB in locations that would otherwise be sulfate limited.

Sulfate reduction by SRB in the presence of bioavailable Hg(II) leads to both MeHg production (Choi et al. 1994a) and an accumulation of sulfide (Benoit et al. 1999. Sulfate has a stimulatory effect on Hg-methylation, in concentrations from 0.01 mM - 0.2 mM (Orem et al. 2019), whereas greater concentrations have been shown to lead to an accumulation of sulfide sufficient to inhibit MeHg production. Sulfide has been found to suppress MeHg production at concentrations >10 μM in porewater (Benoit et al. 2001binfluence) or >1.8 mg sulfide/g sediment (Craig and Moreton, 1983). However, more recent work has shown that maximum MeHg production in cultures occurred when the culture medium had a range of sulfide concentrations from 0.1 to 0.5 mM, regardless of the form of sulfur added initially (Barrouihet et al. 2022). It seems that higher sulfide concentrations than have been previously reported can lead to different effects on k_{meth} values in a culture experiment with a single model organism than were observed for environmental samples. The lack of consensus for a sulfide concentration threshhold at which MeHg production is suppressed suggests results may have limited applicability across site types or experimental conditions and thus require site specific investigation.

Vineyards are another system, like the Everglades, that receive agricultural S applications. Wine grapes receive elemental S to prevent powdery mildew disease (CDPR, 2018). Atmospheric deposition of S would otherwise be the sole source to this region which would leave it sulfate-limited for SRB activity. Wine grapes grown in Napa receive an average of 80 kg/hectacre/year of elemental sulfur applications and this crop type covers over 45,000 acres of the Napa River Watershed (Napa Valley Vintners, 2024). Applied

elemental S is oxidized to sulfate in dry fields, leaving the soil enriched in the substrate known to stimulate SRB metabolism.

The soils of this upland region provide a contrasting study region to the previously investigated, water saturated soils of the Everglades Agricultural Area (EAA), and to the more recently studied agricultural soils of rice paddies as vineyards have aspects of both of these systems. Vineyards receive S applications, as did sites in the Everglades, though vineyard soils are not continuously saturated. Vineyard soils experience alternating wet and dry (AWD) periods, akin to rice paddies, as California has a dry season (May-September) and a wet season (October-April). AWD has been shown to select for SRB (Guan et al. 2023) in rice paddies and has also been shown to lead to spikes in soil MeHg levels following reflooding, as opposed to continuous flooding management practices (Rothenberg et al. 2014). While oxygenated vineyard soils may seem an implausible location for harboring microbes who thrive in anoxic conditions, the work of Angle et al. (2017) suggests that oxic soils can host microsites (soil aggregates) capable of supporting anaerobic processes. Unlike other agricultural crops, wine grapes do not typically receive N fertilizer, providing a unique environment to study the effects of S on MeHg-production without the confounding variable of nitrogen addition that could favor nitrate-reduction. Furthermore, terrestrial Hg could be enriched in the Napa River watershed as a result of historic Au mining (Smith et al. 2008), fossil fuel combustion (Conaway et al. 2005), and wet (Weiss-Penzias et al. 2016) and dry (Wright et al. 2014) deposition.

Thus, as conditions of sulfate-enrichment, zones of anoxia, and Hg-deposition are met, it is hypothesized that agricultural soils of the Napa River watershed could be locations of enhanced MeHg production which could potentially affect the water quality and wetland ecosystems of San Pablo Bay and San Francisco Bay. To test this hypothesis, we measured the specific Hg methylation rates in S-amended vineyard soils and nearby unamended forest and grassland soils in wet and dry seasons, as well as other geochemical variables, to assess whether land-use and S-amendment drives changes in the production of MeHg.

Primary goals of the study are to answer whether upland soils that undergo periods of wetting and drying are zones of MeHg production, to examine whether sulfate-enriched soils have different potential methylation rates than unamended soils, and to detail the geochemical characteristics that support enhanced potential methylation rates in agricultural and non-agricultural soils of the Napa River Watershed.

4.2 Methods

Site Description

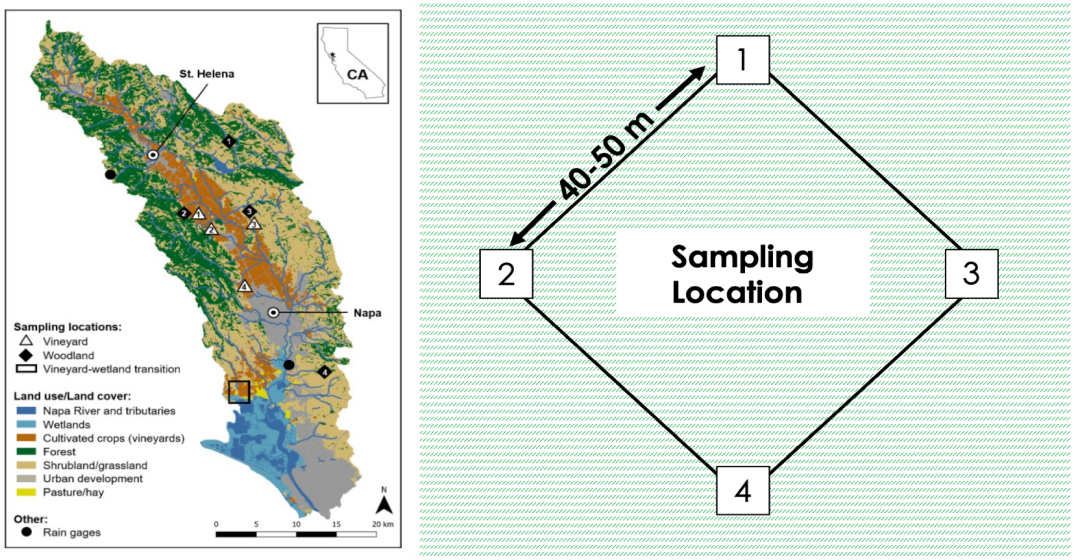

Figure 21. A map of the Napa River Watershed from Hermes et al. (2022) (left) and a schematic diagram of the arrangement of the four "nodes" sampled within each site type (right). On the map, vineyards are shown in brown, forests in green, and grasslands in tan. The hydrologic connection to San Pablo Bay is illustrated with dark blue lines representing the Napa River and its tributaries entering the wetlands of the bay illustrated in light blue. On the schematic diagram, the locations of 4 sampling nodes within each site type were spaced ~40-50 m apart in a diamond shape.

The Napa River Watershed (NRW) is 1103 km^2 and experiences a Mediterranean climate with distinct dry (April through September) and wet (October through March) seasons. Wine grapes, grown in the dry season and dormant in the wet season, are the primary crop grown in this region (Figure 21). During the growing season, wine grapes receive weekly to biweekly applications of elemental S as a fungicide. The NRW receives more annual

precipitation to the north, with 931 mm in St. Helena, than to the south, with 518 mm in Napa (Arguez et al. 2012). During the wet season, fields can become saturated to ≥0.5 m depth below the soil surface (Hinckley et al. 2008). The range of elevation for sampled sites was 36 – 564 m above sea level and included grasslands and vineyards at both the low and high end of the range. The range of elevations for forested sites was 101-131 m.

Field Sampling

Field sampling was conducted in October 2022 (dry season) and February 2023 (wet season) in Napa, CA at 4 vineyards, 2 grasslands, and 2 forested sites. Soil was sampled from four locations, or "nodes", at each site (Figure 21), with each node ~40-50 meters apart. The arrangement of the nodes across a site was designed to provide spatial representation of the location. Two soil cores (0-10 cm depth) were sampled at each node in both the dry and wet seasons using a hand-operated corer or bulb-planting trowels. One core was used to prepare microcosms (described in detail below) and a "companion core" was for bulk geochemical analyses. Leaves and debris were cleared away from the soil before cores were taken. Cores were bagged in zip-sealed bags and placed in mylar bags with oxygen-scrubbers for transport to the lab. Samples were kept on ice packs during transport and were stored on ice in coolers in the lab until microcosm preparation (~24 hr after collection).

Isotope-Enriched Standard Solutions

Following the methods of Martin-Doimeadios et al. (2002) and Filipelli and Baldi (1993), isotopically enriched $Me^{198}Hg$ and $Me^{199}Hg$ were synthesized for use in the microcosm experiments from ^{198}HgO and ^{199}HgO sourced from Oak Ridge National Labs. $Me^{198}Hg$ and $Me^{199}Hg$ had final concentrations of 2.97 ug/ml and 115 ng/ml, respectively. A solution of $^{200}Hg(II)$ in 0.1% HCl and deionized water was prepared using isotopically enriched $^{200}HgCl_2$ from Oak Ridge National Labs and had a final concentration of 165 ug/ml. A Thermo Element XR Inductively Coupled Plasma Mass Spectrometer (ICPMS;

ThermoFisher Scientific, USA), hyphenated to a Tekran 2700 Methylmercury Analyzer, was used to determine the isotopic composition of all three enriched-isotope solutions. The Thermo Element XR was also used to determine the concentration of the isotopically enriched $Me^{199}Hg$ solutions by reverse isotope dilution (Hintelmann and Evans, 1997).

To prepare the final spike solution added to microcosms $^{200}Hg(II)$ and $Me^{198}Hg$ enriched isotopes were added to one liter of deionized water and bubbled with nitrogen gas for 30 minutes within a glove bag to deoxygenate the solution. Within the dry season spike the $^{200}Hg(II)$ concentration was 23.1 ng/ml and the $Me^{198}Hg$ was 0.101 ng/ml For the dry season, the average concentration of $^{198}MeHg$ within the dry microcosm soil was 0.057+/- 0.002 ng/g and the average $^{200}Hg(II)$ concentration was 12.9 +/- 0.48 ng/g dry soil. The $^{198}MeHg$ spike in the dry season was too low for demethylation to be quantified above background MeHg and the amount of $^{198}MeHg$ in the spike solution for the wet season was increased to yield a final concentration of ~0.6 ng/g dry soil and the $^{200}Hg(II)$ concentration was kept the same as the dry season (~13 ng/g dry soil), allowing for both potential methylation (k_{meth}) and demethylation (k_{demeth}) rate constants to be calculated. A final version of the data presented here will be available in a forthcoming publication. Readers are encouraged to refer to the published manuscript for the most up to date information, as concentrations of spike solutions are being reanalyzed and reported k_{meth} and k_{demeth} values may shift after recalculation.

Isotope-Spiked Microcosm Preparation

Microcosms were prepared with soil sampled from four vineyards and four non-agricultural sites, two forests and two grasslands, so that potential methylation (k_{meth}) and demethylation (k_{demeth}) rate constants (assuming pseudo-first order kinetics) derived from the conversion of stable Hg-isotope tracers (Hintelmann et al. 2000) could be compared between site types. Soil from a single node was homogenized and subsampled to prepare three microcosms, one each to be incubated for 0 h, 24 h, and 48 h. A homogenized subsample of

a soil core (~20 g) was added to a glass serum jar in a glove bag filled with N_2 gas to maintain anoxic conditions. A spike solution (~10 mL; consisting of $^{200}Hg(II)$ to track methylation and $^{198}MeHg$ to track demethylation) was added to the soil in each serum jar before being capped with a butyl rubber septa and crimp sealed. Duplicate microcosms of each of the 3 time points (0 h, 24 h, 48 h) were prepared from one vineyard and one non-vineyard location for both wet and dry season to reveal biological variability within soil from a single location. Microcosm jars were placed in boxes and allowed to incubate in the dark at room temperature for periods of 24 or 48 h. The t=0 replicates were "killed" by freezing promptly (6-22 min) after the spike solution with enriched isotope standards was added. All samples were frozen at -80°C until solid, and lyophilized to a constant weight and then homogenized by hand with a clean spatula.

Microcosm Sample Distillation

Lyophilized soil subsamples (~0.24-0.37 grams) from microcosms were distilled following the methods described in Hammerschmidt and Fitzgerald (2006) and consistent with EPA Standard Method 1630. In summary, the dry material was weighed into a tared Teflon distillation vial and ~45 mL of MilliQ water was added atop the sediment followed by 450 µL of 2 M sulfuric acid, 450 µL of 1 M copper sulfate, and 212 µL of 20% (w/v) KCl solution. Approximately 100 pg (as ^{199}Hg) of $^{199}MeHg$ spike was added as an internal standard to allow for quantification by species-specific stable isotope dilution following established techniques described in Hintelmann and Ogrinc (2009). The samples were then steam distilled under constant N_2 flow using an all Teflon system at 110°C into collection vessels pre-filled with 5 mL of MilliQ water and placed in an ice bath for 2.75-3.5 hours. Samples were distilled until ~75% (35 ml) of the liquid on the distillation side had transferred. A 35 ml volume allowed for technical replicates to be analyzed in duplicate. Samples were stored refrigerated and in the dark for approximately 24 hours prior to ethylation and analysis. A distillation reagent blank and a soil certified reference material (CRM) (IAEA-456) were

distilled along with each set of 6 soil subsamples. A reagent blank was prepared by adding ~45 mL of MilliQ water to a distillation vessel, then adding 450 µL of 2M sulfuric acid, 450 µL of 1M copper sulfate, 212 µL of 20% (w/v) KCl solution, and a ^{199}MeHg spike, as was done for a soil sample, and subjecting the vessel to the distillation procedure within the hot block.

ICPMS Analysis

Subsamples (~10-12 mL volumes) of distillates were placed in septum-sealed amber vials, buffered with 40 µL of 2 M potassium acetate solution, treated with 20 µL of 2.5% (w/v) ascorbic acid and ethylated with 25 µL of 1% (w/v) sodium tetraethyl borate (NaTEB) and allowed to react for a minimum of 2 h. The derived methylethylmercury was then quantified as Hg by cold-vapor atomic fluorescence spectroscopy (CVAFS) following isothermal gas chromatography using a Tekran 2700 methylmercury analyzer (5 min purge, 60 mL/min carrier gas flow, 70 °C oven temperature, 700 °C pyrolysis temperature). The Tekran 2700 was used to provide GC-separation of Hg species prior to their introduction into the ICPMS, allowing for detection of peaks corresponding to Hg0, MeHg, and Hg(II). Isotope-specific peak areas were integrated using a Python script available at https://github.com/chlamborg/HgICPPeakIntegration (Lamborg, 2023). Peak areas were used in the matrix algebra calculations of Ouerdane et al. (2009) following the technique of Hintelman and Ogrinc (2009) for separating the signal from Me^{200}Hg produced from the spike from that of the background pool of ^{200}Hg(II) in the soil. Peak areas modified by the calculations were used to calculate the ratio of the peak areas of Me^{200}Hg to Me^{199}Hg. The ratio of Me^{200}Hg/Me^{199}Hg was used to solve for the final amount of "excess Me^{200}Hg" by multiplying the ratio times the known amount of Me^{199}Hg spiked into the distillation. The quantity of excess Me^{200}Hg from each sample replicate was blank corrected by subtracting the quantity of Me^{200}Hg coming from the daily average reagent blank (one distillation blank per day, with 2 technical replicates analyzed). Tabulated values of isotopic abundance were used to determine the portion of MeHg coming from any isotope other than measured

$Me^{200}Hg$. The resulting "corrected value" was used to calculate the average concentration in pg/g dry soil of a given sample.

Calculation of Potential Methylation Rate Constants

Potential methylation rate constants (k_{meth}) were calculated using a modified version of the equation reported in Hintelmann et al. (2000). Pseudo-first order rate constants are described as "potential rate constants" or "methylation/demethylation potentials" as the isotope-enriched spikes may be more bioavailable than native Hg(II) (Mitchell and Gilmour, 2008). The modification was to subtract the concentration of $Me^{200}Hg$ from t = 0 h microcosms from that of the t = 24 h or 48 h microcosms to remove a contribution from "initial" methylation. Munson (2014) describes the importance of making this correction. Following that, the "time-zero corrected" concentration value was divided by the calculated spiked concentration of $^{200}Hg(II)$ for each t = 0 h microcosm. This ratio was subtracted from 1, and the natural log taken. Finally, the proportion of the spike methylated was converted to a rate constant by multiplying by negative 1, dividing by the number of days (2), and multiplying by 100 to express as a percent. The following equation was used to calculate potential methylation rate constants with units of percent per day:

$$k_{meth} = (-\ln(1-[Me^{200}Hg]_{time} - [Me^{200}Hg]_0)/[^{200}Hg]_0)/time)*100$$

$[Me^{200}Hg]_{time}$ is the amount of excess $Me^{200}Hg$ measured in the sample of microcosm soil in ng/g at the final time of incubation, either 24 or 48 hours. $[Me^{200}Hg]_0$ is the amount of excess $Me^{200}Hg$ measured in the sample of microcosm soil in ng/g from the instantaneous control (time = 0). $[^{200}Hg]_0$ is the amount of $^{200}Hg(II)$ spiked into the instantaneous microcosm in ng/g and time is the amount of time incubated in days. Multiplying by 100 gives units of percent per day.

Calculation of Potential Demethylation Rate Constants

Potential demethylation rate constants (k_{demeth}) were calculated from a modified form of the following equation:

$$k_{demeth} = (-\ln([Me^{198}Hg]_{time} / [Me^{198}Hg]_0) / time) * 100$$

$[Me^{198}Hg]_{time}$ is the amount of excess $Me^{198}Hg$ measured in the sample of microcosm soil in ng/g at the final time of incubation, either 24 or 48 hours. $[Me^{198}Hg]_0$ is the amount of excess $Me^{198}Hg$ measured in the sample of microcosm soil in ng/g from the instantaneous control (time = 0). Time is the amount of time incubated in days. Multiplying by 100 gives units of percent per day. As some t = 48 h microcosms had higher $Me^{198}Hg$ concentrations than did corresponding t = 0 h microcosms, suggesting that "remethylation" of demethylated $Me^{198}Hg$ took place, a modification to the rate constant calculation was made. Rather than dividing the t = 48 h $Me^{198}Hg$ concentration by that of the t = 0 h, the t = 48 h $Me^{198}Hg$ concentration was divided by the calculated spike amount of $Me^{198}Hg$ in the t = 48 h condition. In doing so, we no longer have a snapshot of instantaneous demethylation, and instead are making the (potentially erroneous) assumption that the amount of demethylation occurring between 0 and 48 h is representative of the potential demethylation happening in the field. Not all microcosms had a t = 48 h that was lower than that of the t = 0 h. However, dividing by the calculated spike amount of $Me^{198}Hg$ in the t = 48 h microcosm was done for all samples for consistency in reporting and comparing potential demethylation rate constants between locations.

Companion Core Processing

The companion cores described above, were sampled, transported and lyophilized according to the methods described for the microcosm core. Companion core soils were

sieved at 2 mm prior to subsampling for analysis with DMA-80 (HgT) or Tekran 2700 analysis (MeHg).

Companion Core HgT Analysis

A Direct Mercury Analyzer (DMA-80) was used to analyze HgT concentrations from ~0.1 g subsamples of the companion cores. Three to five replicates were analyzed for each sample, and the final concentration for each sample was determined as an average of the replicates having RSD within 15%. The DMA-80 was calibrated with serial dilutions of a NIST-3133 $HgCl_2$ standard and liquid standards were analyzed in acid-cleaned and heated (550 ^oC) quartz sample boats. Boat blanks produced < 0.003 ng of Hg, the limit of detection. For a 0.1 g sample this gives a method limit of 0.03 ppb. Liquid standards and certified reference materials (CRMs) were run on the DMA-80 at the beginning and end of the run sequence and between every 20 samples. Samples were considered valid if the % recovery of the CRMs was between 90-110% of the accepted values. CRMs used were IAEA BCR-320R (Channel Sediment) and IAEA-456 (Marine Sediment).

Companion Core MeHg Analysis

Distillation and ethylation were carried out as described previously, without the use of $Me^{199}Hg$ as an internal standard. MeHg concentrations in soil were determined using a calibration curve prepared from bulk MeHg working standard solution (~1 pg/μL), diluted from a 10 μg/mL primary standard obtained from Brooks Rand Inc.. A range of standards bracketing the sample concentrations was run on Tekran 2700 each day of analysis along with a distillation CRM (IAEA-456) and blank. The CRM distillation and analysis yielded an overall recovery of 99 $\pm$ 11% and for each day, the data were considered valid if the % recovery was between 80-120%. The lowest standard run on any day was 10 pg MeHg which was lower than all samples. The method detection limit as determined by 3 x the standard deviation of the reagent blanks was 0.27 pg.

Companion Core Sulfate, LOI, and pH Analysis

Soil sulfate concentrations were determined from subsamples of a lyophilized and homogenized companion soil core. Soil anions from a ~10 g sample were extracted with calcium dihydrogen phosphate. Extracts were analyzed on a Metrohm Ion Chromatograph. The average blank concentration was 0.46 +/- 0.03 mg/L sulfate and the LOD was 0.08 mg/L. Loss-on-ignition was used to determine percentage (w/w) of organic carbon (ash-free carbon content) in soils after the methods described in Heiri et al. (2001). Briefly, lyophilized soil sieved at 2mm was crushed in a rolling mill for 24 hrs. Two subsamples (~10 g each) were weighed into tared tins, and dried in a muffle furnace overnight at 105°C. Dry mass was recorded and then samples were combusted for 4 hours at 550 °C in a muffle furnace. Percent organic matter (w/w) was determined gravimetrically by mass lost during combustion. LOI was calculated with the following equation:

$$LOI = ((DW105 - DW550)/DW105)*100$$

DW105 is the dry weight of soil after 24 hours of drying at 105 °C and DW550 is the dry weight of soil after 4 hours of combustion at 550 °C.

Soil pH was determined by preparing a suspension of soil (~10 g) in an electrolyte buffer solution (0.01 M $CaCl_2$) with a 1:2 soil-to-liquid mixture (1:4 for organic soils) following the methods of Schofield and Taylor (1955), McKeague (1978), and Davey and Conyers (1988). Soil pH was measured potentiometrically in the supernatant liquid of the soil/buffer suspension after soil was allowed to flocculate and settle. For organic soils the following modifications were used: 5 g of soil and a 1:4 soil-to-liquid mixture. Soil pH was only determined in the dry season as pH has previously been found to be stable across seasons.

Quality Assurance, Quality Control

CRM (IAEA-456) recovery was 111 +/- 34 % (n = 96) across all days of analysis. The variability of data from multiple soil subsamples, each distilled and analyzed separately, was investigated. These technical replicates were found to give answers ranging from 20.2 - 44.7% RSD. A comparison of replicate soil subsamples from vineyard and forest microcosms were used to determine these metrics (Figure 22). The relative standard deviation (%RSD) varies by site type and node (Table 18), but despite variability within a given location, the difference in k_{meth} values between forest and vineyards can still be detected.

Table 18. Percent relative standard deviation for technical replicates analyzed at FOR_1 & VYD_2

Site and Node ID	%RSD	Number of Replicates
FOR_1_1	24.2	n=4
FOR_1_2	20.7	n=4
FOR_1_4	31.8	n=4
VYD_2_1	33.9	n=4
VYD_2_2	20.2	n=4
VYD_2_3	37.4	n=4
VYD_2_4	44.7	n=3

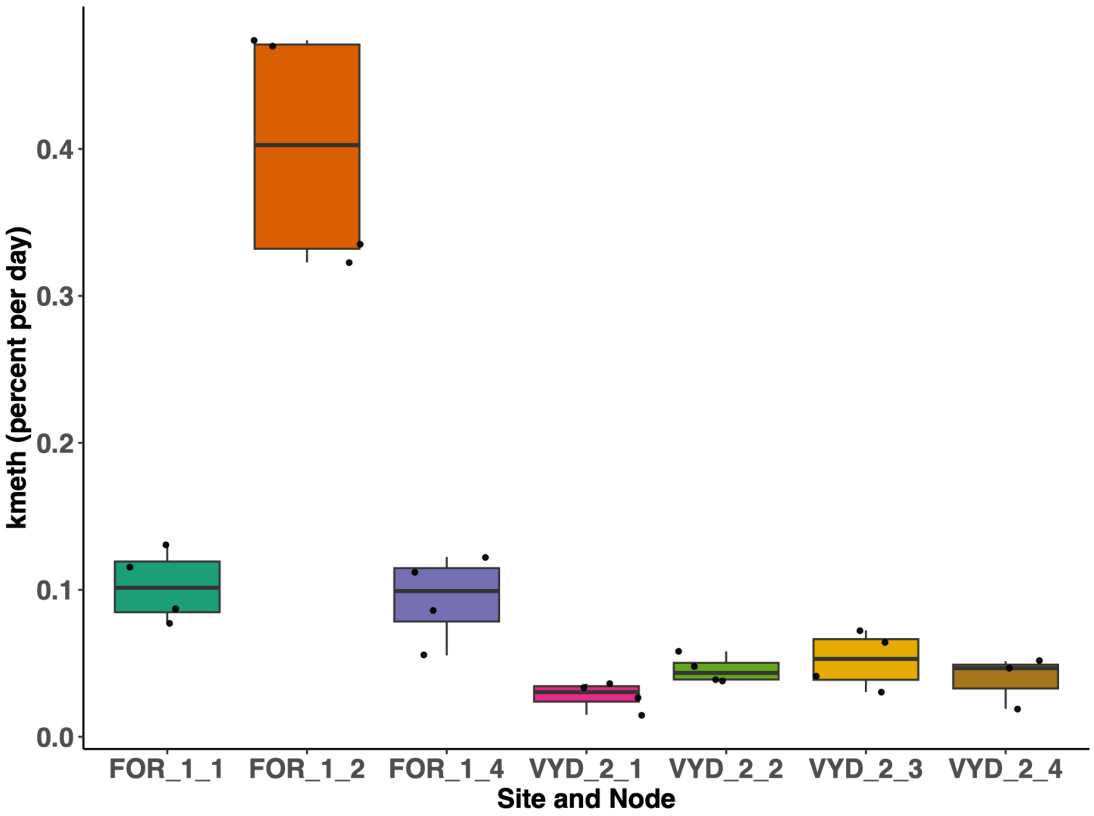

Figure 22. The results of repeated determination of k_{meth} values for wet season surface soils at one forested (FOR) site (3 nodes: _1, _2, _4) and one vineyard (VYD) site (4 nodes: _1, _2, _3, 4)). Each box is composed of 3 or 4 replicate measurements so that the full variability (from microcosm construction to analysis) of these measurements can be captured. Data from FOR_1_3 is not shown as samples were destroyed in transport and could not be analyzed.

Data Analysis

The parameters k_{meth}, sulfate concentration, HgT concentration, MeHg concentration, and percent MeHg in surface samples were examined using an unbalanced design (type = "III"), 2-way ANOVA with site type, season, and their interaction as factors. Tukey's Honest Significant Differences test (Tukey's HSD) was used as a post-hoc test of multiple comparisons. Values for k_{meth}, MeHg concentration and sulfate concentration were log_{10}-transformed to ensure that residuals met expectations of normal distribution. An unbalanced design (type = "III"), 1-way ANOVA was used to determine if k_{demeth} in surface samples was statistically significantly different by site type. K_{demeth} values were not log_{10}-transformed.

Site Type Characterization with Principal Component Analysis

Variables of k_{meth}, HgT concentration, MeHg concentration, organic matter (w/w), sulfate concentration, pH, percent moisture (w/w), and percent MeHg (w/w) data from dry season soils were included in a principle component analysis (PCA) to visualize how variables clustered by each of three site types. For wet season soils, k_{meth}, k_{demeth}, HgT concentration, MeHg concentration, organic matter (w/w), sulfate concentration, percent moisture (w/w), and percent MeHg (w/w) were included in a PCA model of three site types. All variables were z-scored before inclusion in the model. The 'prcomp' function from the R package 'stats' was used to produce the model and plots were prepared with the 'ggbiplot' function from the package of the same name (R Core Team, 2023; Vu, 2011). Results were used to confirm that the assigned site type categories contained samples with geochemical characteristics like others of the same type. PCA was also used to guide selection of variables for linear regression modeling with k_{meth} .

Linear Regression Models

HgT concentration, sulfate concentration, percent moisture (w/w), pH, and LOI (as a proxy for % organic matter) were investigated as explanatory variables with k_{meth} as the dependent variable. All variables examined for correlation, with the exception of percent moisture, were $\log_{10}$-transformed prior to modeling. Linear models were constructed between each variable and k_{meth} with data grouped in three ways: all site types and both seasons, vineyards only both seasons, and non-agricultural site types (forests and grasslands) both seasons. All statistical analyses were conducted in RStudio Version 2023.12.1 + 402, using the 'stats', 'car', 'ggplot2', and 'dplyr' packages (R Core Team, 2023; Fox and Weisberg, 2019; Wickham, 2016; Wickham et al. 2023). The significance level was 0.05.

4.3 Results & Discussion

4.3.1 Ambient HgT & MeHg Concentrations of Upland Soils in Two Seasons

4.3.1.1 HgT Concentrations

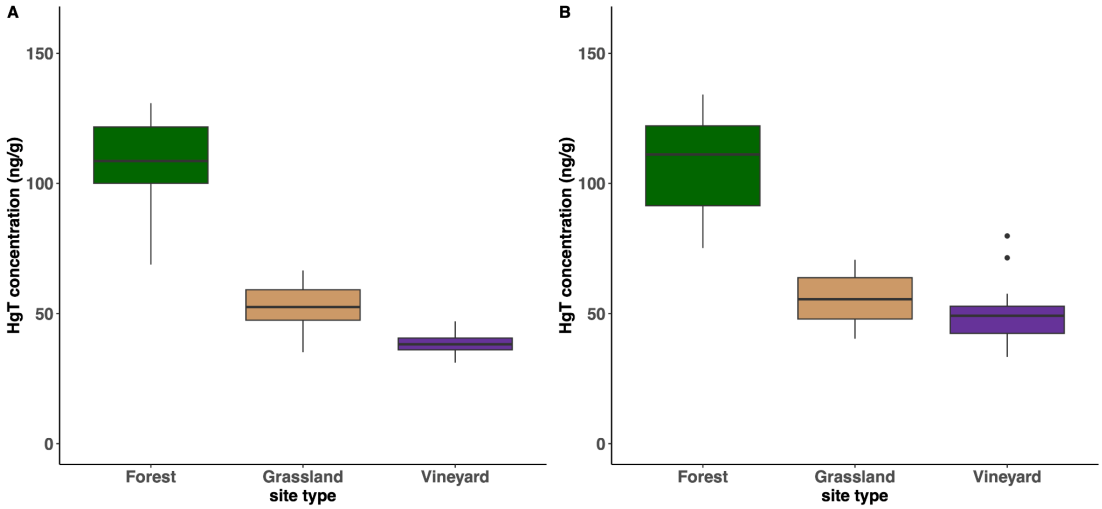

Figure 23. Box plots showing HgT concentrations at three site types in dry (A) and wet (B) seasons. HgT concentrations were higher in forests than in grasslands or vineyards. Grasslands and vineyards had similar HgT concentrations. HgT concentrations were not different between dry and wet seasons.

Forests had higher concentrations of HgT than did grasslands or vineyards ($p < 0.001$), while HgT concentrations between grasslands and vineyards were not significantly different ($p = 0.2$). The HgT concentration at wet season grasslands and vineyards was similar, with concentrations of 56 +/- 10 and 50 +/- 12 ng/g, respectively, while the HgT concentration in wet forests was greater (117 +/- 34 ng/g) than the other two site types (Figure 23). This may be due to wet and dry deposition onto foliage which then delivers HgT to the soil in forested locations through litterfall. Dry and wet season HgT concentrations were not significantly different ($p = 0.4$) (Table 19).

Table 19. HgT concentration selected ANOVA contrasts & adjusted p-values with site type and season as factors

Group and/or Interaction Compared	Adjusted p-value
Grassland-Forest	<0.001
Vineyard-Forest	<0.001
Vineyard-Grassland	0.2
Wet-Dry	0.4

4.3.1.2 MeHg Concentrations

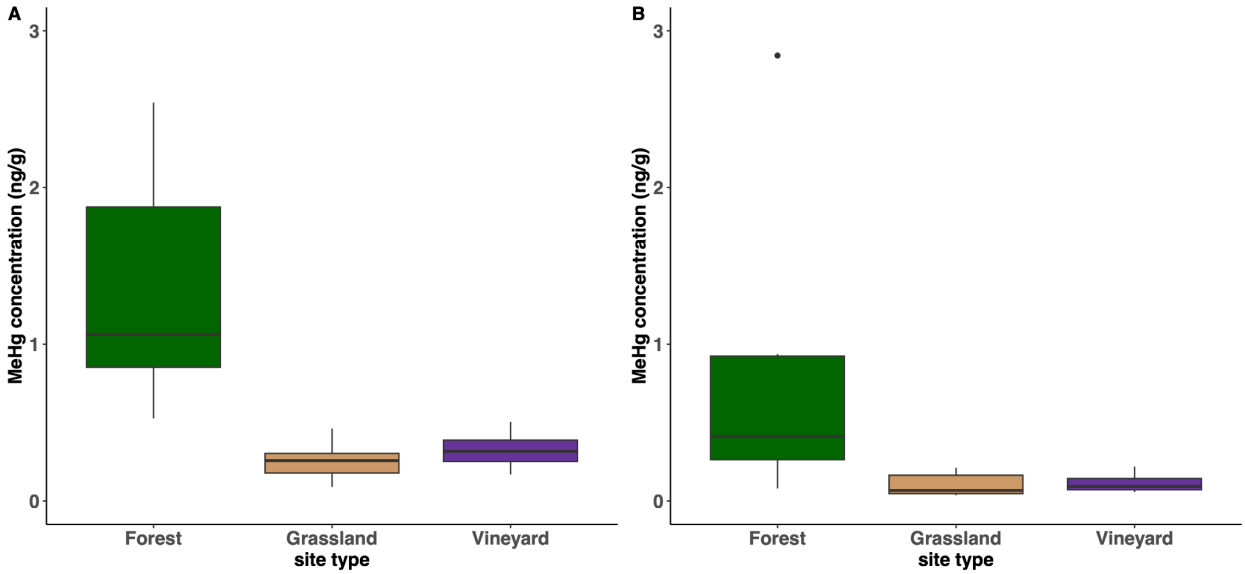

Figure 24. Box plots showing MeHg concentrations at three site types and in dry (A) and wet (B) seasons. MeHg concentrations were highest in forests in both the dry and wet seasons. The MeHg concentrations of grasslands and vineyards did not differ from one another in either season. At each of the three site types, wet season MeHg concentrations were lesser than in the dry season.

Table 20. MeHg concentration selected ANOVA contrasts & adjusted p-values with site type and season as factors

Group and/or Interaction Compared	Adjusted p-value
Grassland-Forest	<0.001
Vineyard-Forest	<0.001
Vineyard-Grassland	0.4
Wet-Dry	0.002

Similar to HgT concentrations, MeHg concentrations were greater at forests (Figure 24) than at the other two site types ($p < 0.001$ for both), while MeHg concentrations at vineyards and grasslands were not significantly different ($p = 0.4$) (Table 20). The average MeHg concentration in wet forests was 0.76 +/- 0.90 ng/g, whereas at grasslands it was 0.10 +/- 0.07 ng/g and at vineyards 0.11 +/- 0.05 ng/g. Unlike HgT concentrations, there was a significant difference between MeHg concentrations in the wet and dry seasons ($p = 0.002$). The difference in MeHg concentrations in the dry vs. wet seasons at each site type were significant; $p = 0.03$ for forests, $p = 0.01$ for grasslands, and $p < 0.001$ for vineyards. The average MeHg concentration at each of the three site types was lesser in the wet season than in the dry season (Table 21). The lower MeHg concentrations measured in the wet season may reflect removal of MeHg from the soil by mobilization into waterways.

Table 21. Average k_{meth} and k_{demeth} values, HgT concentrations, MeHg concentrations, and sulfate concentrations for 3 site types of the Napa River Watershed.

DRY SEASON SURFACE	48 hour k_{meth} (percent per day)	48 hour k_{demeth} (percent per day)	THg Concentration ng/g	MeHg Concentration ng/g	% MeHg (w/w)	Sulfate Concentration (mg/L)
Mean Across 2 Forests	0.13	NA	123	1.3	1.1	0.89
Standard Deviation Across 2 Forests	0.11	NA	35.6	0.73	0.38	0.19
Mean Across 2 Grasslands	0.094	NA	54.3	0.26	0.48	1.1
Standard Deviation Across 2 Grasslands	0.093	NA	13.3	0.12	0.23	0.29
Mean Across 4 Vineyards	0.021	NA	39.5	0.32	0.82	6.6
Standard Deviation Across 4 Vineyards	0.028	NA	5.69	0.09	0.25	11
WET SEASON SURFACE	**48 hour k_{meth} (percent per day)**	**48 hour k_{demeth} (percent per day)**	**THg Concentration ng/g**	**MeHg concentration ng/g**	**% MeHg (w/w)**	**Sulfate Concentration (mg/L)**
Mean Across 2 Forests	0.16	30	117	0.76	0.55	0.8
Standard Deviation Across 2 Forests	0.087	9.1	34.2	0.9	0.47	0.25
Mean Across 2 Grasslands	0.11	23	55.5	0.1	0.19	2.6
Standard Deviation Across 2 Grasslands	0.12	7.2	10.4	0.072	0.14	3.8
Mean Across 4 Vineyards	0.13	19	50	0.11	0.24	1.3
Standard Deviation Across 4 Vineyards	0.17	6.1	12	0.05	0.15	0.61

4.3.2 Correlation Analysis of HgT Concentration, MeHg Concentration, k_{meth}, and Ratio of MeHg/HgT vs. k_{meth}/k_{demeth}

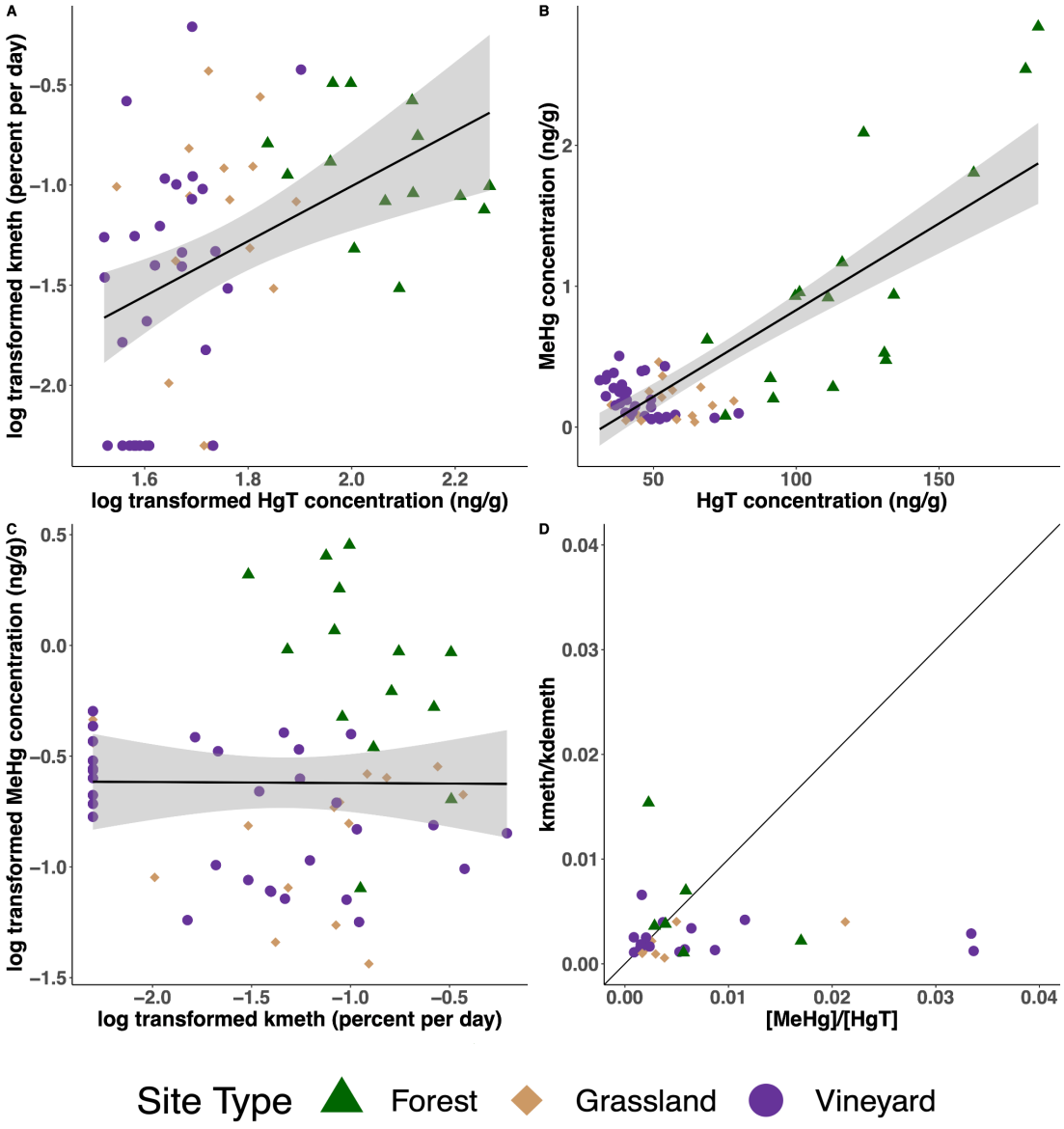

Figure 25. Linear regression models between HgT concentration and k_{meth} (A), HgT and MeHg concentration (B), and k_{meth} and MeHg concentration (C). Site types are indicated by circles for vineyards, triangles for forests, and diamonds for grasslands. Regression lines are for all site types grouped. The ratio of MeHg/HgT plotted against the ratio of k_{meth}/k_{demeth} with a 1:1 line in black (D).

Table 22. Correlations between HgT concentration and k_{meth}, HgT and MeHg concentration, & k_{meth} and MeHg

Independent Variable (x)	Dependent Variable (y)	Adjusted r^2	p-value
HgT (ng/g)	k_{meth}	0.2	<0.001
HgT (ng/g)	MeHg (ng/g)	0.19	<0.001
k_{meth}	MeHg (ng/g)	-0.02	1.0

A correlation between HgT concentration and k_{meth} was explored, as microbes at locations with elevated HgT could be reasonably expected to be primed for performing Hg cycling. The statistically significant, positive linear relationship between HgT and k_{meth} across both seasons and all site types (Figure 25 (A); Table 22) suggests that locations with more Hg are indeed primed to methylate faster and this effect is captured in the k_{meth} value. Forested sites had the highest HgT concentrations and had some of the highest potential methylation rate constants observed. HgT concentrations and MeHg concentrations across all sites and seasons also have a statistically significant positive correlation (Figure 25 (B)) meaning that sites with more HgT also have the propensity to methylate the Hg that is present. Both of the aforementioned relationships share the same sign (positive), which tells us that the microcosms and resulting k_{meth} values are reasonably representative of the processes taking place in the field.

The relationship between k_{meth} and MeHg concentration is not significant (Figure 25 (C)), though one might expect it to be, as locations with the potential to methylate faster (higher k_{meth}) would be anticipated to have more MeHg. This means that the microcosms may not have captured all aspects of the processes taking place in the field that can affect Hg methylation. This finding is unsurprising as microcosms only provide short term “snapshots” of variables’ effects on Hg cycling, though in the field, processes affecting concentrations of MeHg may be approaching equilibrium on time scales longer than two days. The

bioavailability of Hg(II) added to microcosms is another reason why k_{meth} derived from microcosms may not be significantly correlated with MeHg concentrations, and previous work has also noted a disconnect between k_{meth} values and ambient MeHg concentrations (Hoggarth et al. 2015). Another possibility for the lack of a significant relationship between $k_{meth}$and MeHg concentration is the effect of demethylation. This leads to the plot comparing the ratio of MeHg/HgT concentrations to the ratio of k_{meth}/k_{demeth} potential rate constants (Figure 25 (D)). If a data point falls to the right side of the 1:1 line it means the site has more MeHg than would be expected based on the ratio of k_{meth}/k_{demeth} and is approaching equilibrium by experiencing net demethylation. Conversely, if a data point falls to the left side of the 1:1 line, it means that the location has less MeHg than expected based on the ratio of the potential rate constants, and that the system would approach equilibrium through net demethylation. Here, solely grasslands plot either on the 1:1 line or to the right side, indicating this site type has more MeHg than predicted by the ratio of the rate constants. Forest and vineyards plot to either side of the 1:1 line.

4.3.3 MeHg Production in Upland Soils

4.3.3.1 Potential Methylation Rates

Upland soils that experience dry and wet seasons do produce MeHg (Figure 26), and methylation potentials in vineyards in the dry season (0.02+/-0.03 percent per day) are low and similar to those in boreal forests (0.011 %/day) (Huang and Mitchell, 2023). Dry season methylation potential rate constants at vineyards were statistically significantly lower than forests (0.13+/- 0.11%/ day) ($p < 0.001$). K_{meth} values were generally higher in the wet season and season was a significant factor ($p < 0.001$; Table 23). Wet season k_{meth} values were more similar across site types (Figure 26). K_{meth} values in wet season vineyards were higher (0.13 +/- 0.17 %/day) ($p < 0.001$) than for dry season vineyards, but not statistically different than those found at wet forests (0.16 +/- 0.09 %/day) ($p = 0.8$) or wet grasslands (0.11+/-0.12 %/day) ($p = 1.0$).

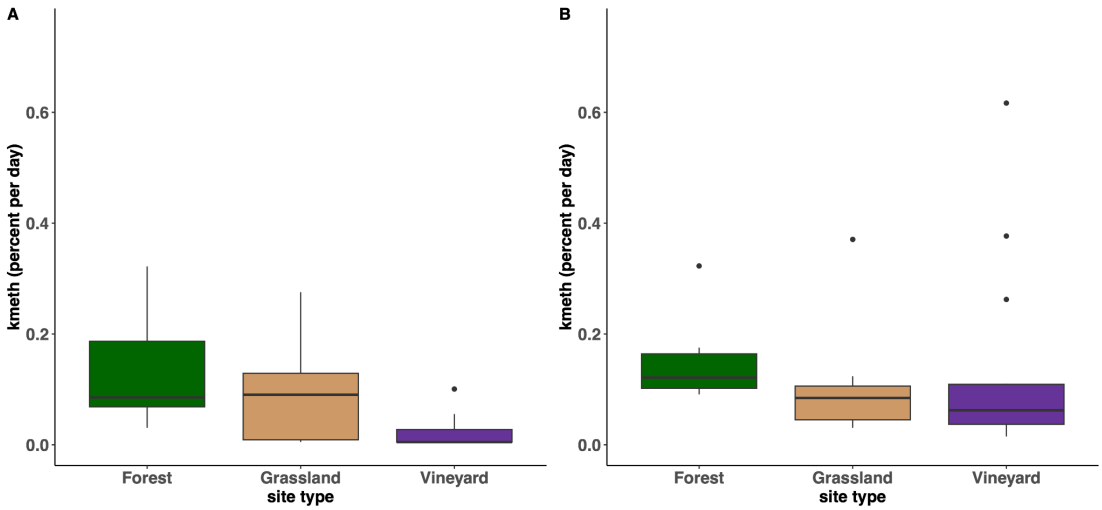

Figure 26. Box plots showing potential methylation rate constants (k_{meth}) across three site types in the dry (A) and wet (B) seasons. The variability of k_{meth} values observed in vineyard soil was greater in the wet season than the dry, and k_{meth} values were more similar across wet season site types than in the dry season, where dry vineyards were different from dry grasslands or dry forests.

Table 23. k_{meth} selected ANOVA contrasts & adjusted p-values with site type & season as factors

Group and/or Interaction Compared	Adjusted p-value
Vineyard-Forest	<0.001
Wet-Dry	<0.001
Vineyard:Dry-Forest:Dry	<0.001
Forest:Wet-Vineyard:Dry	<0.001
Grassland:Wet-Vineyard:Dry	0.002
Vineyard:Wet-Vineyard:Dry	<0.001

4.3.3.2 Potential Demethylation Rates

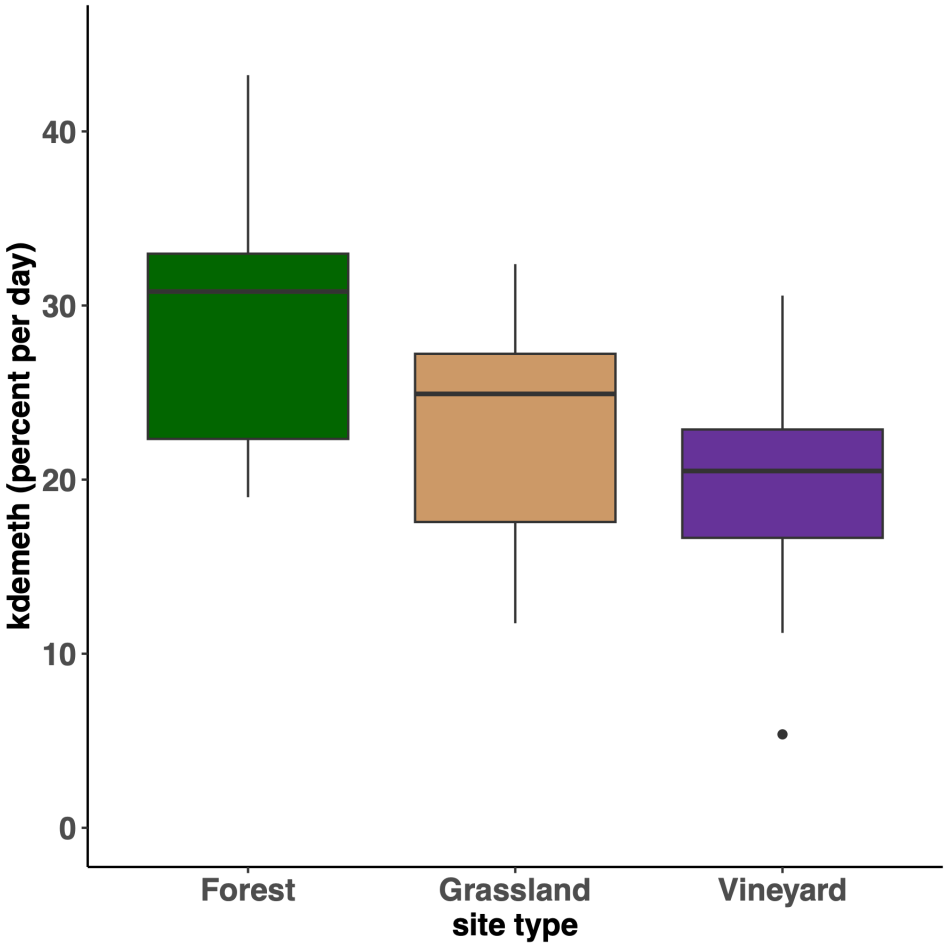

Figure 27. Potential demethylation rate constants (k_{demeth}) across three site types in the wet season. k_{demeth} values were examined as a function of site type and were only determined in the wet season. The most different mean potential demethylation rates were between forests and vineyards, though this difference was not statistically significant.

Demethylation potentials in upland soils ranged from 5 - 43 %/day, which were similar to k_{demeth} values measured in boreal forests (2 - 48%/day) and in brackish sediment in San Pablo Bay (2 - 33%/day) (Huang and Mitchell, 2023; Marvin-DiPasquale et al. 2003). K_{demeth} values in upland soils were less than those found in rice paddy soil (Chen et al. 2023) and overlapped with demethylation potentials in Mediterranean lagoon sediment (Hines et al. 2012) (Table 24). Hg demethylation potential was compared across site types in the wet

season (Figure 27), and while k_{demeth} values were highest at forests (30 +/- 9.1 %/day), there were no significant differences across site types ($p = 0.07$). No significant differences in wet season k_{meth} nor k_{demeth} values leaves observed differences in MeHg concentrations across site types to be explained by alternative variables.

Table 24. A comparison of k_{meth} and/or k_{demeth} values across a selection of study sites

Source	Environment	Description	k_{meth} (percent per day)	k_{demeth} (percent per day)
This Study	Napa Valley Watershed, California, USA	Freshwater, Upland Soil	BD (0.005)-0.62	5.4-43
Huang and Mitchell, 2023	Boreal Soil, Northwestern Ontario, Canada	Freshwater, Upland Soil	0.011	Feb-48
Marvin-DiPasquale et al., 2003	Marsh and Open Water Sediment, San Pablo Bay, California, USA	Brackish, Sediment	< 0.03-1.4	1.7-33
Chen et al., 2023	Rice Paddy Fields, Guizhou Province, Southwest China	Freshwater, Soil	0.03-2.5	60-160
Hines et al., 2012	Marano and Grado Lagoons, Italy	Brackish, Sediment	~0-5.4	~1-60
Roth et al., 2021	Subarctic Peatlands Fen, Alaska, USA	Freshwater, Peat Soil	9.3	ND
Gilmour et al., 1998	Florida Everglades, USA	Freshwater, Surficial Sediment	0-12	23-Mar
Hoggarth et al., 2015	Prairie Pothole Ponds, Saskatchewan, Canada	Freshwater, Sediment	2-17	ND

***BD indicates below limit of detection and ND indicates no data available. K_{demeth} values provided for the FL Everglades are from Marvin-DiPasquale et. al., 2000.**

4.3.4 Linking Sulfate Concentration and Hg Methylation Potential

4.3.4.1 Sulfate Concentration Characterization of Upland Soils in Two Seasons

Characterization of sulfate concentration by site type, to establish if sites receiving elemental S applications (vineyards) had significantly higher sulfate concentrations, was necessary to address the question of whether sulfate-enriched upland soils have different methylation potentials than unamended soils. Mean concentrations of sulfate in the dry season were significantly enriched in vineyards (6.6 +/- 11 mg/L) compared to forests (0.89 +/-0.19 mg/L) ($p = 0.02$) though were not significantly different than dry grasslands (1.1 +/- 0.29 mg/L) ($p = 0.07$). Sulfate concentrations were also highly variable in vineyards as indicated by relative standard deviation (RSD) of 168% ($n = 16$) in the dry season. Inspection of the temporal aspect of the sulfate concentrations reveals that wet vineyards are not elevated compared to wet forests or wet grasslands ($p = 0.9$ for vineyards vs. forests; $p = 0.7$ for grasslands vs. forests; $p = 1.0$ for vineyards vs. grasslands); Figure 28; Table 21. Wet vineyards have significantly lower sulfate concentrations (1.3 +/- 0.61 mg/L) than dry vineyards ($p = 0.03$) and this speaks to the solubility of sulfate and how it is known to enter the watershed (Hermes et al. 2022).

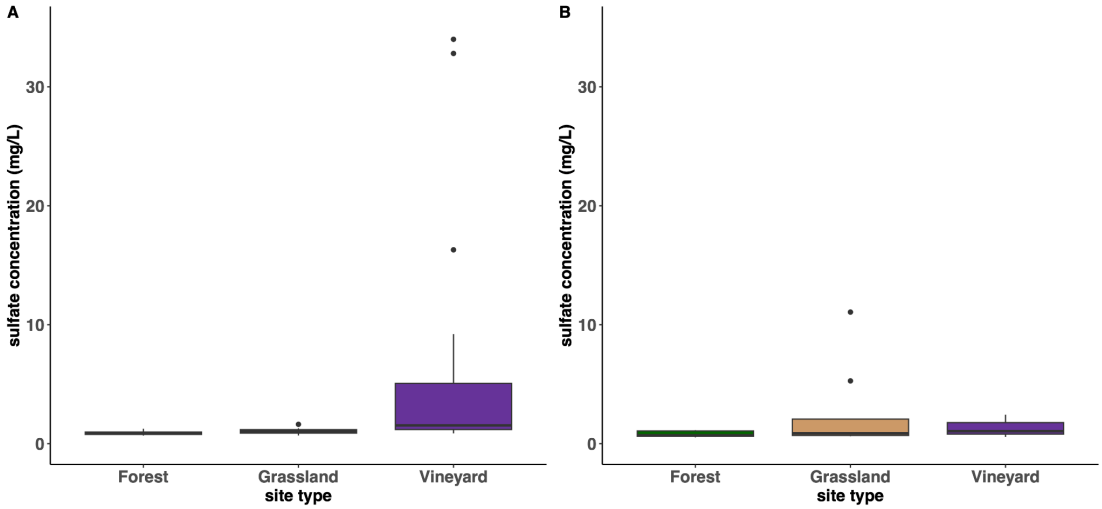

Figure 28. Sulfate concentrations across three site types from the dry (A) and wet (B) seasons.

Table 25. Sulfate concentration ANOVA contrasts & adjusted p-values with site type and season as factors

Group and/or Interaction Compared	Adjusted p-value
Vineyard-Forest	0.008
Wet-Dry	0.05
Vineyard:Dry-Forest:Dry	0.02
Forest:Wet-Vineyard:Dry	0.007
Vineyard:Wet-Vineyard:Dry	0.03

4.3.4.2 Sulfate Enrichment's Relationship with k_{meth}

Vineyards were associated with elevated sulfate concentrations in the dry season (Figure 28). Locations with elevated sulfate concentrations ultimately had, in general, lower potential methylation rate constants (Figure 29), yielding a weak, negative trend between sulfate concentration and k_{meth} across all site types (adjusted $r^2 = 0.08$, p-value = 0.01; Figure 3.4.2). Vineyard soils in the dry season are sulfate enriched relative to dry forests (p = 0.02; Table 25), however, dry vineyards have lower k_{meth} values than dry forests (p<0.001). This finding, along with no significant differences between sulfate concentrations across site types in the wet season paired with no significant differences across site types in the wet season for k_{meth} (p = 0.8 for vineyards vs. forests; p = 0.9 for grasslands vs. forests; p = 1.0 for vineyards vs. grasslands; Figure 28) suggest that variables other than sulfate may be responsible for controlling MeHg production in upland soils.

Sulfate concentrations did not have a statistically significant relationship with k_{meth} for a subset of forests and grasslands only (non-agricultural sites) (p-value = 0.7) when wet and dry season data is combined. For vineyards only across both seasons, the relationship between sulfate and k_{meth} was not significant (p = 0.06). When all sites have more similar sulfate concentrations, they also all have more similar k_{meth} values, as seen in the wet season. When differences in sulfate across site types are significant, as in the dry season, sites with highest sulfate concentrations (vineyards) have the lowest k_{meth} values. As sulfate did not explain much of the variability in k_{meth} (adjusted $r^2 = 0.06$) and was weakly negatively correlated, we turn to other variables for consideration as controls on Hg methylation.

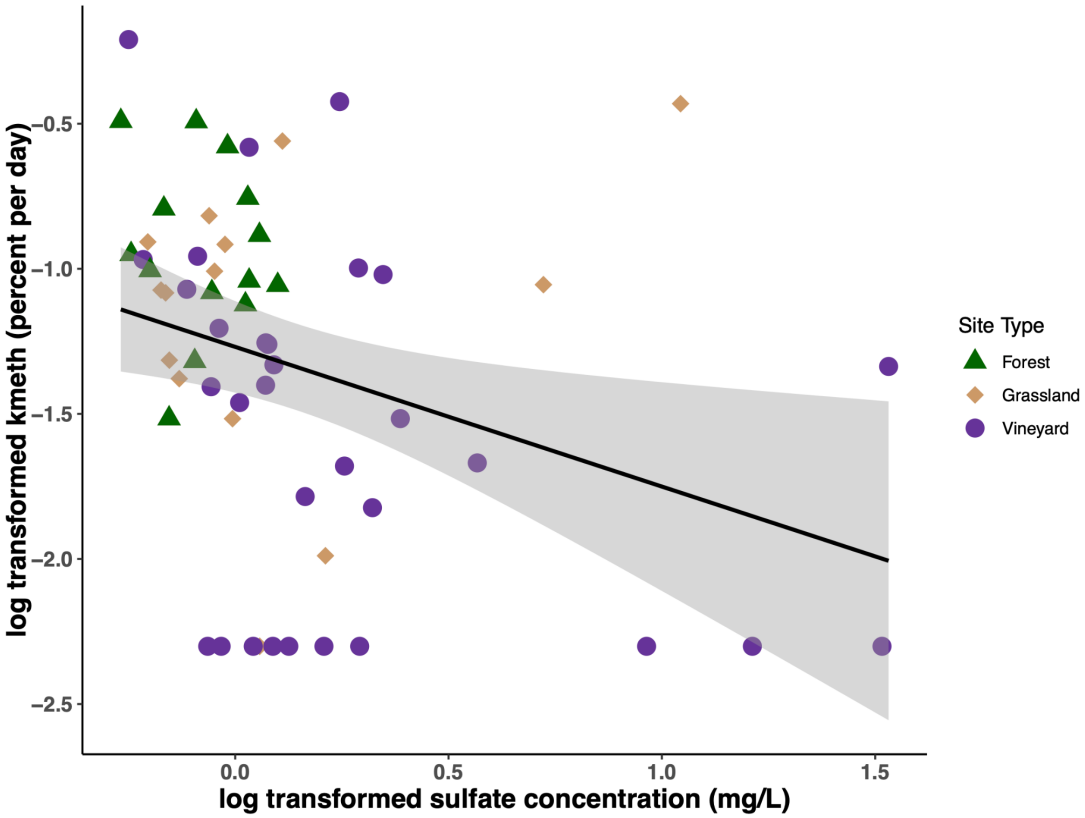

Figure 29. K_{meth} as a function of sulfate concentration. Regression is for all sites combined. Across all site types and both dry and wet season surface samples, a significant though weak trend exists between sulfate concentration and k_{meth}.

4.3.5 Principal Component Analysis (PCA) Plots

The results of the principal component analyses provide support for the site type categorizations. The colored ellipses surround data points with shared characteristics, and data points from given locations of forests, grasslands, and vineyards tend to group similarly to others within the same site type. Forests are unlike vineyards and grasslands in the dry season (Figure 30), whereas vineyards and grasslands are more similar to one another. In the wet season (Figure 31), all three site type categorizations overlap to some extent, but it can be seen that forests are less like vineyards and grasslands, where again, grasslands and vineyards group more similarly. Sulfate and pH cluster with vineyards in the dry season

whereas moisture content and organic matter cluster with forests. As relationships between sulfate and k_{meth} were explored with linear regression models, we now turn to investigating the relationships between k_{meth} and pH, percent moisture (w/w) and percent organic matter (w/w) across all site types and at vineyards only, in an effort to reveal biogeochemical controls on k_{meth}.

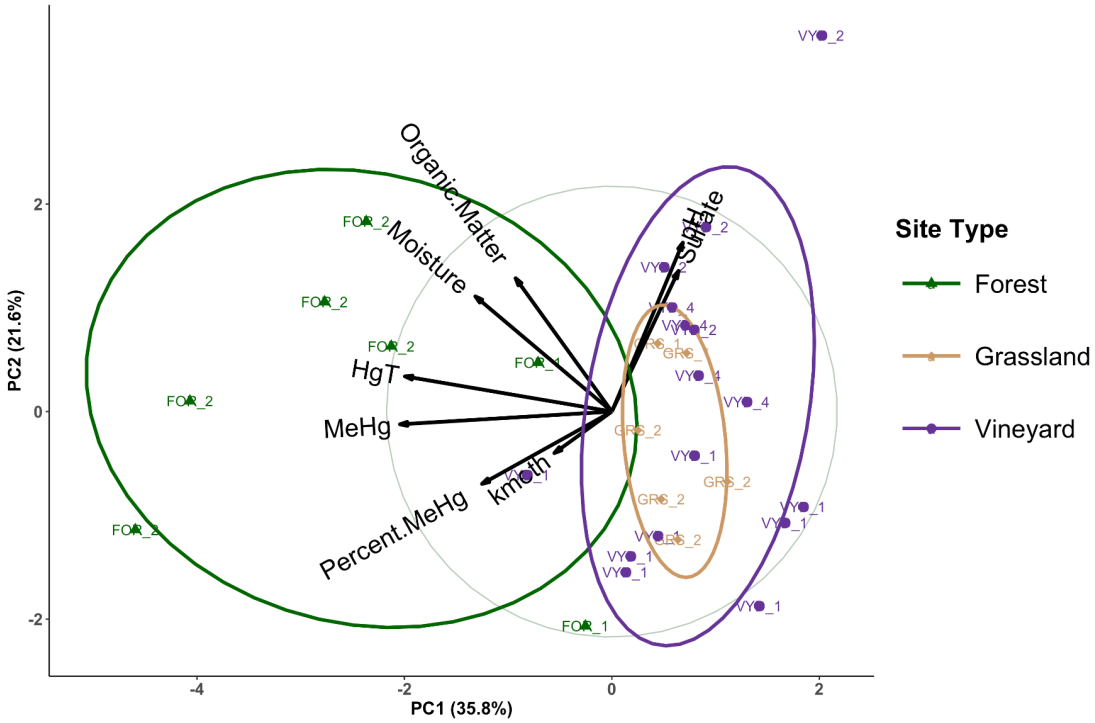

Figure 30. A principal component analysis for dry season biogeochemical variables, grouped by three site types. When clustered by site type, forested sites were associated with higher amounts of HgT, MeHg, organic matter, and percent moisture, along with higher k_{meth} values. Vineyards were associated with conditions of elevated sulfate concentrations and pH, and grasslands exhibited characteristics that were similar to that of vineyards.

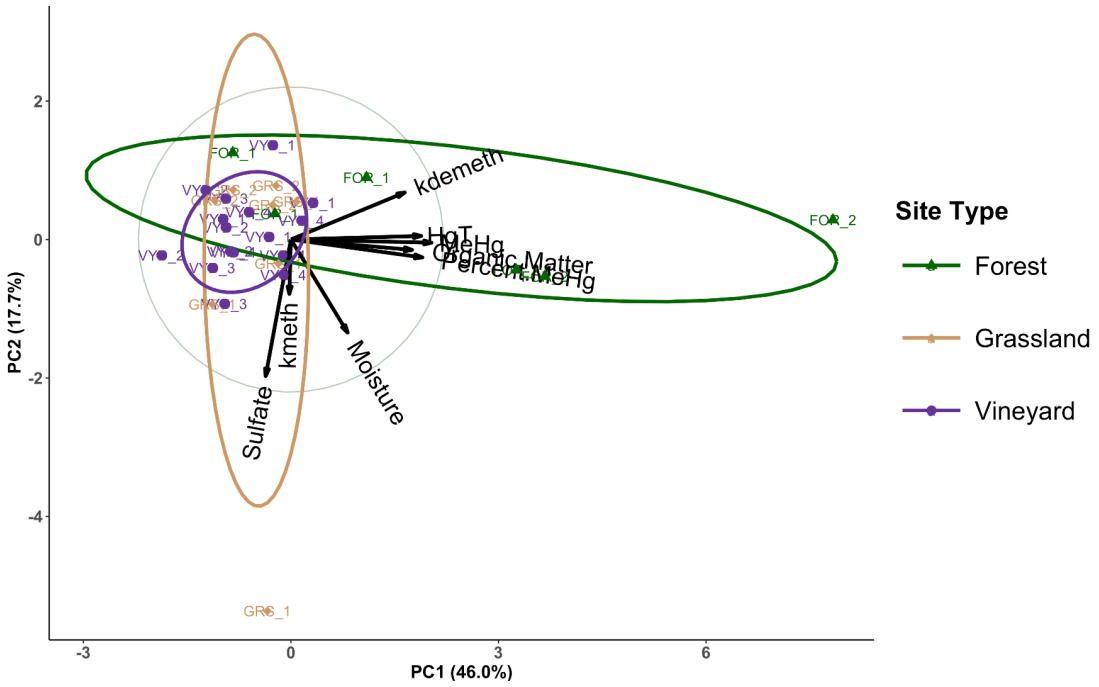

Figure 31. A principal component analysis for wet season biogeochemical variables, grouped by three site types. When clustered by site type, forested sites were associated with higher amounts of HgT, MeHg, percent MeHg, and organic matter, along with higher k_{demeth} values. Vineyards overlapped with both other site types, and clustered somewhat more similarly to grasslands. Grasslands were associated with higher sulfate concentrations and higher k_{meth} values.

4.3.6 Geochemical Variables and Correlations with k_{meth}

Sulfate concentration and HgT only go so far to explain the variability in k_{meth}, as HgT concentration and k_{meth} had a statistically significant relationship across all sites and both seasons (Figure 25 (A); $p < 0.001$), and within vineyards only ($p = 0.01$), but the relationship was not significant for non-agricultural sites ($p = 0.2$). Thus, an increased concentration of HgT alone is insufficient to explain higher potential rates of Hg methylation. In an effort to identify a geochemical control on Hg methylation in upland soils, percent moisture (w/w), pH, and LOI (as a proxy for % organic matter) were investigated as explanatory variables with k_{meth} as the dependent variable.

Akin to HgT, percent moisture (w/w) was a significant predictor of k_{meth} across all site types (Figure 32) and for vineyards only ($p = 0.006$; $p<0.001$, respectively), yet failed to be a

significant predictor of k_{meth} within non-agricultural sites (p = 0.8). A linear relationship between LOI and k_{meth} across both seasons was not statistically significant across all site types (p = 0.3), vineyards only (p = 0.06), nor for non-agricultural sites (p = 0.7). This finding is inconsistent with the expectation that higher percentages of organic matter mean that microbes have more carbon to oxidize, and that this in turn leads to higher k_{meth} values. A lack of significance between LOI and k_{meth} suggests that 1) carbon limitation is not the variable controlling Hg methylation and therefore having more OM does not lead to more Hg methylation and/or 2) organic matter as a bulk property has a limited relationship with bioavailable carbon capable of supporting microbial metabolisms. Linear models of pH vs. k_{meth} across both seasons did not yield any significant relationships across all site types (p = 0.09), vineyards only (p = 0.6), nor non-agricultural sites only (p = 0.4). However, for a linear model of dry season pH vs. wet season k_{meth} in vineyards only, the correlation is negative and statistically significant (p = 0.006), explaining 41% of the variability in k_{meth} (Figure 33).

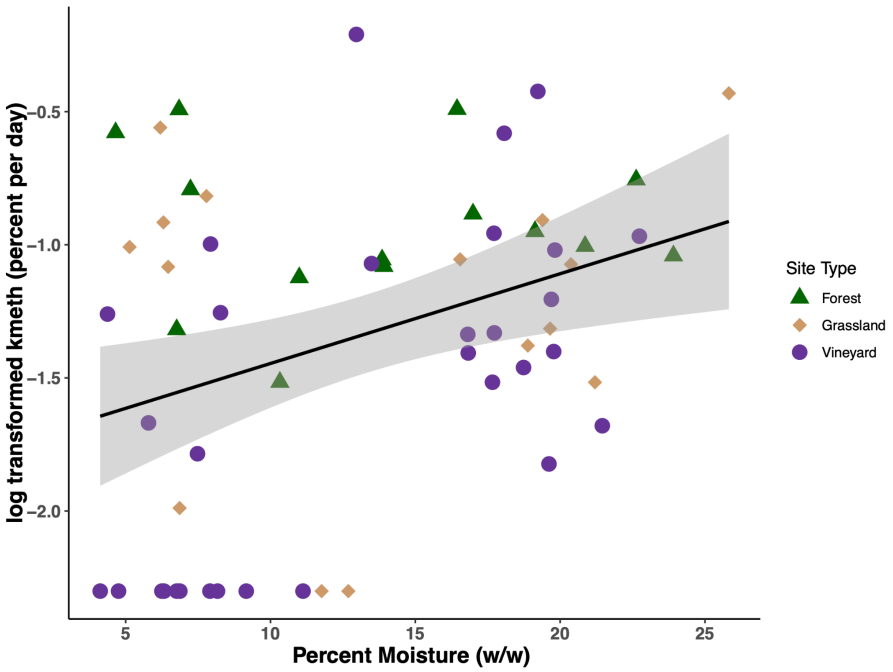

Figure 32. A linear regression model of percent moisture vs. k_{meth} across all site types and both seasons. More moisture is associated with faster potential methylation rates, though the trend is weak as only 11% of the variability in k_{meth} is explained.

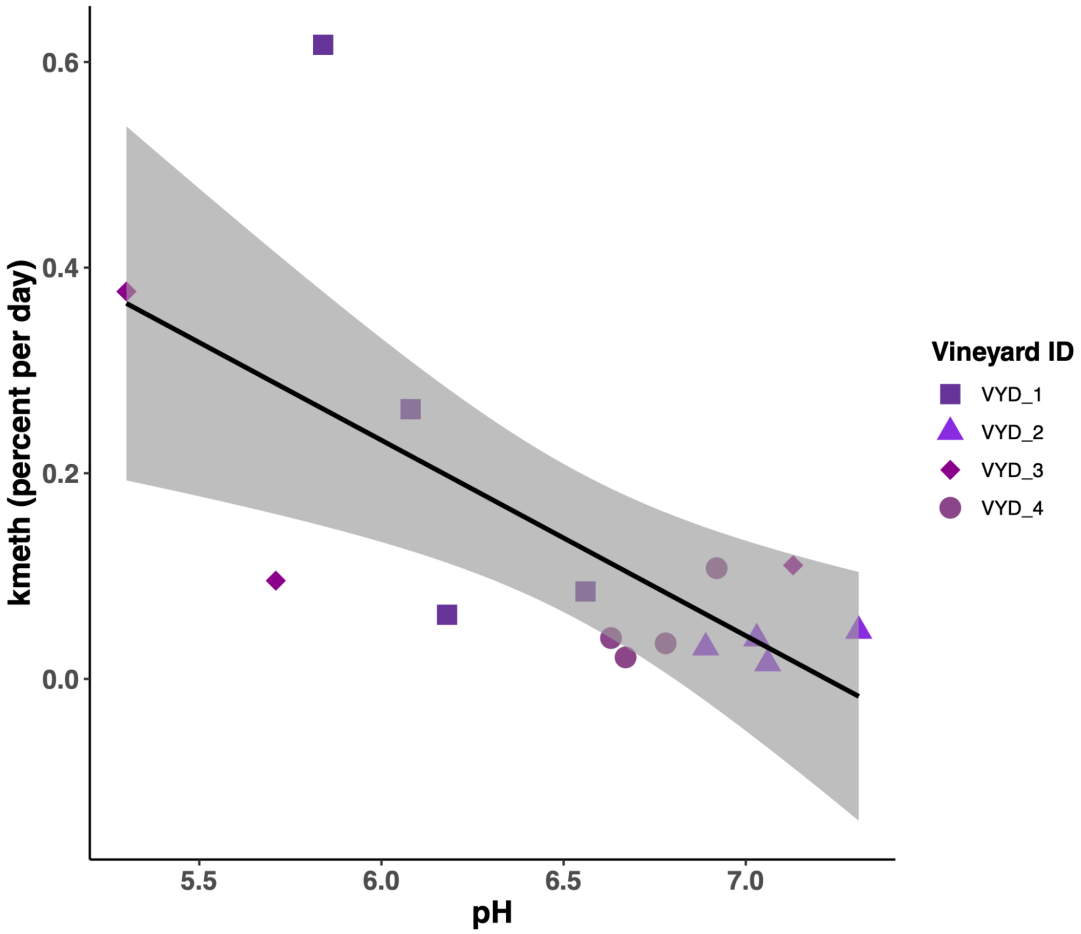

Figure 33. Wet season k_{meth} as a function of dry season soil pH. For a linear model of vineyards only, pH and potential methylation rate constant have a statistically significant negative relationship. More acidic sites were associated with higher k_{meth} values in the wet season.

4.3.7 Comparing High Sulfate and Low Sulfate Vineyards & Hypothetical Influence of pH

Figure 34 summarizes the results of sulfate concentrations, HgT concentrations, and processes potentially affecting k_{meth} in the dry and wet seasons. Elemental S applied during the growing season has accumulated and has converted to sulfate in vineyards during the dry season. Wet season sulfate concentrations in vineyards (1.3 +/- 0.61 mg/L) are lower than in the dry season (6.6 +/- 11 mg/L) ($p = 0.03$), suggesting that other processes affecting its removal are at work. One possible explanation for this finding is mobilization of sulfate during

the rainy season, documented by Hermes et al. (2022) which is additionally supported by the lack of statistically significant difference between sulfate concentrations in wet vineyards compared to wet grasslands (2.6 +/- 3.8 mg/L) ($p = 1.0$). Another possible outcome is that sulfate is lower in wet season vineyards because it has been converted to sulfide by sulfate-reducing bacteria. The negative relationship observed between sulfate concentration and k_{meth} suggests that the presence of sulfate may have exerted an influence on reduced sulfur/sulfide concentrations in turn affecting methylation potential due to changes in Hg(II) availability to microbes (Benoit et al. 2001; Gilmour and Henry, 1991). The presence of sulfide or reduced sulfur species, though not measured in this study, would be anticipated to occur as a result of microbial sulfate reduction if SRB are active in upland soils.

Orem et al. (2019) identified a range of sulfate concentrations, ~1-20 mg/L (0.01 - 0.2 mM), that were found to enhance Hg methylation in the Everglades, whereas sulfate concentrations surpassing this threshold suppressed Hg methylation by favoring sulfide accumulation. Whether this concentration range was applicable to the processes taking place in upland soils was investigated and some supporting evidence exists. For example, in the dry season, VYD_1 had sulfate concentrations ranging from 1.2 -1.9 mg/L (0.012 - 0.020 mM) while VYD_2 had a sulfate concentration range of 1.2-34 mg/L (0.012 -0.35 mM), and these results were significantly different ($p=0.04$). Correspondingly, k_{meth} values in the wet season were also significantly different ($p =0.04$), with k_{meth} values of 0.06 - 0.62 %/day for VYD_1 compared to 0.02-0.05 %/day for VYD_2. At VYD_1, sulfate may have played a role in stimulating Hg methylation, as k_{meth} values were higher in the wet season than in the dry, though the enhancement of k_{meth} could have been partially due to another factor such as increased moisture content. For VYD_2, it is possible that sulfate concentrations >20 mg/L (0.20 mM) led to sulfide accumulation that limited Hg bioavailability, as k_{meth} values in the wet season were of a similar range (0.02-0.05 %/day) to those in the dry season (0.005-0.05 %/day). pH was also significantly negatively correlated with wet season methylation potential in vineyards (Figure 33; $p = 0.006$) and, though speculative, may have an influence on the

fate of sulfide generation or preservation. Higher pH vineyards had lower potential methylation than lower pH vineyards in microcosm experiments, and results were significant ($p = 0.02$). However, for multiple comparisons, only one of the higher pH vineyards was significantly different than a lower pH vineyard ($p= 0.04$). At higher pH vineyards, one of which also had sulfate concentrations surpassing 20 mg/L (0.20 mM), lower methylation potential suggests that Hg may not have been bioavailable to microbes, as has been observed when charged HgS complexes are formed under conditions of elevated sulfide. Future work may further explore whether pH conditions, in conjunction with sulfate concentrations surpassing a threshold of 20 mg/L (~0.2mM), play a role in the effects of sulfate on k_{meth}.

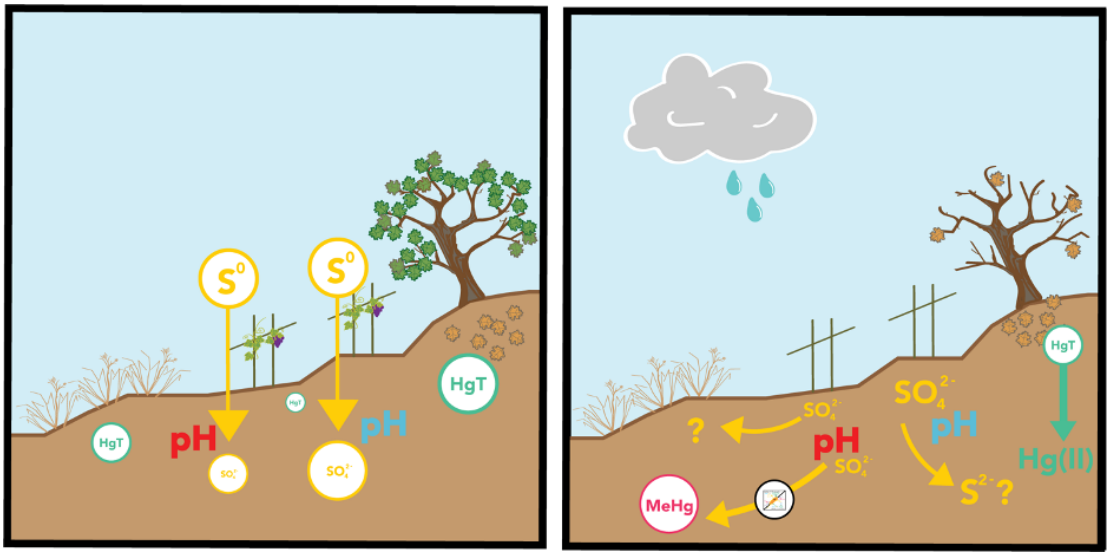

Figure 34. Schematic showing dry (left) and wet (right) season conditions in upland soils. The size of the sulfate circles depict the relative magnitude of concentrations at vineyards. The red pH label indicates dry season conditions less than 6.5, while the blue pH label represents conditions above 6.5. The size of HgT circles indicates the relative magnitude of concentrations of total Hg measured in the dry season soils. The yellow arrows show possible fates of sulfate in the wet season, where sulfate in low pH vineyards could stimulate MeHg production and also mobilize to a nearby grassland. Higher pH vineyards had lower potential methylation than lower pH vineyards in microcosm experiments, and results were significant ($p = 0.02$). At higher pH vineyards, one of which also had sulfate concentrations surpassing 20 mg/L, lower methylation potential suggests that Hg may not have been bioavailable to microbes, as has been observed when charged HgS complexes are formed under conditions of elevated sulfide.

4.3.8 Comparison of k_{meth} in Upland Soils to Other Sulfate-Impacted Sites

A comparison of k_{meth} values and sulfate concentrations across a variety of sulfate-impacted sites show that the potential methylation rate constants in upland soils are lesser than comparison sites (Table 26), even when sulfate concentrations overlap as they do for upland sites and locations within the EAA. k_{meth} values in upland soils (0.005 - 0.62 %/day) were similar to those found in rice paddies (0.03-2.5 %/day), despite a higher range of sulfate concentrations for rice paddy soil 12-140 mg/L (0.12-1.5 mM) than for upland soil 0.5 - 34 mg/L (0.005 - 0.35 mM). K_{meth} values in upland soils were less than in sulfate-impacted freshwater prairie potholes (2-17 %/day (Hoggarth et al. 2015)) or sulfate-impacted, saturated agricultural soils of the Everglades (0-12 %/day (Gilmour et al. 1998)). The range of sulfate concentrations in upland soils 0.5 - 34 mg/L (0.005 - 0.35 mM) does extend beyond the 0.01 - 0.2 mM range found to stimulate MeHg production (Orem et al. 2019), suggesting that at some vineyards, sulfate concentrations may be high enough to suppress Hg methylation via accumulation of sulfide.

Table 26. Sulfate concentrations and k_{meth} across a selection of sulfate-impacted locations

Location	Sulfate Concentration (mM)	k_{meth} (%/day)	Source
Upland Soils, Napa CA, USA	0.005 - 0.35	BD(0.005) - 0.62	This Study
Everglades Agricultural Area, Florida, USA	0 - 0.40	0-12	Gilmour et al. 1998
Rice Paddies, Guizhou Province, China	0.12 - 1.5	0.03-2.5	Chen et al. 2023
Prairie Pothole Ponds, Saskatchewan, Canada	0.10 - 33	2-17	Hoggarth et al. 2015

***BD indicates below limit of detection.**

4.3.9 Conclusion

Sites receiving agricultural S applications (vineyards) had higher sulfate concentrations relative to reference sites in the dry season, though vineyards had lower k_{meth} values. Therefore, sulfate is associated with an effect on Hg cycling, though this effect is not stimulatory to the production of MeHg. Sulfate concentration was weakly correlated with k_{meth} across all site types, with a negative relationship, further supporting the conclusion that elevated sulfate concentration does not lead to enhanced k_{meth}. There were not significant differences in sulfate concentration across site types in the wet season, nor were differences in k_{meth} significant for the wet season. Sulfate failed to have a significant correlation with k_{meth} at vineyards only and non-agricultural sites only. It is possible that sulfur transformations led to accumulated sulfide in vineyard soils. The presence of sulfide or reduced sulfur moieties may have formed HgS complexes with Hg(II) in the microcosms, rendering it not bioavailable to microbes, which could help explain the low k_{meth} values in very high sulfate concentration 20 mg/L (>0.2 mM) vineyards. However, microcosms had added Hg(II) in excess, and it is difficult to say whether there was sufficient sulfide to convert the majority of the Hg(II) spike to HgS complexes. Linear regression models with k_{meth} vs. other geochemical variables revealed that higher concentrations of HgT are significantly correlated with greater k_{meth} values, though this relationship only holds up for models of all site types and vineyards only, and not for a model of non-agricultural sites. Like HgT, percent moisture had a significant relationship across all site types and for vineyards only, but was not correlated with k_{meth} for non-agricultural sites. LOI was not correlated with k_{meth} within any of the data groupings. While the data suggests that MeHg is indeed produced in upland soils, the process does not appear to be stimulated by sulfur and occurs at potential rates greater than that of boreal soils and similar to rice paddies.

MeHg production in upland soils proceeds at low potential rates and this finding could be due to one of several possible mechanisms. First, the soils of the Napa River Watershed

are broadly oxic, and sulfate reduction and Hg methylation would be expected to happen within anoxic microsites, providing only limited amounts of MeHg per unit of soil when compared with anoxic locations such as wetlands. Methylation potential rates determined in Napa vineyards are smaller than those found by Gilmour et al. (1998) in the Everglades, despite having a similar range of sulfate concentrations (Table 26). This finding provides support for the hypothesis that upland soils are a unique regime in regards to Hg methylation when compared to the sulfate-impacted, inundated agricultural soils of the EAA. Second, it is possible that sulfate was utilized by SRB within microsites, drawing down sulfate concentrations by conversion to sulfide, which in turn formed HgS complexes. Under this scenario, limited potential methylation in vineyards would come as a result of Hg(II) not being bioavailable. Thirdly, it is worth considering that sulfate was not found to be associated with increased Hg methylation potential due to low abundance of SRB to utilize sulfate as a terminal electron acceptor. Therefore, k_{meth} does not respond to added sulfate because another clade of bacteria is responsible for methylation. This conclusion is further supported by dry forests having the highest k_{meth} values across site types in the dry season, while not having elevated sulfate concentrations, which suggests that the Hg methylating community in upland soils, or at least in forests, may consist of microbes other than SRB, such as Fe-reducers or methanogens.

While no clear overarching control on Hg methylation in upland soils has been revealed, HgT and percent moisture are the most useful in explaining variability in k_{meth} across all site types. It is possible that geochemical variables not measured in this study could be responsible for controlling MeHg production in the Napa River Watershed. With that in mind, future work might consider assessing nitrate concentrations, sulfide/reduced sulfur concentrations, and microbial identity and abundance as potential variables exerting control on MeHg production in upland soils. Additionally, the question as to whether pH influences sulfur speciation at vineyards with sulfate concentrations > 0.2 mM could be investigated with regard to bioavailability of Hg(II).

APPENDIX A. Chapter 3 Supplementary Data Table S1. R Package version, RStudio version & R language version used.

Package	Version	RStudio Version	R Language Version
dada2	1.22.0	1.4.1717	4.1.2
phyloseq	1.38.0	1.4.1717	4.1.1
BiocManager	1.30.16	1.3.1093	4.1.3
Bioconductor	3.14	1.3.1093	4.1.3
DESeq2	1.34.0	1.31093	4.1.3
stats	4.1.1	1.4.1717	4.1.1
car	3.0.13	1.4.1717	4.1.1
lsr	0.5.2	1.4.1717	4.1.1
DescTools	0.99.44	1.4.1717	4.1.1
FSA	0.9.3	1.4.1717	4.1.1
ggplot2	3.3.5	1.4.1717	4.1.1
wesanderson	0.3.6	1.4.1717	4.1.1

APPENDIX B. Chapter 3 Supplementary Data Table S2. Extended table of results from one-predictor models at East Fork.

Predictor	EF Estimate of Coefficient	EF p-value	EF R^2	EF Residual Sum of Squares	EF F-statistic	EF Shapiro-Wilk Test p-value
Depth (cm)	-0.46	0.01*	0.21	20.42	6.83	4.90E-06
Sed. HgT (ng/g dry)	0.06	0.77	0	25.91	0.08	4.00E-08
LOI %	0.31	0.12	0.09	23.57	2.58	3.80E-07
Ammonium (µM)	-0.46	0.02*	0.21	20.5	6.7	3.50E-07
Porewater AVS (mM)	-0.32	0.1	0.11	23.26	2.95	2.10E-07
Porewater O2 % saturation	0.5	0.01*	0.25	19.41	8.49	4.70E-04
Porewater HgT (pM)	-0.09	0.65	0.01	25.78	0.21	8.00E-08
Nitrate (µM)	0.77	2.2E-6*	0.6	10.43	37.31	9.60E-04
pH	-0.03	0.9	0	25.98	0.02	5.20E-08
Salinity (ppt)	-0.37	0.06	0.14	22.46	3.94	8.00E-09
Temp. (Celcius)	-0.34	0.09	0.11	23.07	3.18	1.00E-06

APPENDIX C. Chapter 3 Supplementary Data Table S3. Extended table of results from one-predictor models at Beach Zone.

Predictor	BZ Estimate of Coefficient	BZ p-value	BZ R^2	BZ Residual Sum of Squares	BZ F-statistic	BZ Shapiro-Wilk Test p-value
Depth (cm)	-0.42	0.03*	0.18	21.32	5.49	0.32
Sed. HgT (ng/g dry)	0.04	0.84	0	25.95	0.04	0.30
LOI %	0.11	0.57	0.01	25.66	0.33	0.19
Ammonium (µM)	-0.43	0.03*	0.18	21.29	5.53	0.07
Porewater AVS (mM)	-0.49	0.01*	0.24	19.76	7.9	0.04
Porewater Dissolved O2 % saturation	0.28	0.16	0.08	24	2.09	0.15
Porewater HgT (pM)	0.21	0.29	0.04	24.84	1.17	0.96
Nitrate (µM)	0.22	0.27	0.05	24.72	1.29	0.20
pH	-0.32	0.1	0.1	23.36	2.83	0.21
Salinity (ppt)	-0.2	0.33	0.04	25	1	0.14
Temp. (Celcius)	-0.27	0.18	0.07	24.17	1.89	0.04

APPENDIX D. Chapter 3 Supplementary Data Table S4. Results of post-hoc tests after Kruskal-Wallis & ANOVA for 2020 microcosm assay.

Site	Post-hoc Test	Comparison	p-value
Beach Zone	Dunn's after Kruskal-Wallis	48 hour Control - Ammonium	0.49
Beach Zone	Dunn's after Kruskal-Wallis	48 hour Control - Molybdate	0.30
Beach Zone	Dunn's after Kruskal-Wallis	48 hour Control - Molybdate + Nitrate	0.43
Beach Zone	**Dunn's after Kruskal-Wallis**	**48 hour Control - Nitrate**	**0.18**
Beach Zone	Dunn's after Kruskal-Wallis	Ammonium - Molybdate	0.10
Beach Zone	Dunn's after Kruskal-Wallis	Ammonium - Molybdate + Nitrate	0.14
Beach Zone	Dunn's after Kruskal-Wallis	Molybdate - Molybdate + Nitrate	0.74
Beach Zone	Dunn's after Kruskal-Wallis	Ammonium - Nitrate	0.52
Beach Zone	Dunn's after Kruskal-Wallis	Molybdate - Nitrate	0.03
Beach Zone	Dunn's after Kruskal-Wallis	Molybdate + Nitrate - Nitrate	0.03
East Fork	Dunnett's after ANOVA	Nitrate-48 hour Control	0.91
East Fork	Dunnett's after ANOVA	Ammonium-48 hour Control	1.0
East Fork	**Dunnett's after ANOVA**	**Molybdate-48 hour Control**	**0.07**
East Fork	Dunnett's after ANOVA	Molybdate + Nitrate-48 hour Control	0.12

APPENDIX E. Chapter 3 Supplementary Data Table S5. Table of omnibus test critical value comparisons for 2020 microcosm assay.

Test	Total Number of Samples	Calculated Test Statistic (H or F)	chi^2 or F Critical value
Kruskal-Wallis with df =4	14	H = 7.49	chi^2 = 9.49
Kruskal-Wallis with df = 4	19	H = 12.6	chi^2 = 9.49
ANOVA with numerator df =4 and denominator df = 10	15	F = 3.33	F = 3.48
ANOVA with numerator df = 4 and denominator df = 15	20	F = 3.33	F = 3.06

BIBLIOGRAPHY

Acha, D., Hintelmann, H. and Pabon, C. , 2012. Sulfate-reducing Bacteria and Mercury Methylation in the Water Column of the Lake 658 of the Experimental Lake Area. Geomicrobiology Journal, 29, 667–674.

Aiken GR. 2004. Carbon, sulfur, and mercury—A biogeochemical axis of evil. Proceedings of the 2004 CALFED science conference, "Getting results: integrating science and management to achieve system-level responses", Sacramento, CA, October 4–6, 2004. http://pubs.er.usgs.gov/ publication/70195438

Angle, J.C., Morin, T.H., Solden, L.M., Narrowe, A.B., Smith, G.J., Borton, M.A., Rey-Sanchez, C., Daly, R.A., Mirfenderesgi, G., Hoyt, D.W. and Riley, W.J., 2017. Methanogenesis in oxygenated soils is a substantial fraction of wetland methane emissions. Nature communications, 8, 1567.

Arguez, A.; Durre, I.,; Applequist, S.; Vose, R.S.; Squires, M.F.; Yin, X.; Heim, R.R.. & Owen, T., 2012. NOAA's 1981–2010 U.S. climate normals: an overview. Bulletin of the American Meteorological Society. 93, 1687-1697. 10.1175/BAMS-D-11-00197.1.

Barkay, T., & Gu, B., 2022. Demethylation–the other side of the mercury methylation coin: A critical review. ACS Environmental Au, 2, 77–97.

Barrouilhet, S., Monperrus, M., Tessier, E., Khalfaoui-Hassani, B., Guyoneaud, R., Isaure, M. P., & Goñi-Urriza, M., 2023. Effect of exogenous and endogenous sulfide on the production and the export of methylmercury by sulfate-reducing bacteria. Environmental science and pollution research international, 30, 3835–3846. https://doi.org/10.1007/s11356-022-22173-y

Benoit, J. M., Gilmour, C. C.; Mason, R. P.; and Heyes, A., 1999a. Sulfide controls on mercury speciation and bioavailability to methylating bacteria in sediments pore waters. Environ. Sci. Technol. 33, 951–957.

Benoit J.M., Mason R.P, and Gilmour CC., 1999b. Estimation of mercury-sulfide speciation in sediment pore waters using octanol-water partitioning and implications for availability to methylating bacteria. Environ Toxicol Chem 18:2138–2141

Benoit, J. M.; Gilmour, C. C. and Mason, R. P., 2001a, Aspects of Bioavailability of Mercury for Methylation in Pure Cultures of Desulfobulbus propionicus (1pr3). Appl. Environ. Microbiol. 67, 51-58.

Benoit, J.M., Gilmour, C.C., and Mason, R.P., 2001b The Influence of Sulfide on Solid-Phase Mercury Bioavailability for Methylation by Pure Cultures of Desulfobulbus propionicus (1pr3). Environ. Sci. Technol., 35, 127-132.

Bentzen G, Smith AT, Bennett D, Webster NJ, Reinholt F, Sletholt E & Hobson J.,1995. Controlled dosing of nitrate for prevention of H2S in a sewer network and the effects on the subsequent treatment process. Water Sci Technol 31, 293–302.

Blum JE, Bartha R.,1980. Effect of salinity on methylation of mercury. Bull Environ Contam Toxicol. 25, 404-8. doi: 10.1007/BF01985546.

Boening DW., 2000. Ecological effects, transport, and fate of mercury: a general review. Chemosphere, 40, 1335–1351. PMID:10789973. doi:10.1016/S0045-6535(99)00283-0.

Bourceau, O. M., Ferdelman, T., Lavik, G., Mussmann, M., Kuypers, M. M. M., & Marchant, H. K., 2023. Simultaneous sulfate and nitrate reduction in coastal sediments. ISME communications, 3(1), 17. https://doi.org/10.1038/s43705-023-00222-y

Bowman, K., Collins, R., Agather, A., Lamborg, C., Hammerschmidt, C., Kaul, D., Dupont, C. & Christensen, G. & Elias, D., 2019. Distribution of mercury-cycling genes in the Arctic and equatorial Pacific Oceans and their relationship to mercury speciation. Limnology and Oceanography, 9999, 1–11.

Bravo, A.G. and Cosio, C., 2020. Biotic formation of methylmercury: A bio–physico–chemical conundrum. Limnol Oceanogr, 65, 1010-1027. https://doi.org/10.1002/lno.11366

Callahan BJ, McMurdie PJ, Rosen MJ, Han AW, Johnson AJA, Holmes SP., 2016. "DADA2: High-resolution sample inference from Illumina amplicon data." Nature Methods, 13, 581-583.

Carrell, A. A., Schwartz, G. E., Cregger, M. A., Gionfriddo, C. M., Elias, D. A., Wilpiszeski, R. L., Klingeman, D. M., Wymore, A. M., Muller, K. A., & Brooks, S. C., 2021. Nutrient Exposure Alters Microbial Composition, Structure, and Mercury Methylating Activity in Periphyton in a Contaminated Watershed. Frontiers in microbiology, 12, 647861. https://doi.org/10.3389/fmicb.2021.647861.

(CDPR, 2018). (Online: https://cdpr.ca.gov)

Celo, V., Lean, D.R. and Scott, S.L., 2006. Abiotic methylation of mercury in the aquatic environment. Science of the Total Environment, 368, 126-137.

Chen, C., Amirbahman, A., Fisher, N., Harding, G., Lamborg, C., Nacci, D., & Taylor, D., 2008. Methylmercury in marine ecosystems: spatial patterns and processes of production, bioaccumulation, and biomagnification. EcoHealth, 5, 399–408. https://doi.org/10.1007/s10393-008-0201-1.

Chen, J., Hu, G., Liu, J., Poulain, A. J., Pu, Q., Huang, R., Meng, B., & Feng, X., 2023. The divergent effects of nitrate and ammonium application on mercury methylation, demethylation, and reduction in flooded paddy slurries. Journal of hazardous materials, 460, 132457. https://doi.org/10.1016/j.jhazmat.2023.132457

Chiasson-Gould, S. A., Blais, J. M., & Poulain, A. J., 2014. Dissolved organic matter kinetically controls mercury bioavailability to bacteria. Environmental Science & Technology, 48, 3153–3161.

Chidthaisong, A., Conrad, R., 2000. Turnover of glucose and acetate coupled to reduction of nitrate, ferric iron and sulfate and to methanogenesis in anoxic rice field soil. FEMS Microbiol Ecol 31, 73–86.

Choi[a], S.-C., T. Chase, Jr., and R. Bartha.,1994a. Enzymatic catalysis of mercury methylation by Desulfovibrio desulfuricans LS. Appl. Environ. Microbiol. 60, 1342–1346.

Choi[b], S.-C., T. Chase, Jr., and R. Bartha., 1994b. Metabolic pathways leading to mercury methylation in Desulfovibrio desulfuricans LS. Appl. Environ. Microbiol. 60, 4072–4077.

Christensen, G.A., Somenahally, A.C., Moberly, J.G., Miller, C.M., King, A.J., Gilmour, C.C., Brown, S.D., Podar, M., Brandt, C.C., Brooks, S.C. and Palumbo, A.V., 2018. Carbon amendments alter microbial community structure and net mercury methylation potential in sediments. Applied and environmental microbiology, 84, e01049-17.

Clarkson, T.W., Magos, L. nd Myers, G.J., 2003. The toxicology of mercury—current exposures and clinical manifestations. New England Journal of Medicine, 349(18), 1731-1737.

Cline, J.D., 1969. Spectrophotometric determination of hydrogen sulfide in natural waters 1. Limnology and Oceanography, 14, 454-458.

Cohen, J. 1977. Statistical power analysis for the behavioral sciences (revised ed.). New York: Academic Press.

Compeau, G. C.; Bartha, R.,1985. Sulfate-reducing bacteria: Principal methylators of mercury in anoxic estuarine sediment. Appl. Environ. Microbiol. 50, 498−502.

Conaway, C.H., Mason, R.P., Steding, D.J. and Flegal, A.R., 2005. Estimate of mercury emission from gasoline and diesel fuel consumption, San Francisco Bay area, California. Atmospheric Environment, 39(1), 101-105

Conover, W. J. 1999. Practical nonparametric statistics. John Wiley & Sons.

Coolican, H. 2017. Research methods and statistics in psychology. Psychology press.

Corrales, J., Naja, G.M., Dziuba, C., Rivero, R.G. and Orem, W., 2011. Sulfate threshold target to control methylmercury levels in wetland ecosystems. Science of the total environment, 409(11), 2156-2162.

Craig, P. J. Moreton; P. A., 1983. Total Mercury, Methyl Mercury and Sulphide in River Canon Sediments. Mar. Poll. Bull. 14, 408-411.

Cristol, D.A., Brasso, R.L., Condon, A.M., Fovargue, R.E., Friedman, S.L., Hallinger, K.K., Monroe, A.P. and White, A.E., 2008. The movement of aquatic mercury through terrestrial food webs. Science, 320(5874), 335-335.

Crump, K. S., Van Landingham, C., Shamlaye, C., Cox, C., Davidson, P. W., Myers, G. J., & Clarkson, T. W., 2000. Benchmark concentrations for methylmercury obtained from the Seychelles Child Development Study. Environmental Health Perspectives, 108(3), 257-263.

Cypionka, H., 2000. Oxygen respiration in Desulfovibrio species. Ann. Rev. Microbiol. 54, 827–848.

Davey, BG, and Conyers, MK. 1988. Determining the pH of acid soils. Soil Sci. 146, 141-150.

De Gusseme, B., De Schryver, P., De Cooman, M., Verbeken, K., Boeckx, P., Verstraete, W. and Boon, N., 2009. Nitrate-reducing, sulfide-oxidizing bacteria as microbial oxidants for rapid biological sulfide removal. FEMS microbiology ecology, 67, 151-161.

Doronina, N. V., Trotsenko, Y. A., & Tourova, T. P., 2000. Methylarcula marina gen. nov., sp. nov. and Methylarcula terricola sp. nov.: novel aerobic, moderately halophilic, facultatively methylotrophic bacteria from coastal saline environments. International journal of systematic and evolutionary microbiology, 50 Pt 5, 1849–1859. https://doi.org/10.1099/00207713-50-5-1849.

Drake, H.L., Aumen, N.G., Kuhner, C., Wagner, C., Grießhammer, A. and Schmittroth, M., 1996. Anaerobic microflora of Everglades sediments: effects of nutrients on population profiles and activities. Applied and Environmental Microbiology, 62, 486-493.

Driscoll CT, Han Y-J, Chen CY, and Evers DC., 2007. Mercury contamination in forest and freshwater ecosystems in the northeastern United States. BioScience, 57, 17–28. doi:10.1641/B570106.

Driscoll, C. T., Chen, C. Y., Hammerschmidt, C. R., Mason, R. P., Gilmour, C. C., Sunderland, E. M., Greenfield, B. K., Buckman, K. L., & Lamborg, C. H., 2012. Nutrient supply and mercury dynamics in marine ecosystems: a conceptual model. Environmental research, 119, 118–131. https://doi.org/10.1016/j.envres.2012.05.002

Eckley, C.S., Luxton, T.P., Stanfield, B., Baldwin, A., Holloway, J., McKernan, J. and Johnson, M.G., 2021. Effect of organic matter concentration and characteristics on mercury mobilization and methylmercury production at an abandoned mine site. Environmental Pollution, 271, 116369.

Filippelli, M. & Baldi, F., 1993. Alkylation of Ionic Mercury to Methylmercury and Dimethylmercury by Methylcobalamin: Simultaneous Determination by Purge-and-Trap GC in Line with FTIR. Applied Organometallic Chemistry 7, 487 - 493.

Fishman, M.J and Friedman, L.C., Eds. USGS Methods for Determination of Inorganic Substances in Water and Fluvial Sediments, Open-File Report 85-495; U.S. Geological Survey: Denver, CO, 1985.

Fleming, E. J., E. E. Mack, P. G. Green, and Nelson, D. C. 2006. Mercury methylation from unexpected sources: molybdate-inhibited freshwater sediments and an iron- reducing bacterium. Appl. Environ. Microbiol. 72, 457–464. doi:10.1128/AEM.72.1.457

Fox, J. and Weisberg, S. 2019. An {R} Companion to Applied Regression, Third Edition. Thousand Oaks CA: Sage. URL: https://socialsciences.mcmaster.ca/jfox/Books/Companion/

Fritz, C. O., Morris, P. E. and Richler, J. J., 2012. Effect size estimates: current use, calculations, and interpretation. Journal of experimental psychology: General 141, 2.

Garcia-de-Lomas, J.; Corzo, A.; Gonzalez, J.M.; Andrades, J.A.; Iglesias, E.; and Montero, M.J.; 2006. Nitrate promotes biological oxidation of sulfide in wastewaters: experiment at plant-scale. Biotechnol Bioeng 93:,801–811.

Gascón Díez E, Loizeau J-L, Cosio C, Bouchet S, Adatte T, Amouroux D, Bravo AG., 2016. Role of settling particles on mercury methylation in the oxic water column of freshwater systems. Environ Sci Technol 50, 11672–11679.

Gentès, S., Löhrer, B., Legeay, A., Mazel, A.F., Anschutz, P., Charbonnier, C., Tessier, E. and Maury-Brachet, R., 2021. Drivers of variability in mercury and methylmercury bioaccumulation and biomagnification in temperate freshwater lakes. Chemosphere 267, 128890.

Gentleman, R.C., Carey, V.J., Bates, D.M., Bolstad, B., Dettling, M., Dudoit, S., Ellis, B., Gautier, L., Ge, Y., Gentry, J. and Hornik, K., 2004. Bioconductor: open software development for computational biology and bioinformatics. Genome biology, 5, 1-16.

Giblin, A.E., Tobias, C.R.; Song, B.; Weston, N.; Banta, G.T.; and Rivera-Monroy, V.H., 2013. The importance of dissimilatory nitrate reduction to ammonium (DNRA) in the nitrogen cycle of coastal ecosystems. Oceanography 26(3), 124–131, http://dx.doi.org/10.5670/oceanog.2013.54.

Gill, G. A., and Fitzgerald, W. F., 1987. Picomolar mercury measurements in sea water and other materials using stannous chloride reduction and two-stage gold amalgamation with gas phase detection. Marine Chemistry 20, 227-243.

Gilmour, C. and Henry, E. ,1991. Mercury Methylation in Aquatic Systems Affected by Acid Deposition. Environmental Pollution 71, 131-169.

Gilmour, C.C.; Riedel, G.S.; Ederington, M.C.; Bell, J.T.; Benoit, J. M.; Gill, G. A.; Stordal, M. C. Biogeochemistry 1998, 80, 327.

Gilmour, C.C., Podar, M., Bullock, A.L., Graham, A.M., Brown, S.D., Somenahally, A.C., Johs, A., Hurt Jr, R.A., Bailey, K.L. and Elias, D.A., 2013. Mercury methylation by novel microorganisms from new environments. Environmental science & technology 47, 11810-11820.

Gionfriddo, C.M., Tate, M.T., Wick, R.R., Schultz, M.B., Zemla, A., Thelen, M.P., Schofield, R., Krabbenhoft, D.P., Holt, K.E. and Moreau, J.W., 2016. Microbial mercury methylation in Antarctic sea ice. Nature microbiology 1, 1-12.

Gionfriddo, C., Capo, E., Peterson, B., Lin, H., Jones, D., Bravo, A., Bertilsson, S., Moreau, J., McMahon, K., Elias, D. and Gilmour, C., 2021. Hg-MATE-Db v1. 01142021. https://doi.org/10.25573/serc.13105370.v1

Greene EA, Hubert C, Nemati M, Jenneman GE, Voordouw G., 2003. Nitrite reductase activity of sulphate-reducing bacteria prevents their inhibition by nitrate-reducing, sulphide-oxidizing bacteria. Environ Microbiol. 5, 607-17. doi: 10.1046/j.1462-2920.2003.00446.x

Griffith, C.M., Woodrow, J.E., & Seiber, J.N., 2015. Environmental behavior and analysis of agricultural sulfur. Pest management science, 71(11), 1486–1496. https://doi.org/10.1002/ps.4067

Guan, Z., Wei, R., Liu, T., Li, J., Ao, M., Sun, S., Deng, T., Wang, S., Tang, Y., Lin, Q. and Ni, Z., 2023. Water Management Impacts on Chromium Behavior and Uptake by Rice in Paddy Soil with High Geological Background Values. Toxics, 11: 433.

Hamelin S, Amyot M, Barkay T, Wang YX, and Planas D., 2011. Methanogens: principal methylators of mercury in lake periphyton. Environmental Science & Technology 45, 7693–7700. PMID:21875053. doi:10.1021/es2010072.

Hammerschmidt CR, and Fitzgerald WF., 2004. Geochemical controls on the production and distribution of methylmercury in near-shore marine sediments. Environmental Science & Technology, 38, 1487–1495.

Hammerschmidt, C.R., & Fitzgerald, W.F., 2006. Methylmercury cycling in sediments on the continental shelf of southern New England. Geochimica et Cosmochimica Acta, 70, 918-930.

Hao, Z., Zhao, L., Liu, J., Pu, Q., Chen, J., Meng, B. and Feng, X., 2024. Relative importance of aceticlastic methanogens and hydrogenotrophic methanogens on mercury methylation and methylmercury demethylation in paddy soils. Science of The Total Environment 906, 167601.

Harrell, Jr, F.E. and Harrell, F.E., 2015. Multivariable modeling strategies. Regression modeling strategies: With applications to linear models, logistic and ordinal regression, and survival analysis, 63-102.

Heiri, O., Lotter, A.F., Lemcke G., 2001. Loss on ignition as a method for estimating organic and carbonate content in sediments: reproducibility and comparability of results. Journal of Paleolimnology 25, 101–110.

Herlemann, D. P., Labrenz, M., Jürgens, K., Bertilsson, S., Waniek, J. J., and Andersson, A. F., 2011. Transitions in bacterial communities along the 2000 km salinity gradient of the Baltic sea. ISME J. 5, 1571–1579. doi: 10.1038/ismej.2011.41

Hermes, A.L., Logan, M.N., Poulin, B.A., McKenna, A.M., Dawson, T.E., Borch, T. and Hinckley, E.L.S., 2023. Agricultural sulfur applications alter the quantity and composition of dissolved organic matter from field-to-watershed scales. Environmental Science & Technology 57, 10019-10029.

Heyes, A., Mason, R.P., Kim, E.H. and Sunderland, E., 2006. Mercury methylation in estuaries: Insights from using measuring rates using stable mercury isotopes. Marine chemistry 102, 134-147.

Hinckley, E.L.S., Kendall, C. and Loague, K., 2008. Not all water becomes wine: Sulfur inputs as an opportune tracer of hydrochemical losses from vineyards. Water resources research, 44.

Hines, M.E., Poitras, E.N., Covelli, S., Faganeli, J., Emili, A., Žižek, S. and Horvat, M., 2012. Mercury methylation and demethylation in Hg-contaminated lagoon sediments (Marano and Grado Lagoon, Italy). Estuarine, Coastal and Shelf Science 113, 85-95.

Hintelmann, H. and Evans, R. D., 1997. Application of stable isotopes in environmental tracer studies – Measurement of monomethylmercury (CH3Hg+) by isotope dilution ICP-MS and detection of species transformation. Fresenius J Anal Chem 358, 378–385.

Hintelmann, H., Keppel-Jones, K. and Evans, R.D., 2000. Constants of mercury methylation and demethylation rates in sediments and comparison of tracer and ambient mercury availability. Environmental Toxicology and Chemistry: An International Journal 19, 204-2211.

Hintelmann, H. and Ogrinc, N., 2003. Determination of stable mercury isotopes by ICP/MS and their application in environmental studies.

Hoggarth, C.G., Hall, B.D. and Mitchell, C.P., 2015. Mercury methylation in high and low-sulphate impacted wetland ponds within the prairie pothole region of North America. Environmental pollution 205, 269-277.

Hollander, M.; Wolfe, D. A.; and Chicken, E., 2013. Nonparametric statistical methods. John Wiley & Sons.

Hollweg, T.A., Gilmour, C.C. and Mason, R.P., 2010. Mercury and methylmercury cycling in sediments of the mid-Atlantic continental shelf and slope. Limnology and Oceanography, 55, 2703-2722.

Horvat, M; Liang, L.; Bloom, N.S., 1993. Comparison of distillation with other current isolation methods for the determination of methyl mercury compounds in low level environmental samples. Part II. Water. Analytica Chimica Acta 282, 153-168.

Huang, H. and Mitchell, C.P.J., 2023. Spatial and seasonal patterns of mercury concentrations, methylation and demethylation in central Canadian boreal soils and stream sediment, Science of The Total Environment 891,164447. https://doi.org/10.1016/j.scitotenv.2023.164447.

Hubert, C., and Voordouw, G., 2007. Oil field souring control by nitrate-reducing Sulfurospirillum spp. that outcompete sulfate-reducing bacteria for organic electron donors. Applied and environmental microbiology, 73, 2644–2652. https://doi.org/10.1128/AEM.02332-06.

Jensen, S. and Jernelöv, A., 1969. Biological methylation of mercury in aquatic organisms. Nature 223(5207), 753-754.

Kang-Yun, C.S., Liang, X., Dershwitz, P., Gu, W., Schepers, A., Flatley, A., Lichtmannegger, J., Zischka, H., Zhang, L., Lu, X. and Gu, B., 2022. Evidence for methanobactin “Theft” and novel chalkophore production in methanotrophs: impact on methanotrophic-mediated methylmercury degradation. The ISME Journal 16, 211-220.

Karimi, R., Fitzgerald, T.P. and Fisher, N.S., 2012. A quantitative synthesis of mercury in commercial seafood and implications for exposure in the United States. Environmental Health Perspectives 120(11), 1512-1519.

Kassambara, A. 2021. Pipe-friendly framework for basic statistical tests [R package rstatix version 0.7. 0]. February. https://mran.microsoft. com/web/packages/rstatix/index. html.

Kerin, E. J., C. C. Gilmour, E. Roden, M. T. Suzuki, J. D. Coates, and R. P. Mason, 2006. Mercury methylation by dissimilatory Iron-reducing bacteria. Appl. Environ. Microbiol. 72, 7919–7921. doi:10.1128/AEM.01602-06

King, A., and R. Eckersley. 2019. Chapter 6-Inferential Statistics III: Nonparametric Hypothesis Testing. Statistics for Biomedical Engineers and Scientists, AP King and RJ Eckersley, Eds. Academic Press: 119-145.

Kögel-Knabner, I., Amelung, W., Cao, Z., Fiedler, S., Frenzel, P., Jahn, R., Kalbitz, K., Kölbl, A. and Schloter, M., 2010. Biogeochemistry of paddy soils. Geoderma 157, 1-14.

Kögler, F., Hartmann, F.S., Schulze-Makuch, D., Herold, A., Alkan, H. and Dopffel, N., 2021. Inhibition of microbial souring with molybdate and its application under reservoir conditions. International Biodeterioration & Biodegradation 157, 105158.

Krabbenhoft, D.P., Benoit, J.M., Babiarz, C.L., Hurley, J.P., Andren, A.W., 1995. Wat. Air Soil Poll. 80, 425-433.

Kraft, B., 2014. Competition in nitrate-reducing microbial communities (Doctoral dissertation, University of Bremen, Bremen, Germany).

Kronberg, R. M.; Schaefer, J. K.; Bjorn, E.; Skyllberg, U., 2018. Mechanisms of methylmercury net degradation in Alder swamps: The role of methanogens and abiotic processes. Environ. Sci. Technol. Lett. 5 (4), 220−225.

Lachat Group. 2015. Quikchem Method 10-107-06-2-A Determination of Ammonia by Flow Injection Analysis. Lachat Instruments. 5600 Lindbergh Drive, Loveland, CO 80539 USA.

Lamborg, C.; Mincer, T.; Buchanan, W.; Collins, C.; Swarr, G.; Ganguli, P.; Whalen, K.; Bothner, M. and Valiela, I., 2019. Mercury speciation and retention in a salt marsh undergoing long-term fertilization. Estuarine, Coastal and Shelf Science 218, 188-196.

Lamborg, C.H. ICP Peak Integration Script, (2023), GitHub repository, https://github.com/chlamborg/HgICPPeakIntegration

Lang, C.-Y., Y.-W. Chen, J. Tong, M. Wang, and N. Belzile, 2005. Determination of total mercury in porewater of lake sediments: control of interference from dissolved organic carbon and sulphide. Can J Anal Sci Spectrosc 50, 167-174.

Laverman, A.M., Pallud, C., Abell, J. and Van Cappellen, P., 2012. Comparative survey of potential nitrate and sulfate reduction rates in aquatic sediments. Geochimica et Cosmochimica Acta, 77: 474-488.

Lehnherr, I.; St. Louis, V. L. Importance of ultraviolet radiation in the photodemethylation of methylmercury in freshwater ecosystems. Environ. Sci. Technol. 2009, 43 (15), 5692−5698.

Levipan, H. A., Molina, V. & Fernandez, C., 2014. Nitrospina-like bacteria are the main drivers of nitrite oxidation in the seasonal upwelling area of the Eastern South Pacific (Central Chile ~36°S). Environ. Microbiol. Rep. 6, 565–573.

Li, S., Jiang, Z. and Ji, G., 2022. Effect of sulfur sources on the competition between denitrification and DNRA. Environmental Pollution 305, 119322.

Liem-Nguyen, V., Jonsson, S., Skyllberg, U., Nilsson, M.B., Andersson, A., Lundberg, E. and Bjorn, E., 2016. Effects of nutrient loading and mercury chemical speciation on the formation and degradation of methylmercury in estuarine sediment. Environmental Science & Technology 50(13), 6983-6990.

Love MI, Huber W, Anders S., 2014. Moderated estimation of fold change and dispersion for RNA-seq data with DESeq2. Genome Biology 15, 550.

Lu, X., Gu, W., Zhao, L., Farhan Ul Haque, M., DiSpirito, A.A., Semrau, J.D. and Gu, B., 2017. Methylmercury uptake and degradation by methanotrophs. Science Advances 3, e1700041.

Lutz, M. A., M. E. Brigham, and M. Marvin-DiPasquale. 2008. Procedures for collecting and processing streambed sediment and pore water for analysis of mercury as part of the National Water-Quality Assessment Program. US Geological Survey Reston, VA.

Ma, M., Du, H., Wang, D., Sun, T., 2018. Mercury methylation in the soils and sediments of Three Gorges Reservoir Region. J Soils Sediments 18, 1100–1109. https://doi.org/10.1007/s11368-017-1827-9

Marietou, A., Griffiths, L. and Cole, J., 2009. Preferential reduction of the thermodynamically less favorable electron acceptor, sulfate, by a nitrate-reducing strain of the sulfate-reducing bacterium Desulfovibrio desulfuricans 27774. Journal of bacteriology 191, 882-889.

Martin-Doimeadios, R. C., Stoichev, T., Krupp, E., Amouroux, D., Holeman, M., and Donard, O. F. X., 2002. Micro-scale preparation and characterization of isotopically enriched monomethylmercury. Appl. Organometal. Chem. 16, 610-615.

Marvin-DiPasquale, M.C. and Oremland, R.S., 1998. Bacterial methylmercury degradation in Florida Everglades peat sediment. Environmental Science & Technology 32, 2556-2563.

Marvin-DiPasquale, M., Agee, J., Bouse, R. and Jaffe, B., 2003. Microbial cycling of mercury in contaminated pelagic and wetland sediments of San Pablo Bay, California. Environmental Geology 43, 260-267.

Marvin-DiPasquale, M., 2007. SOP USGS-MP #5 Assaying Bulk Sediment-Acid Volatile Sulfur (AVS) and Chromium Reducible Sulfur (CRS) and/or Total Reduced Sulfur (TRS). Updated: 16 January, 2007 U.S. Geological Survey, Menlo Park, CA.

Marvin-DiPasquale M, Windham-Myers L, Agee JL, Kakouros E, Kieule H, Fleck JA, Alpers CN, Stricker CA., 2014. Methylmercury production in sediment from agricultural and nonagricultural wetlands in the Yolo Bypass, California, USA. Sci Total Environ 484, 288 – 299. http://dx.doi.org/10.1016/j.scitotenv.2013.09.098.

Mason, R.P., Fitzgerald, W.F. and Morel, F.M., 1994. The biogeochemical cycling of elemental mercury: anthropogenic influences. Geochimica et cosmochimica acta 58, 3191-3198.

Mason, R.P., Reinfelder, J.R. and Morel, F.M., 1996. Uptake, toxicity, and trophic transfer of mercury in a coastal diatom. Environmental Science & Technology 30, 1835-1845.

McKeague, JA, ed. 1978. Manual on soil sampling and methods of analysis. Can. J. Soil Sci. Ottawa, ON.

McLaren, Michael R., & Callahan, Benjamin J., 2021. Silva 138.1 prokaryotic SSU taxonomic training data formatted for DADA2 [Data set]. Zenodo. https://doi.org/10.5281/zenodo.4587955

McMurdie, P. J., & Holmes, S., 2013. Phyloseq: An R package for reproducible interactive analysis and graphics of microbiome census data. PloS One 8(4), e61217.

McMurdie PJ, Holmes S., 2014. Waste not, want not: why rarefying microbiome data is inadmissible. PLoS Comput Biol. 10, e1003531. doi: 10.1371/journal.pcbi.1003531.

Mitchell CPJ, and Gilmour CC., 2008. Methylmercury production in a Chesapeake Bay salt marsh. Journal of Geophysical Research—Biogeosciences 113, G00C04. doi:10.1029/2008JG000765.

Morgan, M. 2021. BiocManager: Access the Bioconductor Project Package Repository. R package version 1.30.16. https://CRAN.R-project.org/package=BiocManager

Munson, K.M., 2014. Transformations of mercury in the marine water column (Doctoral dissertation, Massachusetts Institute of Technology).

Muyzer, G. and Stams, A.J., 2008. The ecology and biotechnology of sulphate-reducing bacteria. Nature reviews microbiology 6, 441-454.

Napa Valley Vintners, 2024. (Online: https://napavintners.com/about/ag_land_preservation.asp#:~:text=While%20it%20may%20appear%20to,Napa%20County%20Watershed%20Task%20Force.)

Navarro, D. J. 2015. Learning statistics with R: A tutorial for psychology students and other beginners. (Version 0.6) University of New South Wales. Sydney, Australia.

Nica D, Davis JL, Kirby L, Zuo G & Roberts DJ, 2000. Isolation and characterization of microorganisms involved in the biodeterioration of concrete in sewers. Int Biodeterior Biodegrad 46, 61–68.

Ogle, D. and Ogle, M.D., 2017. Package 'fsa'. Cran Repos, 1: 206.

Okabe, S., Odagiri, M., Ito, T. and Satoh, H., 2007. Succession of sulfur-oxidizing bacteria in the microbial community on corroding concrete in sewer systems. Applied and environmental microbiology 73, 971-980.

Olson, M. L., L. B. Cleckner, J. P. Hurley, D. P. Krabbenhoft, and T. W. Heelan, 1997. Resolution of matrix effects on analysis of total and methyl mercury in aqueous samples from the Florida Everglades. Fresen J Anal Chem 358, 392-396.

Orem, W.H., Krabbenhoft, D.P., Poulin, B.A. and Aiken, G.R., 2019. Sulfur contamination in the Everglades, a major control on mercury methylation. Mercury and the Everglades. A Synthesis and Model for Complex Ecosystem Restoration: Volume II–Aquatic Mercury Cycling and Bioaccumulation in the Everglades, 13-48.

Oremland, R. S., Culbertson, C. W., & Winfrey, M. R., 1991. Methylmercury decomposition in sediments and bacterial cultures: Involvement of methanogens and sulfate reducers in oxidative demethylation. Applied and Environmental Microbiology 57, 130–137.

Ortiz VL, Mason RP, Ward JE., 2015. An examination of the factors influencing mercury and methylmercury particulate distributions, methylation and demethylation rates in laboratory-generated marine snow. Mar Chem. 177(Pt 5), 753-762. doi: 10.1016/j.marchem.2015.07.006.

Ouerdane, L.; Mester, Z.; Meija, J., 2009. General Equation for Multiple Spiking Isotope Dilution Mass Spectrometry. Anal. Chem. 81, 5075–5079.

Parks JM, Johs A, Podar M, Bridou R, Hurt RA, Jr, Smith SD, Tomanicek SJ, Qian Y, Brown SD, Brandt CC, Palumbo AV, Smith JC, Wall JD, Elias DA, Liang L., 2013. The genetic basis for bacterial mercury methylation. Science 339, 1332–1335. https://doi.org/10.1126/science.1230667.

Personal Communication, Francois Birgand via Brian Dreyer and Emilio Grande. Precipitate Fe(III) with $CaCl_2$. Email November 16th, 2020.

Personal Communication, Emilio Grande, Dilute Samples to Reduce Interference By A Sulfidic Matrix, Email Nov. 24, 2020.

Personal Communication, Kristine Prelich, Time Series of N Concentration at Younger Lagoon, Email June 2, 2024.

Podar, M., Gilmour, C.C., Brandt, C.C., Soren, A., Brown, S.D., Crable, B.R., Palumbo, A.V., Somenahally, A.C. and Elias, D.A., 2015. Global prevalence and distribution of genes and microorganisms involved in mercury methylation. Science advances 1, e1500675.

Pollman CD. 2015. The role of sulfate as a driver for mercury methylation in the Everglades—what does statistics really have to say? Invited paper. Greater Everglades Ecosystem Restoration Conference 2015, Coral Springs, FL, April 21–23, 2015.

Poulain, A.J., Aris-Brosou, S., Blais, J.M., Brazeau, M., Keller, W. and Paterson, A.M., 2015. Microbial DNA records historical delivery of anthropogenic mercury. The ISME journal 9, 2541-2550

Podar, M., Gilmour, C. C., Brandt, C. C., Soren, A., Brown, S. D., Crable, B. R., Palumbo, A. V., Somenahally, A. C., & Elias, D. A., 2015. Global prevalence and distribution of genes and microorganisms involved in mercury methylation. Science advances 1(9), e1500675. https://doi.org/10.1126/sciadv.1500675

Pohlert, T., and M. T. Pohlert. 2018. Package 'PMCMRplus'. R Foundation for Statistical Computing, Vienna, Austria.

Quast C, Pruesse E, Yilmaz P, Gerken J, Schweer T, Yarza P, Peplies J, Glöckner FO., 2013. The SILVA ribosomal RNA gene database project: improved data processing and web-based tools. Nucl. Acids Res. 41(D1), D590-D596.

R Core Team. 2023._R: A Language and Environment for Statistical Computing_. R Foundation for Statistical Computing, Vienna, Austria. <https://www.R-project.org/>.

Ram, K. and Wickham, H. 2018. wesanderson: A Wes Anderson Palette Generator. R package version 0.3.6. https://CRAN.R-project.org/package=wesanderson

Roth, S., Poulin, B. A., Baumann, Z., Liu, X., Zhang, L., Krabbenhoft, D. P., Hines, M. E., Schaefer, J. K., & Barkay, T., 2021. Nutrient Inputs Stimulate Mercury Methylation by Syntrophs in a Subarctic Peatland. Frontiers in microbiology 12, 741523. https://doi.org/10.3389/fmicb.2021.741523

Rothenberg, S.E., Windham-Myers, L. and Creswell, J.E., 2014. Rice methylmercury exposure and mitigation: a comprehensive review. Environmental research 133, 407-423.

Schartup, A. T.; Mason, R. P.; Balcom, P. H.; Hollweg, T. A.; Chen, C. Y., 2013. Methylmercury production in estuarine sediments: Role of organic matter. Environ. Sci. Technol. 47, 695−700.

Schofield, RK, and AW Taylor, 1955. The measurement of soil pH. Soil Sci. Soc. Am. Proc. 19, 164-167.

Seitz, HJ., Cypionka, H., 1986. Chemolithotrophic growth of Desulfovibrio desulfuricans with hydrogen coupled to ammonification of nitrate or nitrite. Arch. Microbiol. 146, 63–67. https://doi.org/10.1007/BF00690160

Shilova, I.N., Mills, M.M., Robidart, J.C., Turk-Kubo, K.A., Björkman, K.M., Kolber, Z., Rapp, I., Van Dijken, G.L., Church, M.J., Arrigo, K.R. and Achterberg, E.P., 2017. Differential effects of nitrate, ammonium, and urea as N sources for microbial communities in the North Pacific Ocean. Limnology and Oceanography 62(6), 2550-2574.

Signorell, A., Aho, K., Alfons, A., Anderegg, N., Aragon, T., Arachchige, C., Arppe, A., Baddeley, A., Bartoń, K. and Bolker, B., 2021. Package 'DescTools'. R package version 0.99, 41.

Skyllberg, U., Persson, A., Tjerngren, I., Kronberg, R.M., Drott, A., Meili, M. and Björn, E., 2021. Chemical speciation of mercury, sulfur and iron in a dystrophic boreal lake sediment, as controlled by the formation of mackinawite and framboidal pyrite. Geochimica Et Cosmochimica Acta 294, 106-125.

Smith, C.N., Kesler, S.E., Blum, J.D. and Rytuba, J.J., 2008. Isotope geochemistry of mercury in source rocks, mineral deposits and spring deposits of the California Coast Ranges, USA. Earth and Planetary Science Letters 269(3-4), 399-407.

Sonke, J.E., Angot, H., Zhang, Y., Poulain, A., Björn, E. and Schartup, A., 2023. Global change effects on biogeochemical mercury cycling. Ambio 52, 853-876.

Spangler, W. J., Spigarelli, J. L., Rose, J. M., & Miller, H. M., 1973. Methylmercury - bacterial degradation in lake sediments. Science 180, 192–193.

Tan, S.W., Meiller, J.C. and Mahaffey, K.R., 2009. The endocrine effects of mercury in humans and wildlife. Critical reviews in toxicology 39, 228-269.

Tikhonova, T.V., Slutsky, A., Antipov, A.N., Boyko, K.M., Polyakov, K.M., Sorokin, D.Y., Zvyagilskaya, R.A. and Popov, V.O., 2006. Molecular and catalytic properties of a novel cytochrome c nitrite reductase from nitrate-reducing haloalkaliphilic sulfur-oxidizing bacterium Thioalkalivibrio nitratireducens. Biochimica et Biophysica Acta (BBA)-Proteins and Proteomics 1764, 715-723.

Todorova SG, Driscoll CT, Matthews DA, Effler SW, Hines ME, and Henry EA., 2009. Evidence for regulation of monomethyl mercury by nitrate in a seasonally stratified, eutrophic lake. Environmental Science & Technology 43, 6572–6578. PMID:19764219. doi:10.1021/es900887b.

Tomczak, M., and E. Tomczak, 2014. The need to report effect size estimates revisited. An overview of some recommended measures of effect size. Trends in sport sciences 1, 19-25.

Turk-Kubo K.A., Connell, P., Caron D., Hogan, M.E., Farnelid H.M., Zehr J.P., 2018 In Situ Diazotroph Population Dynamics Under Different Resource Ratios in the North Pacific Subtropical Gyre. Frontiers in Microbiology 9. https://www.frontiersin.org/article/10.3389/fmicb.2018.01616.

USEPA. 2002. Method 1631, Revision E: Mercury in Water by Oxidation, Purge and Trap, and Cold Vapor Atomic Fluorescence Spectrometry. U.S. EPA Office of Science and Technology.

Vu, V.Q. 2011. ggbiplot: A ggplot2 based biplot. R package version 0.55. http://github.com/vqv/ggbiplot

Wang YL, Ikuma K, Brown AMV, Deonarine A., 2024. Global survey of hgcA-carrying genomes in marine and freshwater sediments: Insights into mercury methylation processes. Environ Pollut. 352, 124117. doi: 10.1016/j.envpol.2024.124117. Epub 2024 May 5. PMID: 38714231.

Watras, C.J., Back, R.C., Halvorsen, S., Hudson, R.J.M., Morrison, K.A. and Wente, S.P., 1998. Bioaccumulation of mercury in pelagic freshwater food webs. Science of the Total Environment 219(2-3), 183-208.

Weiss-Penzias, P.S., Gay, D.A., Brigham, M.E., Parsons, M.T., Gustin, M.S. and Ter Schure, A., 2016. Trends in mercury wet deposition and mercury air concentrations across the US and Canada. Science of the Total Environment 568, 546-556.

Weiss-Penzias, P.S., Bank, M.S., Clifford, D.L., Torregrosa, A., Zheng, B., Lin, W. and Wilmers, C.C., 2019. Marine fog inputs appear to increase methylmercury bioaccumulation in a coastal terrestrial food web. Scientific Reports 9, 17611.

Wendt, K. 2000. Quikchem® Method 10-107-04-1-A Determination of Nitrate/Nitrite in Surface and Wastewaters by Flow Injection Analysis. Lachat Instruments 6645 West Mill Road, Milwaukee, WI 53218-1239 USA.

West, J., Graham, A. M., Van, L. N., & Jonsson, S., 2020. Dimethylmercury degradation by dissolved sulfide and mackinawite. Environmental Science & Technology 54, 13731–13738.

Whalen K., and Lamborg, C., 2014. Modified Protocol for Extracting DNA from Salt Marsh Sediments.

Wickham, H. 2016. ggplot2: Elegant Graphics for Data Analysis. Springer-Verlag New York. Wickham H, François R, Henry L, Müller K, Vaughan D. 2023. _dplyr: A Grammar of Data Manipulation_. R package version 1.1.4, <https://CRAN.R-project.org/package=dplyr>.

Wright, G., Gustin, M.S., Weiss-Penzias, P. and Miller, M.B., 2014. Investigation of mercury deposition and potential sources at six sites from the Pacific Coast to the Great Basin, USA. Science of the Total Environment 470, 1099-1113.

Wright, E.S. and Baum, D.A., 2018. Exclusivity offers a sound yet practical species criterion for bacteria despite abundant gene flow. BMC Genomics 19, 724. https://doi.org/10.1186/s12864-018-5099-6

Wu, Y. S., Osman, A. I., Hosny, M., Elgarahy, A. M., Eltaweil, A. S., Rooney, D. W., Chen, Z., Rahim, N. S., Sekar, M., Gopinath, S. C. B., Mat Rani, N. N. I., Batumalaie, K., & Yap, P. S., 2024. The Toxicity of Mercury and Its Chemical Compounds: Molecular Mechanisms and Environmental and Human Health Implications: A Comprehensive Review. ACS omega 9(5), 5100–5126. https://doi.org/10.1021/acsomega.3c07047

Yilmaz P, Parfrey LW, Yarza P, Gerken J, Pruesse E, Quast C, Schweer T, Peplies J, Ludwig W, Glöckner FO., 2014. The SILVA and "All-species Living Tree Project (LTP)" taxonomic frameworks. Nucl. Acids Res. 42, D643-D648

Yoon, S., Cruz-García, C., Sanford, R., Ritalahti, K.M. and Löffler, F.E., 2015. Denitrification versus respiratory ammonification: environmental controls of two competing dissimilatory NO3−/NO2− reduction pathways in Shewanella loihica strain PV-4. The ISME journal 9, 1093-1104.

Yu, R.Q., Reinfelder, J.R., Hines, M.E. and Barkay, T., 2013. Mercury methylation by the methanogen Methanospirillum hungatei. Applied and environmental microbiology 79, 6325-6330.

Yu, R.Q. and Barkay, T., 2022. Microbial mercury transformations: molecules, functions and organisms. Advances in applied microbiology 118, 31-90.

Zepp, R.G., 1987. Nitrate-induced photooxidation of trace organic chemicals in water. Environ Sci Technol 21, 443–450.

Zhang, H., Feng, X., Larssen, T., Shang, L. and Li, P., 2010. Bioaccumulation of methylmercury versus inorganic mercury in rice (Oryza sativa L.) grain. Environmental science & technology 44(12), 4499-4504.

Zhang, Y., Soerensen, A. L., Schartup, A. T., & Sunderland, E. M., 2020. A global model for methylmercury formation and uptake at the base of marine food webs. Global Biogeochemical Cycles 34, e2019GB006348. https://doi.org/ 10.1029/2019GB006348